EXPERIMENTAL EVALUATION OF SEVERAL HIGH PERFORMANCE SURFACES FOR COMPACT HEAT EXCHANGERS

CHARLES H. PIERSALL, JR.

EXPERIMENTAL EVALUATION OF SEVERAL HIGH PERFORMANCE SURFACES FOR COMPACT HEAT EXCHANGERS

* * * * * * * *

Charles H. Piersall, Jr.

EXPERIMENTAL EVALUATION OF SEVERAL HIGH PERFORMANCE SURFACES FOR COMPACT HEAT EXCHANGERS

by

Charles H. Piersall, Jr.

Lieutenant, United States Navy

Submitted in partial fulfillment of
the requirements for the degree of

MASTER OF SCIENCE
IN

MECHANICAL ENGINEERING

United States Naval Postgraduate School
Monterey, California

1 9 6 5

EXPERIMENTAL EVALUATION OF SEVERAL HIGH PERFORMANCE SURFACES FOR COMPACT HEAT EXCHANGERS

by

Charles H. Piersall, Jr.

This work is accepted as fulfilling
the thesis requirements for the degree of
MASTER OF SCIENCE
IN
MECHANICAL ENGINEERING
from the
United States Naval Postgraduate School

ABSTRACT

In this report, the basic heat transfer and isothermal flow friction characteristics for five perforated nickel matrices, one perforated nickel fin with solid splitter matrix, and one solid nickel matrix, all of "parallel plate" configuration are presented. In addition, similar information is provided for a 20° skew matrix fabricated from perforated nickel. Finally, performance of two offset rectangular fin matrices constructed from stainless steel, is evaluated. Where meaningful, a comparison of the performance of these surfaces is made. All matrices are investigated by the transient method of testing utilizing the maximum slope analysis of Locke and include the effects of longitudinal thermal conduction as reported by Howard.

ACKNOWLEDGEMENTS

The author takes this opportunity to acknowledge Dr. Paul F. Pucci, Associate Professor of Mechanical Engineering for his patience, understanding, and guidance in this endeavor; and Mr. R. D. Mueller, Chief, Heat Transfer Systems, AiResearch Manufacturing Company, Los Angeles, for his assistance in the project by providing the offset rectangular fin cores that were examined.

Likewise, the assistance of the sponsor, U. S. Navy, Bureau of Ships, Gas Turbine Branch (Code 645), is most gratefully acknowledged.

TABLE OF CONTENTS

LIST OF ILLUSTRATIONS

LIST OF TABLES

NOMENCLATURE

English Letter Symbols

A	Matrix total heat transfer area, ft^2
A_c	Matrix minimum free flow area, ft^2
A_{fr}	Matrix total frontal area, ft^2
A_s	Solid matrix cross sectional area available for thermal conduction, ft^2
A_k	Conduction area corrected for effect of perforations, ft^2
A^*	Plane surface area, ft^2
a	Plate thickness, ft
a	Short side of a rectangular flow passage, ft
b	Plate spacing, ft or in.
b	Long side of a rectangular flow passage, ft
C	Flow stream capacity rate, $(\dot{m}c_p)$, Btu (hr °F)
$\overline{C_s}$	Matrix capacity, $W_s c_s$, Btu/ °F
c_p	Specific heat at constant pressure, Btu/(lb °F)
c_s	Matrix material specific heat, Btu/(lb °F)
D_H	Hydraulic diameter, $4r_h$
d	Inside pipe diameter, in.
E	Flow friction power per unit area, HP/ft^2
f	Mean friction factor, dimensionless. This is the "small" or "Fanning" friction factor. (Ratio of wall shear stress to the fluid dynamic head.)
G	Exchanger flow stream mass velocity, $(\dot{m}/A_c)$, $lb/(hr\ ft^2)$
g_c	Proportionality factor in Newton's Second Law, $g_c = 32.2$ (lb/#) (ft/sec^2)
h	Unit conductance for thermal convection heat transfer, Btu/(hr ft^2 °F), or heat transfer power per unit area per degree temperature difference, Btu/(hr ft^2 °F)

English Letter Symbols (continued)

j	Colburn factor = $N_{ST} N_{PR}^{2/3}$, heat transfer characteristic, dimensionless
j'	Colburn j factor based on plane surface area, A*, dimensionless
K_c, K_e	Contraction loss coefficient for flow at heat exchanger entrance or exit respectively, dimensionless
k	Unit thermal conductivity, Btu/(hr ft^2 °F/ft)
k_s	Matrix thermal conductivity, Btu/(hr ft^2 °F/ft)
L	Total matrix flow length, ft
$\dot{m}$	Mass flow rate, lb/hr
P	Pressure, #/ft^2
p	Porosity for matrix surfaces, dimensionless
q	Heat transfer rate, Btu/hr
R	Universal gas constant, ft-#/lb- °R, (53.35 for air)
r_h	Hydraulic radius, ($A_c L/A$), ft, ($4r_h$ = hydraulic diameter)
s	Solidity of a perforated material, 1-σ, dimensionless
T	Absolute temperature, degrees Rankine, °R
t	Temperature, degrees Fahrenheit, °F
V_m	Matrix volume, ft^3
$\overline{V}_s$	Material volume corrected for effects of perforations
W_s	Mass of matrix, lb
x	Distance along the flow passage in direction of flow, ft

Greek Letter Symbols

α	Aspect ratio of a rectangular flow passage, b/a, dimensionless
β	Compactness; ratio of total heat transfer area to the volume between the plates, ft^2/ft^3
Δ	Denotes difference
δ	Fin thickness, ft

Greek Letter Symbols (continued)

ζ	Conduction area reduction ratio due to perforations in perforated material; cross sectional area of perforations/ cross sectional area, dimensionless
θ	Time
λ	Longitudinal conduction parameter, $\frac{k_s A_s}{\dot{m} L c_p}$, dimensionless
τ	Time parameter
μ	Fluid viscosity coefficient, lb/hr-ft
ν	Area reduction ratio due to perforations in perforated material, dimensionless
ρ	Density, lb/ft^3
σ	Ratio of freeflow area to frontal area, A_c/A_{fr}, dimensionless
φ	Denotes "function of"
$\bar{\beta}$	Compactness for perforated material including the effect of area reduction, A^*s/V_m, dimensionless
$\sum$	Summation

Subscripts

atm	Local atmosphere
f	Fluid
i	Initial, individual
k	Equivalent
m	Mean or matrix, as appropriate
o	At orifice
s	(Matrix material) solid
STD	Standard temperature and pressure
1	Upstream
2	Downstream

Force and Mass Units

lb	Denotes pounds mass to differentiate from
#	Denoting pounds force

Dimensionless Groupings

N_R	Reynolds number, $(4r_h G/\mu)$, a flow modulus
$N_{R(p)}$	Reynolds number for pipe, (dG/μ)
N_{St}	Stanton number, (h/Gc_p), a heat transfer modulus
N_{Nu}	Nusselt number, $(h4r_h/k)$, a heat transfer modulus
N_{Pr}	Prandtl number, $(\mu c_p/k)$, a fluid properties modulus
N_{Tu}	Number of heat transfer units, $(hA/\dot{m}c_p)$
j	Generalized heat transfer grouping - Colburn "j" factor, $(N_{St} N_{Pr}^{2/3})$. This factor versus N_R defines heat transfer characteristics of the surface.
f	Mean friction factor. This is the "small" or "Fanning" friction factor (Ratio of wall shear stress to the fluid dynamic head). This factor versus N_R defines the friction characteristics of the surface.
λ	Conduction parameter, $k_s A_s/\dot{m}Lc_p$ for solid material; $k_s A_k/mLc_p$ for perforated material
λ_k	Equivalent conduction parameter (corrected for equivalent length in perforated material), $\lambda \frac{L}{L_k}$
τ	Time parameter, $\frac{hA}{W_s c_s} \theta$

1. INTRODUCTION

While it is appreciated that the designer of a compact heat exchanger is confronted with many qualitative evaluations, nevertheless he is generally working specifically within limitations relating to flow frontal area, weight, pressure drop and volume. It is for this reason that different heat transfer surfaces may be effectively compared on graphs using coordinates of f and j (or f/j ratio) versus N_R.

As in many other disciplines, model theory is the most satisfactory approach from a cost effectiveness standpoint. The use of such methods as steady state "steam to air" tests or "transient" testing techniques provides the basic flow friction and heat transfer characteristics without necessitating the construction of a full scale heat exchanger.

The data presented herein was obtained by the use of a transient test technique or "single blow". [7] This technique is one of heating a sample core to some predetermined value and then after thermal equilibrium is achieved in the specimen, instantaneously removing the upstream heat source and monitoring the downstream temperature response of the fluid at the core exit.

The objectives of this thesis specifically were: to modify an experimental test rig to operate with a larger capacity blower and to test several offset rectangular fin, of stainless steel, and "modified parallel" plate, of perforated nickel, sample cores.

In the testing of perforated nickel specimens, the effect of varying shape and size of perforations was to be investigated.

2. SUMMARY OF THEORY

The "starting stage of operation", "single blow", or "transient test technique", as it has been called by various authors, had its inception with the analytical treatment by Anzelius in 1926. Nusselt in 1927, Hausen in 1927 and 1929, and finally Schumann in 1929 treated the problem of analytically determining the fluid and solid temperature as a function of position and time for a porous solid, initially at a uniform temperature, when subjected to a change in the entering fluid temperature. Some repetition occurred as the authors were unaware of the work performed by their contemporaries at the time [9] . Anzelius and Schumann made similar assumptions; however, the results are different. Anzelius simplified the problem; whereas, Schumann proceeded to obtain an explicit mathematical solution for the temperature distribution. This solution was for a liquid flowing through a porous solid and consisted of two infinite series which were related to Bessel functions. Schumann states [17] that if the fluid is a gas, the solution to the problem is more formidable. He proceeds to relate how dimensional analysis may be used so that his investigation remains usable for compressible fluids.

The porous solid is considered to be homogeneous and at a uniform temperature throughout with the fluid flowing at this same temperature. With a sudden change in the entering fluid temperature, the temperature of the fluid and the solid as a function of both position and time remains to be evaluated. The theoretical generalized heating curves are developed from an energy balance on the porous solid as presented in [19] and restated in [1] . Inasmuch as experimental procedure used in this report is dependent upon the assumptions and boundary conditions of this energy balance, it is briefly summarized below:

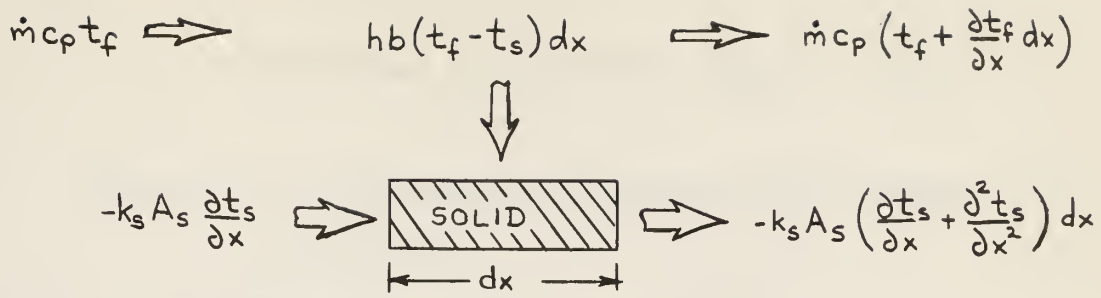

Assumptions made in the analysis are:

a. Properties of the fluid are temperature independent

b. Fluid flow is steady

c. Porous solid is homogeneous

d. Thermal conductivity of both fluid and solid is infinite perpendicular to the fluid flow direction

e. Thermal conductivity of fluid is zero in the flow direction

Boundary conditions are [13] :

(a) The matrix is initially at a uniform temperature

(b) At time equal zero, the temperature of the entering fluid changes instantaneously to a different, constant value, i.e., a step change in fluid temperature

(c) The matrix boundaries are adiabatic

Heat absorbed by solid = $\rho_s A_s c_s \frac{\partial t_s}{\partial \theta} dx$

Heat transferred to the solid by convection = $h b (t_f - t_s) dx$

Heat transferred from the fluid by convection = $\dot{m} c_p \frac{\partial t_f}{\partial x} dx$

Heat transferredfrom solid by conduction = $-k_s A_s \frac{\partial^2 t_s}{\partial x^2} dx$

Thus an energy balance for the fluid and solid yields:

(1) $\rho_s A_s c_s \frac{\partial t_s}{\partial \theta} dx = k_s A_s \frac{\partial^2 t_s}{\partial x^2} dx + h b (t_f - t_s) dx$

(2) $\dot{m} c_p \frac{\partial t_f}{\partial x} dx + h b (t_f - t_s) dx = 0$

Rearranging the above equations and substituting in the following parameters [3] :

$$\tau = \text{generalized time variable} = \frac{hA}{W_s c_s}\left[\Theta - \frac{W_f}{\dot{m}}\frac{x}{L}\right]$$

where h = unit conductance for convective heat transfer, Btu/hr ft^2 °F

A = matrix heat transfer area, ft^2

$W_s c_s$ = matrix capacity, Btu/ °F

Θ = time, hrs.

W_f = mass of fluid contained within the matrix, lb.

$\dot{m}$ = mass flow rate of fluid, lb/hr.

x = distance from entrance of matrix along flow passage in the direction of flow, ft.

L = matrix flow length, ft.

Regrouping the above equation for τ and introducing the specific heat of the fluid, c_p, we get: $$\tau = \frac{hA}{W_s c_s}\Theta - \frac{hA\,W_f\,c_p\,x}{\dot{m}\,W_s c_s c_p L}$$

Since the thermal capacity of the fluid contained at any time within the matrix ($W_f c_p$) is much less than the thermal capacity of the matrix ($W_s c_s$), the second term can be neglected; accordingly:

$$\tau \approx \frac{hA}{W_s c_s}\Theta \qquad (3)$$

$$z = \text{generalized position variable} = \frac{hA}{\dot{m} c_p}\frac{x}{L}$$

Inasmuch as the number of transfer units (N_{Tu}) = $\frac{hA}{\dot{m} c_p}$, this simply becomes

$$z = N_{Tu}\frac{x}{L} \qquad (4)$$

$$\lambda = \frac{k_s A_s}{\dot{m} c_p L} \tag{5}$$

where k_s = matrix thermal conductivity, Btu/hr ft^2 °F / ft.

A_s = solid matrix cross sectional area available for thermal conduction, ft^2.

$\dot{m}$, c_p, and L are as given above.

Equations (1) and (2), together with (3), (4), and (5) yield:

$$\frac{\partial t_s}{\partial \tau} = \lambda N_{Tu} \frac{\partial^2 t_s}{\partial z^2} + (t_f - t_s) \tag{6}$$

$$\frac{\partial t_f}{\partial z} = t_s - t_f \tag{7}$$

where t_s = temperature of the solid

t_f = temperature of the fluid

For the case of thermal conduction in the solid parallel to the direction of flow equal to zero, equations (6) and (7) simplify:

$$\frac{\partial t_s}{\partial \tau} = t_f - t_s \tag{8}$$

$$\frac{\partial t_f}{\partial z} = t_s - t_f \tag{9}$$

It is with these two differential equations, that Schumann utilizing Bessel functions determined the time - temperature history for the solid after a step change in fluid temperature. For a more thorough treatise, the reader is referred to references [13] or [17] .

The task of determining the N_{Tu} value for a test point required the superposition of the experimentally obtained time - temperature heating

or cooling curve on the family of theoretical curves. Although this would uniquely determine the N_{Tu} value, it can be appreciated as being a tedious effort.

Fortunately, in 1950, Locke [13] developed a "maximum slope" technique which bypasses this task. He differentiated the theoretical curves and plotted the slope of the curve versus τ/N_{Tu} with N_{Tu} as a parameter. The expression for the slope is

$$\frac{d\left[\frac{t_{f2}-t_i}{t_{f1}-t_i}\right]}{d\left[\tau/N_{Tu}\right]} = \frac{N_{Tu}^2}{\sqrt{N_{Tu}\tau}}\left[-J_1\left(2i\sqrt{\tau N_{Tu}}\right)e^{-(N_{Tu}+\tau)}\right]$$

where the downstream fluid temperature is evaluated at x = L so that z = N_{Tu} and $t_f = t_{f2}$.

In the efforts of both Locke and Schumann, the thermal conductivity of the solid parallel to the flow was taken as zero. Although the effect of longitudinal conduction is not pronounced at high Reynolds number range, it is considerable at low laminar Reynolds numbers. Several authors have considered the effects of longitudinal conduction, introducing the conduction parameter, λ. When $\lambda \neq 0$, the maximum slope is not a unique function of N_{Tu} but depends on λ as well. Howard [7] has tabulated maximum slopes as functions of N_{Tu} and λ, as well as presenting graphs, which he evaluated by a finite difference technique with the aid of a digital computer. The evaluation of N_{Tu} in this report is based on these tabulated values in so far as practicable.

Satisfying the aforementioned idealizations, initial and boundary conditions, leaves the determination of the conduction parameter, λ, and the experimental evaluation of the maximum slope of the heating or cooling curve as the only two remaining items necessary to determine the heat transfer characteristics of the matrix.

3. EXPERIMENTAL TECHNIQUES

The results of Howard's finite difference calculations in reference [7] were used in this report for evaluating N_{Tu} and ultimately the Colburn j factor. For this reason, the idealizations imposed by Howard were restrictions placed on the experimental set up used. Howard [7] considered transient heating of a porous solid when subjected to a step change in fluid temperature including the material longitudinal conduction effects. The idealizations are restated below:

> "(1) The flow entering the matrix is steady and uniform in velocity and temperature, and remains steady and uniform at any cross-section as it flows through the matrix. The thermal conductivity of the matrix is infinite in the direction normal to the flow and finite in the direction parallel to the flow. Thus the problem is one-dimensional in space.
>
> (2) The thermal capacity of the fluid contained at anytime within the matrix is small compared with the thermal capacity of the matrix. That is, the fluid is normally restricted to a gas and the results to be presented will not be expected to apply for liquid fluids. This also means that for the fluid there will be no time dependent terms in the equations.
>
> (3) The thermal properties of the fluid and matrix are constant and uniform.
>
> (4) The convective heat transfer coefficient is some suitable average and remains uniform and constant.
>
> (5) At time zero the change in fluid temperature will be a step function, with the matrix and its entrained fluid initially at some uniform and equal temperature."

Idealization (1) was achieved, as far as steadiness and uniformity of temperature and velocity were concerned, by responsible experimentation. In an effort to improve on the previously used test apparatus of Bannon [1], a new inlet cone was designed and the test section relocated. The inlet cone was fashioned according to the specifications of Smith and

Wang [18] for contracting cones giving uniform velocity at the throat. Although this design was specifically for circular cones, the resulting square inlet cone fabricated, together with wire screen type flow straighteners provided the required uniform velocity profile. Velocity profiles, taken at the matrix inlet over the entire flow range, verified required uniformity. The test section was placed upstream of the air metering device so that full advantage of the uniform velocity profile could be realized. Uniform temperature profiles within $\pm$ 0.5 °F were obtained by a wire screen type heater explained in detail in APPENDIX B. The latter part of the first idealization pertaining to the thermal conductivity of the matrix cannot be achieved precisely; however, the effects of deviating from it can be made negligible in the solid, if resistance to heat transfer is small within the solid compared to the heat transfer resistance between solid and gas. In other words, "transverse conduction" effects have been neglected; whereas, the effects of longitudinal conduction are considered with the use of λ , the conduction parameter. In a matrix where adequate mixing takes place, no criterion is necessary for "transverse conduction" effects.

The second idealization is self explanatory, i.e., the fluid is restricted to a gas.

Idealization (3) for the thermal properties can be guaranteed if the temperature differences are kept small. A maximum air temperature variation from 70 °F to 90 °F results in a maximum deviation from the arithmetic average in the order of $\pm$ 1.5% in viscosity and is negligible in specific heat.

The convective heat transfer coefficient presented as the final result of this experiment is an overall quantity; accordingly, idealization (4)

is satisfied.

Satisfying the fifth idealization of a step change in fluid temperature is perhaps the most rigorous requirement of all. Several investigators have attempted to meet this requirement by various schemes. The technique of Bannon [1] and Theoclitus and Eckrich [20] appears to be most satisfactory; therefore, it was the one selected for this investigation.

Figure 1 displays a schematic of the experimental set up. Figure 2, is a photograph of the complete test apparatus. The system is comprised of an air source, flow straightener screen section, heater section, matrix test section, air metering device, and pressure and temperature measuring systems. Each of these are discussed at length in APPENDIX B.

Air was drawn through the "wind tunnel" by a Spencer Turboblower. The 0.0031" diameter electric wire heaters upstream of the matrix were energized so as to heat the air to roughly 20 degrees above ambient. The upstream and downstream fluid temperatures at the matrix test section were monitored to ascertain when the matrix had been heated to a uniform temperature. When this condition was satisfied, the heaters were quickly shut down and the time-temperature history of the entering and exit air at the matrix was recorded on a Minneapolis Honeywell "Brown" Recorder. The recorded curve is the experimental cooling curve from which the maximum slope was determined.

The mass rate of flow of air was measured by an ASME orifice meter with pressure taps one diameter upstream and one - half diameter downstream, using a range of orifice plates.

Flow friction performance of the matrix was obtained by measuring the isothermal pressure drop across the matrix and the mass rate of flow of

air through the matrix. Pressure taps upstream of the matrix and upstream of the orifice meter were used to record static pressure entering the system and at the orifice section respectively.

Data reduction relations are discussed in APPENDIX A. A sample calculation for one test run is presented in APPENDIX D.

The following data was recorded for each test run:

(a) Orifice diameter (d_o)

(b) Entering static pressure (P_s)

(c) Pressure drop across the matrix (ΔP_m)

(d) Static pressure upstream of orifice (P_o)

(e) Pressure drop across the orifice (ΔP_o)

(f) Orifice temperature (t_o)

(g) Atmospheric pressure (P_{atm})

(h) Time - temperature cooling curve

(i) Recorder chart speed

4. DESCRIPTION OF SURFACES

Surfaces examined in this experiment fell into one of two major classifications - perforated nickel plate matrices or offset rectangular fin of stainless steel. In the former case, two of the specimens examined - the 20 ° skew matrix and a modified parallel plate matrix, both of 160/40TV perforated nickel - had previously been examined by Bannon [1] . These particular surfaces were selected to provide an additional check on the system reliability.

The 20 ° skew matrix was formed by corrugated sheets, which were skewed relative to one another to prevent meshing of adjacent sheets at an angle of 20 ° . This matrix configuration unlike both the modified parallel plate and the offset rectangular fin matrices does not require splitter plates.

The "modified parallel plate" configuration consists of formed sheets separated by splitter plates to prevent nesting. The assembled matrix is a maze of rectangular passages with a value of α , the aspect ratio of a rectangular flow passage, = 7. The following sketch depicts the ideally formed "modified parallel plate" matrix:

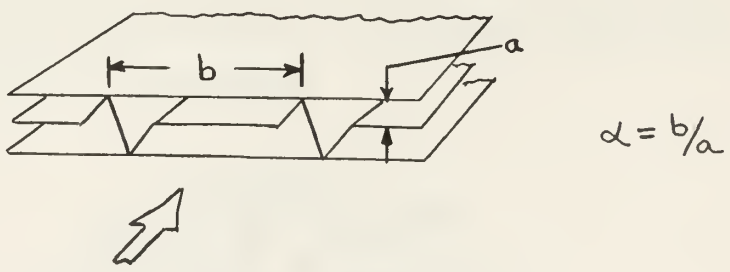

A modified parallel plate matrix of each type of perforated nickel was constructed and tested to examine the effects of varying shape, quantity and size of perforations on this configuration.

The offset rectangular fin surfaces were provided by the courtesy of the AiRsearch Manufacturing Company, Los Angeles. The method of identification employed with this configuration is best illustrated by the following example: [2]

16R - .153 - .143 (0) - .004 - SS
①② ③ ④ ⑤ ⑥ ⑦

① Number of fins per inch

② Type of fin flow cross-section (R = rectangular)

③ Fin height, inches

④ Uninterrupted fin length in the flow direction, inches

⑤ Type of surface (0 = offset)

⑥ Fin metal thickness, δ , inches

⑦ Fin material (SS = stainless steel, Al - Aluminum)

Two matrices of this configuration were investigated: - the 16R - .153 - .143 (0) - .004 - SS and the 20R - .100 - .125 (0) - .004 - SS. The offset - rectangular fin matrix is comprised of offset fins, separated by splitter plates (0.004" thick) to prevent nesting of the fins which would alter the flow characteristics. The isometric sketch below best identifies this plate fin arrangement:

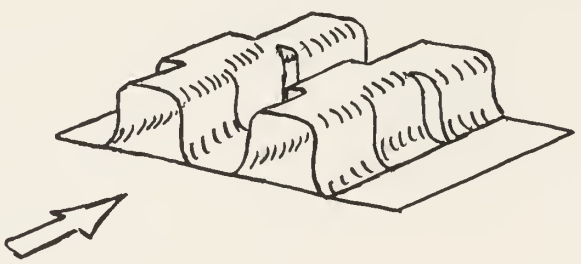

5. PRESENTATION OF RESULTS

Heat transfer and flow friction data for each matrix investigated are exhibited in both tabular and graphical form, TABLES I through X and Figures 9 through 18, using the Colburn j modulus, Fanning friction factor, and Reynolds number. In evaluating the Reynolds number, the hydraulic diameter, which is defined as four times the hydraulic radius, was used. The effects of entrance, exit, and flow acceleration have been considered in the evaluation of f. (See Appendix A).

Geometric and physical properties of the surfaces are given in Figures 3 through 8. Figures 19 through 23 show heat transfer and friction comparisons between various matrices investigated. In Figures 24 and 25, "figure of merit" type curves are presented. The j/f versus Reynolds number thus plotted gives an indication of the required matrix flow frontal area for a given pressure drop.

Lastly, in Figures 26 and 27, heat transfer power versus flow friction power curves on a unit area basis, evaluated for fluid properties at standard conditions of dry air at 500 °F and one atmosphere, are represented. (See Appendix A).

6. EXPERIMENTAL UNCERTAINTIES

Those items of possible error arising from lack of exact duplication of the idealizations, boundary and initial conditions are discussed in the "Experimental Technique" portion of this report and no further attempt was made to evaluate this type of error.

The experimental errors which do not fall into the above area are three fold and are discussed below. These three categories are: (1) uncertainty of physical constants, (2) inaccuracy in the geometric measurements and (3) instrumentation inaccuracies. For the determination of the uncertainties reported, the method of Kline and McClintock [12] was used.

(1) Values for the physical constants required were obtained from [4], [5] and [6]. The uncertainties in these values, as best as can be determined, are listed below:

$$c_s \pm 0.5\%$$

$$c_p \pm 0.5\%$$

$$N_{Pr} \pm 2.0\%$$

$$k_s \pm 0.5\%$$

$$\mu \pm 1.0\%$$

It is noteworthy that the accuracy for the value of c_s depends upon the metal used. Where pure metals are used the accuracy quoted is feasible; however, this is not the case with alloys. Thus the tolerance of c_s can be a major cause for inaccuracy [13].

(2) Due to inconsistencies in construction of the matrices, errors in lineal dimensions are considered to be $\pm$ 0.5%. Inasmuch as the weight of the matrix can be determined as accurately as desired, the error in W_s is considered negligible. Based on this, the uncertainties in geometric measurements are considered to be as follows:

$A, A_{fr}, A_c, A_s, A_k,$	$\pm$ 1.0%
L	$\pm$ 0.5%
W_s	$<$ 0.1%, negligible

(3) Instrumentation inaccuracies were essentially those obtained in pressure measurement. With the exception of the temperature measurement at the orifice, all temperatures recorded were temperature differences which were recorded in inches (See Appendix A). The temperature measurement at the orifice was obtained by a copper-constantan shielded thermocouple which was read by a Leeds and Northrup portable potentiometer. Assuming adequate manufacturer's calibration of the thermocouple wire, the estimated possible error is $\pm$ one-half of the smallest division on the potentiometer, or $\pm$ 0.0025 millivolts which is approximately $\pm$ 0.1 $^{\circ}F$.

Since the range of pressures varied, requiring several different manometers, the maximum uncertainty encountered was used in the uncertainty analysis. These values are listed below:

P_o	$\pm$	1.25%
ΔP_o	$\pm$	1.25%
ΔP_m	$\pm$	1.70%
P_{atm}	$\pm$	0.0005" Hg (negligible)

One final parameter for which uncertainty must be determined before an analysis of the experimental results can be made is N_{Tu}. Inasmuch as Colburn j factor is not a linear function of Reynolds number, uncertainty for high and low N_R values was considered. Using Figure 30 and the uncertainty in Maximum Slope as 2.0% these values were determinable.

For $N_{Tu} = 3.0$, $\lambda = 0$ $\qquad \frac{dN_{Tu}}{N_{Tu}} = \pm$ 7.2%

For $N_{Tu} = 25.0$, $\lambda = 0.05$ $\quad \frac{dN_{Tu}}{N_{Tu}} = \pm 10.0\%$

Now, with the aid of reference [12], the uncertainties in j, $\dot{m}$, N_R, and f were evaluated based on 20: 1 odds.

$$w_R = \left[\left(\frac{\partial R}{\partial v_1} w_1 \right)^2 + \left(\frac{\partial R}{\partial v_2} w_2 \right)^2 + \ldots \left(\frac{\partial R}{\partial v_n} w_n \right)^2 \right]^{1/2}$$

where w_1, w_2, $\ldots w_n$ = uncertainty interval based on certain odds, and w_R is the interval for the result.

Considering the evaluation of the Colburn j factor:

$$j = N_{Tu} \left(\frac{A_c}{A} \right) N_{Pr}^{2/3}$$

then:

$$w_j = \left[\left(\frac{\partial j}{\partial N_{Tu}} w_{N_{Tu}} \right)^2 + \left(\frac{\partial j}{\partial A} w_A \right)^2 + \left(\frac{\partial j}{\partial A_c} w_{A_c} \right)^2 + \left(\frac{\partial j}{\partial N_{Pr}^{2/3}} w_{N_{Pr}^{2/3}} \right)^2 \right]^{1/2}$$

$$= \left[\left(\frac{A_c}{A} N_{Pr}^{2/3} w_{N_{Tu}} \right)^2 + \left(\frac{N_{Tu} A_c N_{Pr}^{2/3}}{A^2} w_A \right)^2 + \left(\frac{N_{Tu}}{A} N_{Pr}^{2/3} w_{A_c} \right)^2 + \left(\frac{2}{3} \frac{N_{Tu} A_c}{A} N_{Pr}^{-1/3} w_{N_{Pr}^{2/3}} \right)^2 \right]^{1/2}$$

Dividing by j yields:

$$\frac{w_j}{j} = \left[\left(\frac{w_{N_{Tu}}}{N_{Tu}} \right)^2 + \left(\frac{w_A}{A} \right)^2 + \left(\frac{w_{A_c}}{A_c} \right)^2 + \left(\frac{2}{3} \frac{w_{N_{Pr}^{2/3}}}{N_{Pr}^{2/3}} \right)^2 \right]^{1/2}.$$

For the $N_{Tu} = 3.0$, $\lambda = 0$ case:

$$\frac{w_j}{j} = \left[(.072)^2 + (.01)^2 + (.01)^2 + \left(\frac{.04}{3}\right)^2 \right]^{1/2} = .0746$$

$$\frac{w_j}{j} \cong 7.5\%$$

For the $N_{Tu} = 25.0$, $\lambda = 0.05$ case:

$$\frac{w_j}{j} = \left[(.1)^2 + (.01)^2 + (.01)^2 + \left(\frac{.04}{3}\right)^2 \right]^{1/2} = .1018$$

$$\frac{w_j}{j} \cong 10.2\%$$

By similar analysis the uncertainties at 20:1 odds were determined for the following:

$\dot{m}$	$\pm$	1.0%
N_R	$\pm$	2.3%
f	$\pm$	4.3%

7. DISCUSSION OF RESULTS

In order to verify the reliability of the data obtained by the test apparatus used, several surfaces on which data was currently available were tested. Two of these matrices, the 160/40TV perforated nickel "parallel plate" and 20° skew, were evaluated by Bannon [1]. These two matrices were originally evaluated by the same transient test technique on basically the same test apparatus; therefore, satisfactory comparison of the data provided the necessary confidence in the test rig. Figures 9 and 16, as well as TABLES I and VIII, present the results.

The two offset rectangular fin matrices tested were essentially tested by Briggs in [2] with the exception of slightly thicker splitter material and using aluminum in lieu of the stainless steel. The data in [2] was obtained by a steady state "steam-to-air" test technique. Although this technique permitted investigation at much higher values of Reynolds number, a sufficient overlap in the Reynold's range existed so that a comparison was possible. A good comparison for the 20R -.100 - .125 - .004 - SS surface for Colburn j factor exists; however, the friction factor reported in [2] differs noticeably. Results are shown in Figure 17 and TABLE IX. For the 16R - .153 - .143 - .004 -SS surface, the values for Colburn j factor for Reynolds number < 1000 are in excellent agreement with those presented in [2]. In the transition range, the j values reported herein are noticeably different; however, the values for friction factor agree nicely throughout the entire duplicated Reynolds number range. It is important to note here that by the "maximum slope" method of analysis an inherently large error is possible in the low N_{Tu} region ($1.5 \leq N_{Tu} \leq 3.5$) [7]. The size of this error in N_{Tu} relative to an error in maximum slope can best be appreciated from Figure 30. Consider, for example, a

2% error in maximum slope with an N_{Tu} value of 2.3 and $\lambda \approx 0$. The percent error in N_{Tu}, from Figure 30, is of the order of 20%. For values of N_{Tu} between 2.0 and 2.3, the percent error has not been evaluated. The $1.5 \leq N_{Tu} \leq 3.5$ region coincides with the Reynolds range for which the reported j values differ from [2], and may account for the difference noted. The results for this matrix appear in Figure 18 and TABLE X.

In spite of the areas of disagreement, the correlation was such that the data for the j in the Reynolds range <1000 and the friction factor data for these matrices are considered reliable. It is noteworthy that the surface tested in [2] is specified as 15.76R - .153 - .143 -.004 - A1, so that the matrix evaluated herein may only be an approximate duplicate. A comparison of the relative performance for these matrices is presented in Figure 23. Additionally, Figure 25 illustrates j/f vs. N_R, a flow area "goodness" factor.

The perforated nickel matrices investigated covered a wide range of percent open area, 12 to 50%. Both slotted and round perforated nickel surfaces were evaluated for the "modified parallel plate" geometry. The perforated nickel geometric properties are given in APPENDIX C for the various types investigated. In order to make a reasonable comparison of the performance among these matrices, the same frontal area and flow length were specified. Results are presented in Figures 9 and 10 and listed in TABLES I and II for the slotted perforated nickel matrices; those for the round perforated matrices are given in Figures 11, 12, and 13 and tabulated in TABLES III, IV, and V.

In order to establish a meaningful fiducial point, a solid nickel matrix of the identical material (obtained from the same manufacturer) with the same frontal area and flow length as the perforated matrices was

fabricated. The performance of this matrix is illustrated in Figure 15 with tabular values given in TABLE VII.

The best performing slotted perforated nickel matrix was the 160/40Q. The 50G round perforated nickel (50% open area) was the best surface investigated among the "parallel plate" nickel matrices.

As another approach to evaluating the Colburn j factor, j' was considered. The parameter j' is based on the plane surface area, A*, as if no perforations were present; whereas, j is based on the heat transfer surface area, A, which includes the solidity correction, s. The value of j' is readily attainable from the relationship

$$j' = j \times s \quad , \qquad \text{where } s = A/A^*.$$ (See Appendix D).

The determination of the solidity is fully described in APPENDIX C. Figure 13 for the 50G perforated nickel matrix includes the values for j' versus Reynold's number in addition to the f and j values.

A comparison of the performance of the two slotted perforated matrices together with the solid nickel matrix is shown in Figure 19. A similar comparison for the round perforated nickel matrices is given in Figure 20.

It is readily apparent that the perforated material yields a higher heat transfer characteristic. Inasmuch as the friction factor also shows an increase, a more appropriate comparison can be made from the flow area "goodness" factor curve in Figure 24. The heat transfer power (h_{STD}) versus flow friction power (E_{STD}) per unit area given in Figures 26 and 27, for the slotted and round perforated nickel matrices respectively, is another "goodness" factor evaluation. Here the information for each of the matrices is presented based on standard conditions for fluid properties and a common hydraulic diameter. (See APPENDIX A).

So that an appreciation for the perforated material might be realized in direct transfer type of heat exchanger application in addition to its use in matrix type for rotary regenerators, a "parallel plate" matrix with the 160/40TV perforated nickel fins and solid nickel splitter plates was fabricated. The performance of this matrix is given in graphical and tabular form in Figure 14 and TABLE VI. A comparison with the solid nickel matrix is made in Figure 21. Figure 24 contains the j/f presentation and Figure 26 shows the h_{STD} vs. E_{STD} for this matrix. Here again is a noticeable increase in heat transfer performance, but with a negligible increase in friction factor.

For the 160/40TV perforated nickel material, a 20° skew matrix was compared in performance against the "modified parallel plate" to see how these two configurations compare with one another. The separate performance for each has been mentioned previously; however, the direct comparison is shown in Figure 22. As with the other nickel surfaces, the flow area "goodness" factor is represented in Figure 24.

In the results of this investigation are several items which are general in nature, but nonetheless extremely important. In the laminar Reynolds number range, friction factor is inversely proportional to Reynolds number. By Reynolds analogy, it was anticipated that the Colburn j factor should likewise be inversely proportional to Reynolds number in this region. However, the experimentally obtained values of j in the low laminar Reynolds range utilizing the equivalent conduction length (defined in APPENDIX C) together with TABLE XI or Figure 29 yielded lower values for j. For this reason, a re-evaluation of the conduction parameter, N_{Tu}, and maximum slope data points for Figure 29 was performed. The equivalent conduction parameter λ_k, was computed and the N_{Tu} value was determined by utilization of the extrapolated j vs. N_R curve, since j is proportional to N_{Tu}. This new

determined value of N_{Tu} was considered to be the actual N_{Tu} for the particular "maximum slope" and conduction parameter. Values determined in this fashion are asterisked in TABLES I through VI and VIII. The tabulated conduction parameter values in these tables are the equivalent conduction parameter (See APPENDIX D).

The second item is that of an equivalent conduction length which was quoted earlier. In the perforated fin material the slots or round holes, as the case may be, provide for a winding heat flow path. It was appreciated that the matrix flow length, L, was not the true conduction path but somewhat less than actual. A mean conduction path length evaluation is presented in APPENDIX C. The conduction parameter, λ , based on the flow length, L, was evaluated, and by simply multiplying by the ratio L/L_k (also given in APPENDIX C), the value of λ_k was determined.

A third item is the inherent error in N_{Tu} in the range $1.5 \leq N_{Tu} \leq 3.5$ which was mentioned earlier. Howard [7] published an error curve for N_{Tu}, including slope vs. N_{Tu}, see Figure 30.

Fourthly, the entrance and exit length effects for a matrix with a small hydraulic radius are small. In the evaluation for Fanning friction factor (APPENDIX A), the effects of exit and entrance length were considered using values of K_c and K_e from Figures 37, 38, or 39, as appropriate. For the perforated surfaces, the K values were taken corresponding to laminar flow conditions; however, in the offset rectangular fin geometry the values were taken from those Figures for $N_R = \infty$ in accordance with reference [11] . The offset fins never have velocity profiles that are fully established, that being a purpose in the design. The same calculations were repeated on the offset rectangular fins using the K values for laminar flow. The friction curves plotted for the offset rectangular fins

were coincident with those obtained earlier; however, some change was noted in tabulated values.

A final item worth mentioning is again concerned with the low Reynolds range. A slight alteration in the conduction parameter value has a marked effect on the N_{Tu} value in this range, which is apparent from Figure 29. For this reason, when utilizing a nickel material, or any other material with a wide range of specified values for thermal conductivity, it is mandatory that the appropriate value of k_s be obtained for calculating purposes. The value of λ is directly proportional to this k_s value, i.e.,

$$\lambda = \frac{k_s A_s}{L \dot{m} c_p}$$

8. CONCLUSIONS

Reliable data is obtainable from the experimental apparatus based on a comparison with those surfaces previously evaluated elsewhere.

A very definite improvement in performance is achieved with the utilization of a perforated material. Kays, in reference [10] , postulated the improved heat transfer characteristic without a "large amount of form drag so characteristic of high performance surfaces". The perforations apparently disturb the heat transfer sub boundary layer so that tubulence increases and the resulting high convection conductance is realized. Inasmuch as the perforations are fine, the downstream edge is considered to be in the wake of the separated region. The perforated nickel matrices investigated herein confirm Kays' hypothesis. Unfortunately, inasmuch as the perforated surface investigated in [10] is greatly different in geometric and physical properties, no meaningful comparison with those tested in this investigation could be made.

As stated previously, the experimentally obtained Colburn j values in the low laminar Reynolds range using TABLE XI or Figure 29 were lower than j values obtained by extrapolating the j versus N_R curve. Inasmuch as friction factor and Colburn j factor are both inversely proportional to Reynolds number in the laminar region owing to Reynolds analogy, the values for Colburn j factor extrapolated from the experimental curves are considered more reliable in the low laminar range.

Effects of longitudinal conduction have been considered in the analysis of data. For the perforated material matrices, corrections for the actual conduction path length and for the area removed by the perforations have been included.

The best performance for a perforated "parallel plate" matrix was attained by the 50G type material. For the offset rectangular fin surfaces,

the 20R - .100 - .125 - .004 - SS matrix was superior.

9. RECOMMENDATIONS FOR FURTHER STUDY

1. Due to the inherent error in the high Reynolds number range where $1.5 \leq N_{Tu} \leq 3.5$, a more reliable means for determining N_{Tu} values should be investigated. Perhaps pursuit of Hausen's cyclic operation [9], a steady state periodic-flow technique, is appropriate in that this method measures effectiveness from which N_{Tu} can be determined subsequently. Since the results obtained using Schumann's analysis, even with longitudinal conduction effects considered, at the low Reynold's range appears inadequate; the use of another testing method may prove fruitful.

2. Inasmuch as the best performing surface for perforated nickel was the 50G type (50% open area), other types, such as the 40G which has a slightly larger hole diameter, with same plate thickness and percent open area as the 50G may prove worthy of test.

10. BIBLIOGRAPHY

[1] Bannon, John M. "An Experimental Determination of Heat Transfer and Flow Friction Characteristics of Perforated Material for Compact Heat Exchanger Surfaces". Unpublished Master's thesis, U. S. Naval Post-graduate School, Monterey, 1964.

[2] Briggs, D. C. and London, A. L. "The Heat Transfer and Flow Friction Characteristics of Five Offset Rectangular and Six Plain Triangular Plate-Fin Heat Transfer Surfaces", International Developments in Heat Transfer, Part I, International Heat Transfer Conference, Boulder, Colorado, 1961.

[3] Coppage, J. E. "Heat Transfer and Flow Friction Characteristics of Porous Media", TR. No. 16, Department of Mechanical Engineering, Stanford University, Stanford, Calif., December 1, 1952.

[4] Eldridge, E. A. and Deem, H. W. Report on Physical Properties of Metals and Alloys from Cryogenic to Elevated Temperatures. Philadelphia: American Society for Testing Materials, 1961.

[5] Goldsmith, A., et.al. Handbook of Thermophysical Properties of Solid Materials. Revised Edition, Vol. I, Elements, New York: The MacMillan Company, 1961.

[6] Hilsenrath, J., et. al. Tables of Thermodynamic and Transport Properties of Air, Argon, Carbon Monoxide, Hydrogen Nitrogen, Oxygen, and Steam. New York: Permagon Press, 1960.

[7] Howard, C. P. "The Single Blow Problem Including the Effects of Longitudinal Conduction", ASME paper, No. 64 - GTP - 11.

[8] Howard C. P. Bureau of Ships, Code 645, U. S. Navy, private communication, February, 1965.

[9] Jakob, M. Heat Transfer, Vol. II, New York: John Wiley and Sons, Inc., 1957.

[10] Kays, W. M. "The Heat Transfer and Flow Friction Characteristics of a Wavy Fin, a Strip Fin, and a Perforated Fin Heat Transfer Surface", TR. No. 39, Department of Mechanical Engineering, Stanford University, Stanford, Calif., October 31, 1958.

[11] Kays, W. M. and London, A. L. Compact Heat Exchangers. Second Edition. New York: McGraw-Hill Book Company, Inc., 1964.

[12] Kline, S. J. and McClintock, F. A. "Describing Uncertainties in Single-Sample Experiments", Mechanical Engineering, January, 1953, pp 3-8.

[13] Locke, G. L. "Heat Transfer and Flow Friction Characteristics of Porous Solids", TR. No. 10, Department of Mechanical Engineering, Stanford University, Stanford, Calif., June 1, 1950.

[14] London, A. L. "New Developments in Compact Exchangers - Design Theory, Surfaces, and Applications", lecture presented at 6th National ASME - AIChE Heat Transfer Conference, Boston, Massachusetts, August, 1963.

[15] Murdock, J. W. "Tables for the Interpolation and Extrapolation of ASME Coefficients for Square-Edged Concentric Orifices", ASME paper, No. 64 - WA/FM - 6.

[16] Power Test Code Supplements, Instruments and Apparatus, PTC - 19. 5.4 Flow Measurement, Chapter 4. New York: American Society of Mechanical Engineers, 1959.

[17] Schumann, T. E. W. "Heat Transfer: A Liquid Flowing Through a Porous Prism", Journal of the Franklin Institute, Vol. 208, 1929, pp. 405 - 416.

[18] Smith, R. H. and Wang, C. T. "Contracting Cones Giving Uniform Throat Speeds", Journal of the Aeronautical Sciences, October, 1944, pp. 356 - 360.

[19] Solar Aircraft Company, Engineering Report ER 1221, Regenerator Core Module Tests - T - 600 Engine, 18 April 1962. Rev. A: 25 October, 1962, AD 290234.

[20] Theoclitus, G. and Eckrich, T. L. "An Experimental Technique for Determining the Effectiveness of Extended Surfaces", presented at 7th National Heat Transfer Conference, Cleveland, Ohio, August, 1964.

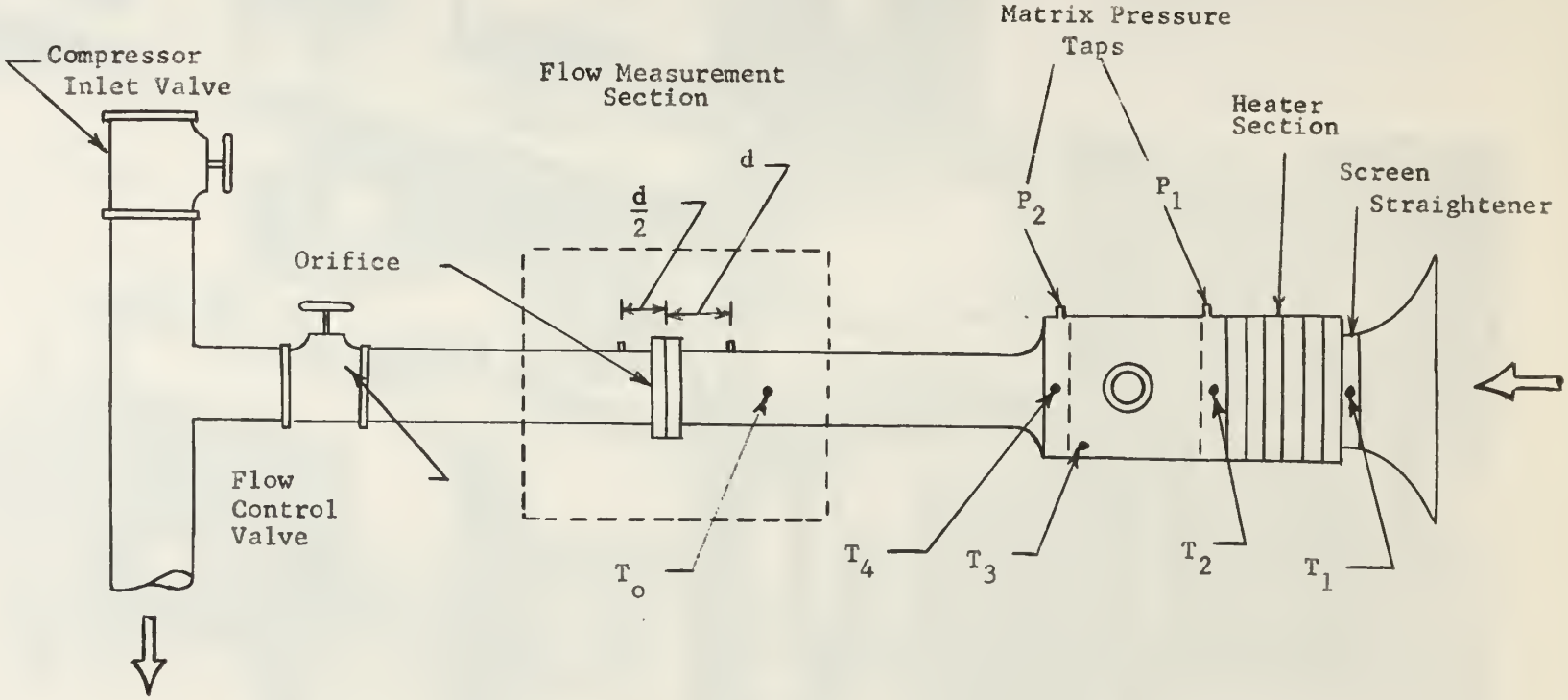

Figure 1. Schematic Diagram of Test Apparatus

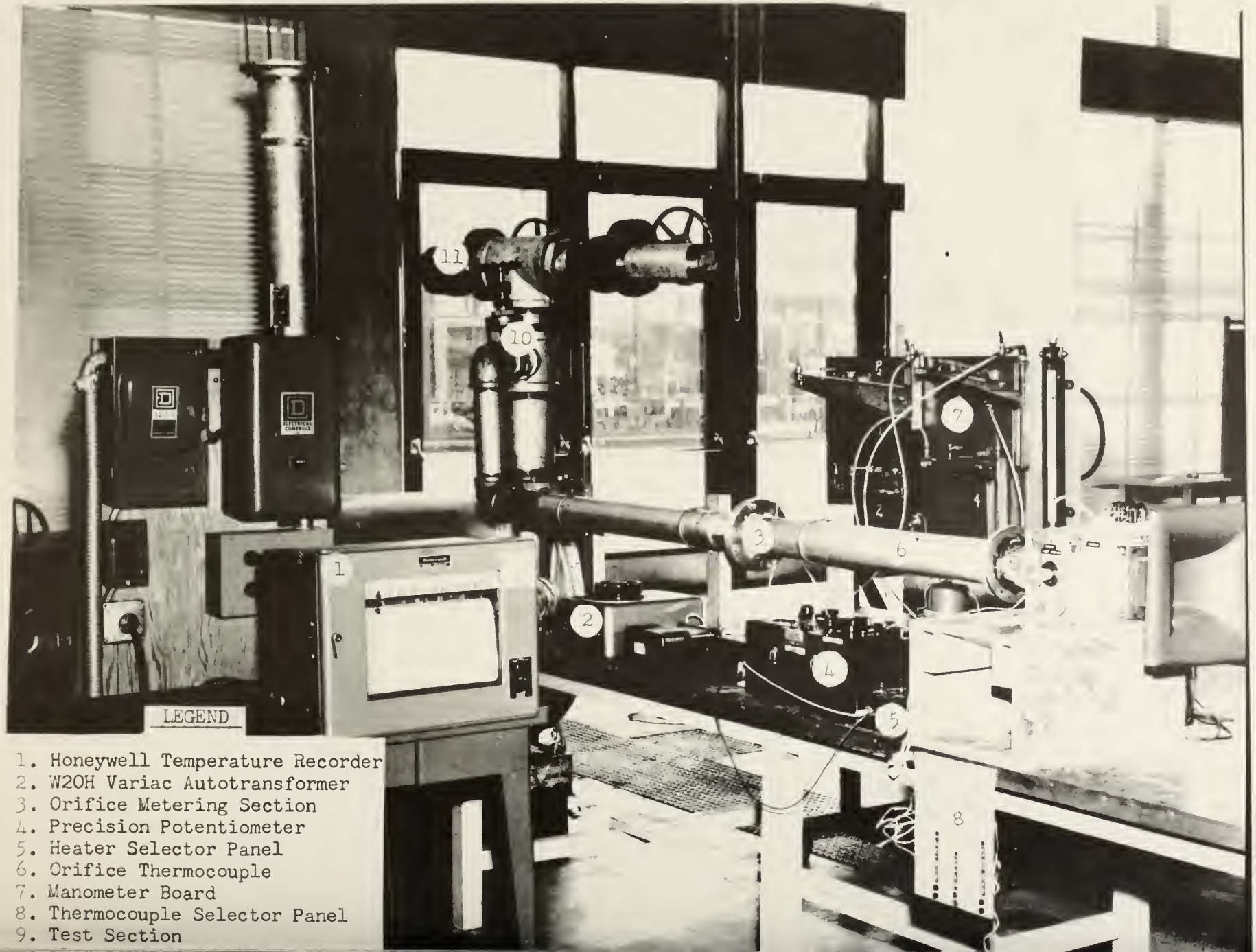
LEGEND
1. Honeywell Temperature Recorder
2. W20H Variac Autotransformer
3. Orifice Metering Section
4. Precision Potentiometer
5. Heater Selector Panel
6. Orifice Thermocouple
7. Manometer Board
8. Thermocouple Selector Panel
9. Test Section

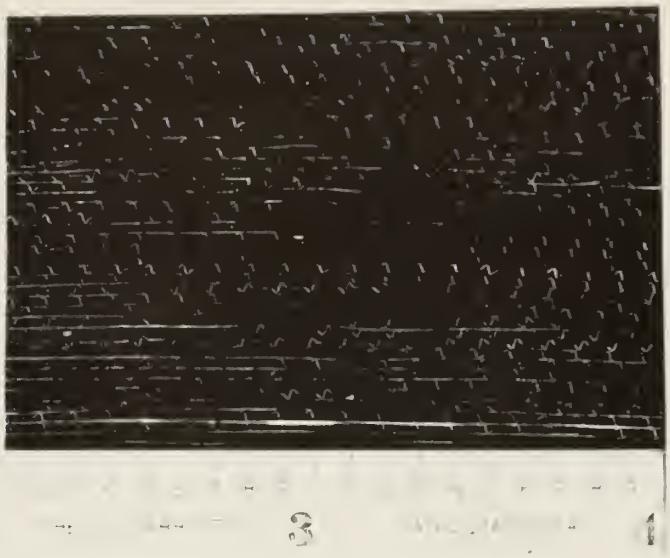

Matrix Material	160/40 TV Perf.Nickel	160/40 S Perf.Nickel
Specific Heat (c_s) Btu/lb F	0.1065	0.1065
Thermal Conductivity (K_s) Btu/ hr ft F	38.7	38.7
Material Thickness, inches	0.0022	0.0016
Total Heat Transfer Area (A) ft^2	18.593	16.2667
Frontal Area (A_{fr}) ft^2	0.06953	0.06953
Total Conduction Area (A_k) ft^2	0.00424	0.002887
Free Flow Area (A_c) ft^2	0.0584	0.06142
Matrix Volume (V_m) ft^3	0.011588	0.011588
Matrix Density (ρ_m) lb/ft^3	58.6	59.2
Hydraulic Diameter (D_H) ft	0.001929	0.002028
Compactness ($\bar{\beta}$) ft^2/ft^3	1604.3	1403.8
Porosity (p)	0.840	0.883

Figure 3. Geometric and Physical Properties of Slotted Perforated Nickel (160/40 TV and 160/40 S) "Parallel Plate" Matrices

Matrix Material	125 M Perf. Nickel	125 P Perf. Nickel	50 G Perf. Nickel
Specific Heat (c_s) Btu/lb °F	0.1065	0.1065	0.1065
Thermal Conductivity (k_s) Btu/ hr ft °F	38.7	38.7	38.7
Material Thickness, inches	0.0016	0.0020	0.0016
Total Heat Transfer Area (A) ft^2	16.2578	17.7024	11.2033
Frontal Area (A_{fr}) ft^2	0.06953	0.06953	0.06953
Total Conduction Area (A_k) ft^2	0.00435	0.00640	0.00243
Free Flow Area (A_c) ft^2	0.06142	0.0 5939	0.06142
Matrix Volume (V_m) ft^3	0.011588	0.011588	0.011588
Matrix Density (ρ_m) lb/ft^3	44.1	41.8	31.6
Hydraulic Diameter (D_H) ft	0.002028	0.001961	0.002028
Compactness ($\overline{\beta}$) ft^2/ft^3	1403.0	1527.7	966.8
Porosity (p)	0.883	0.854	0.883

Figure 4. Geometric and Physical Properties of Round Perforated Nickel (125 M, 125 P, and 50 G) "Parallel Plate" Matrices

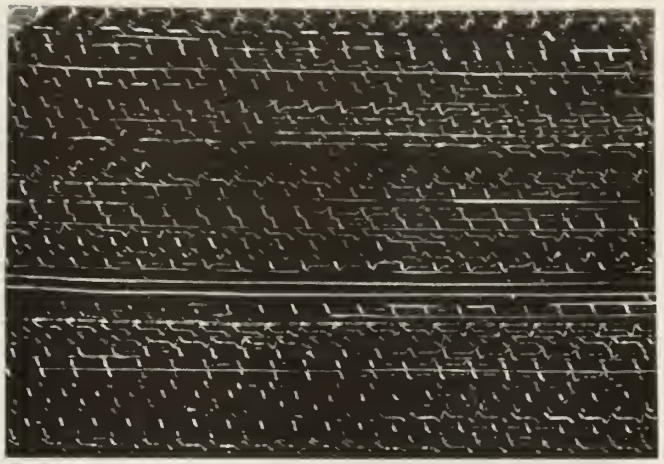

Matrix Material	Solid Nickel Splitters
[illegible]	[illegible]
[illegible]	[illegible]
[illegible]	[illegible]
[illegible]	[illegible]
[illegible]	[illegible]
Frontal Area (A_p), ft^2	[illegible]
[illegible]	[illegible]
[illegible]	[illegible]
Matrix Volume (V_m), ft^3	[illegible]
Matrix Density (ρ_m), lbm/ft^3	[illegible]
Hydraulic Diameter (D_h), ft	[illegible]
Compactness ($\bar{\sigma}$), ft^2/ft^3	[illegible]
Porosity (ϵ)	[illegible]

Figure [illegible]. [illegible] of Slotted Perforated [illegible] Splitters, "Parallel

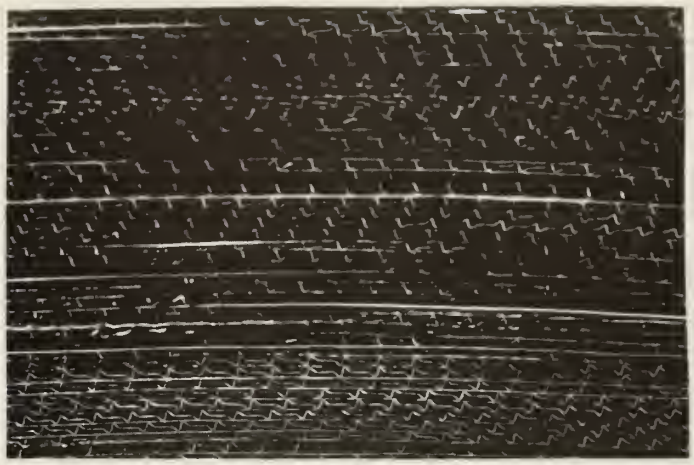

Matrix Material	Solid Nickel
Specific Heat (c_s) Btu/lb ^{o}F	0.1065
Thermal Conductivity (k_s) Btu/ hr ft ^{o}F	38.7
Material Thickness, inches	0.0020
Total Heat Transfer Area (A) ft^2	20.1875
Frontal Area (A_{fr}) ft^2	0.06953
Total Conduction Area (A_s) ft^2	0.01014
Free Flow Area (A_c) ft^2	0.05939
Matrix Volume (V_m) ft^3	0.011588
Matrix Density (ρ_m) lb/ft^3	77.7
Hydraulic Diameter (D_H) ft	0.001961
Compactness ($\bar{\beta}$) ft^2/ft^3	1742.1
Porosity (p)	0.854

Figure 6. Geometric and Physical Properties of a Solid Nickel "Parallel Plate" Matrix

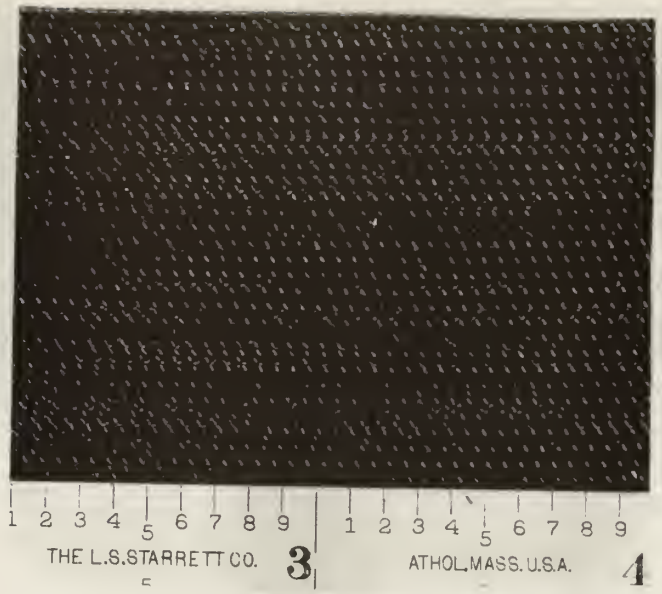

Matrix Material	20 Degree Skew 160/40 TV Perf.Nickel
Specific Heat (c_s) Btu/lb F	0.1065
Thermal Conductivity (k_s) Btu/ hr ft F	38.7
Material Thickness, inches	0.0022
Total Heat Transfer Area (A) ft^2	15.41
Frontal Area (A_{fr}) ft^2	0.0734
Total Conduction Area (A_k) ft^2	0.00349
Free Flow Area (A_c) ft^2	0.06412
Matrix Volume (V_m) ft^3	0.01211
Matrix Density (ϱ_m) lb/ft^3	50.1
Hydraulic Diameter (D_H) ft	0.00252
Compactness ($\bar{\varrho}$) ft^2/ft^3	1272.8
Porosity (p)	0.873

Figure 7. Geometric and Physical Properties of a Slotted Perforated Nickel (160/40 TV) 20° Skew Matrix

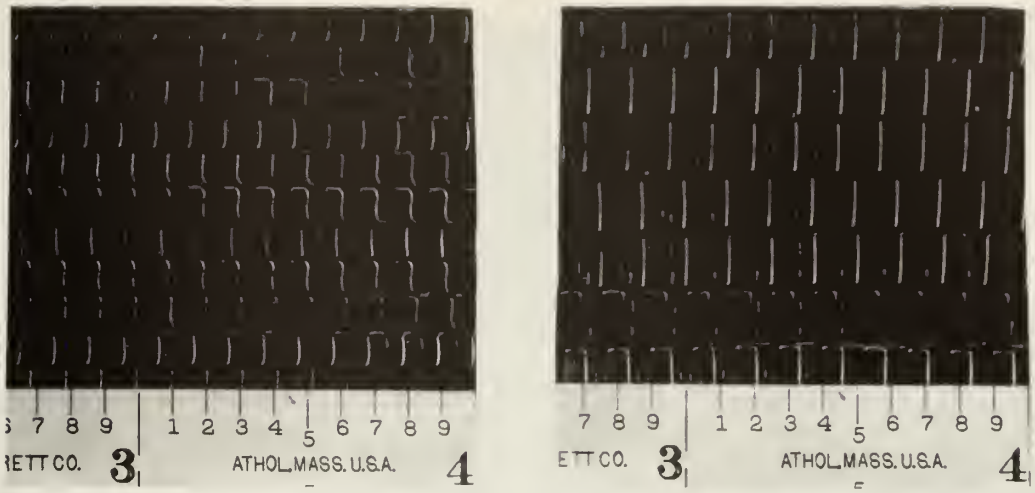

Matrix Material	20R -.100 - .125-.004-SS	16R -.153 - .143-.004-SS
Specific Heat (c_s) Btu/lb F	0.120	0.120
Thermal Conductivity (k_s) Btu/ hr ft F	9.3	9.3
Material Thickness, inches	0.004	0.004
Total Heat Transfer Area (A) ft^2	11.625	9.0625
Frontal Area (A_{fr}) ft^2	0.07083	0.07083
Total Conduction Area (A_s) ft^2	0.01549	0.01201
Free Flow Area (A_c) ft^2	0.05535	0.05882
Matrix Volume (V_m) ft^3	0.0177	0.0177
Matrix Density (ϱ_m) lb/ft^3	66.3	50.4
Hydraulic Diameter (D_H) ft	0.00476	0.00649
Compactness ($\overline{\beta}$) ft^2/ft^3	656.5	511.8
Porosity (p)	0.781	0.830

Figure 8. Geometric and Physical Properties of Stainless Steel Offset Rectangular Fin (20R-.100-.125-.004 -SS and 16R-.153-.143-.004 -SS) Matrices

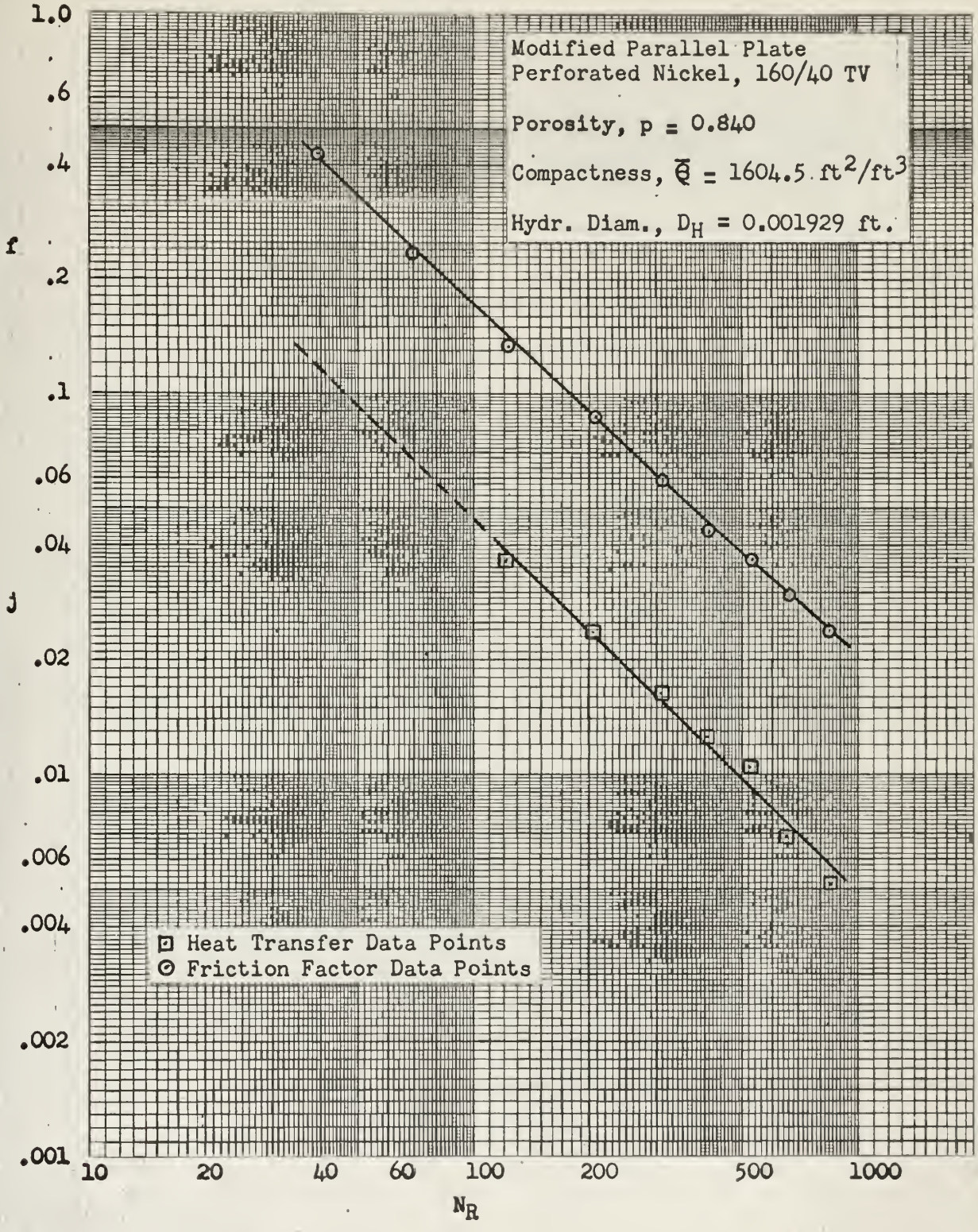

Figure 9. Surface Heat Transfer and Friction Data "Parallel Plate", 160/40 TV Perforated Nickel

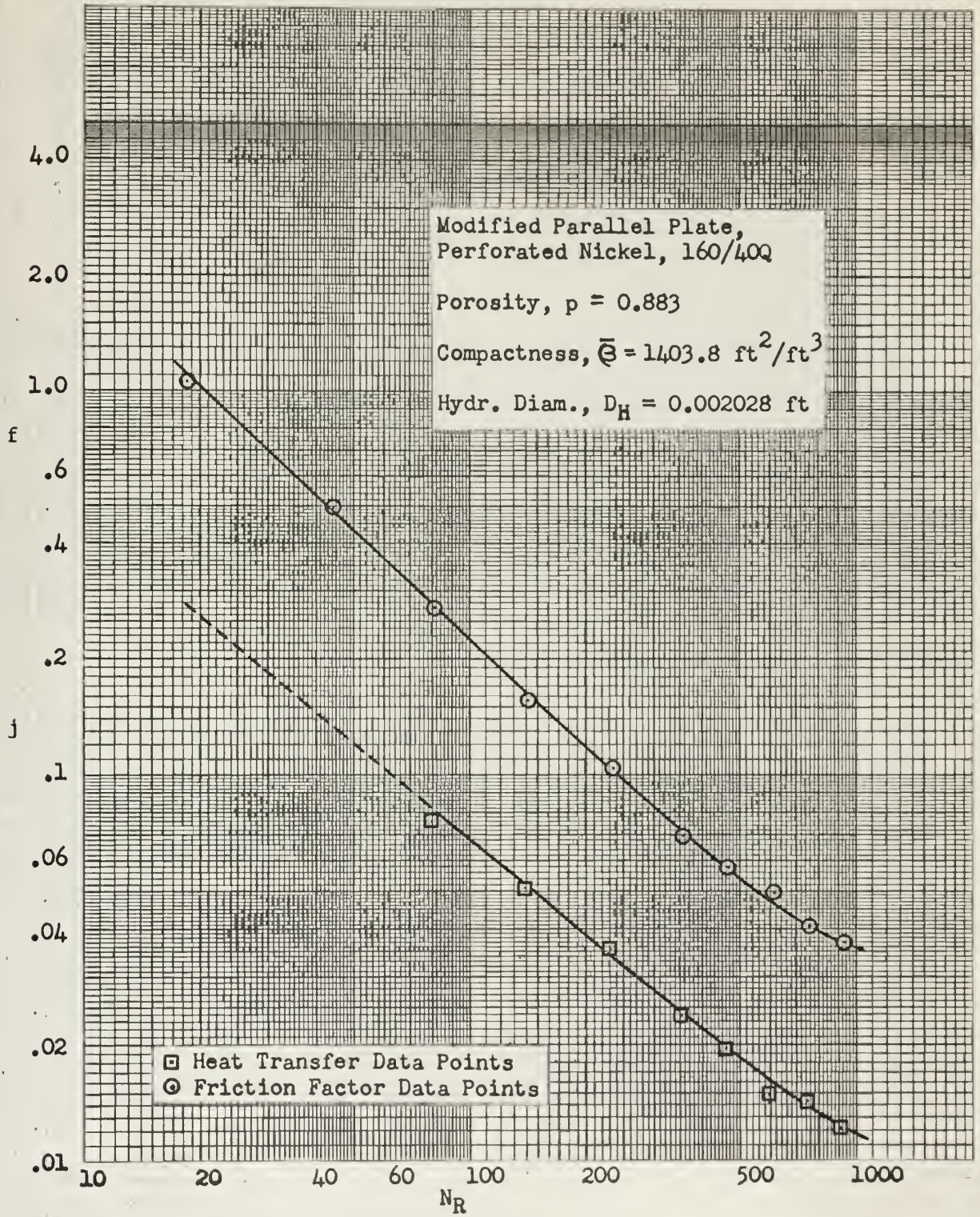

Figure 10. Surface Heat Transfer and Friction Data "Parallel Plate", 160/40 Q Perforated Nickel

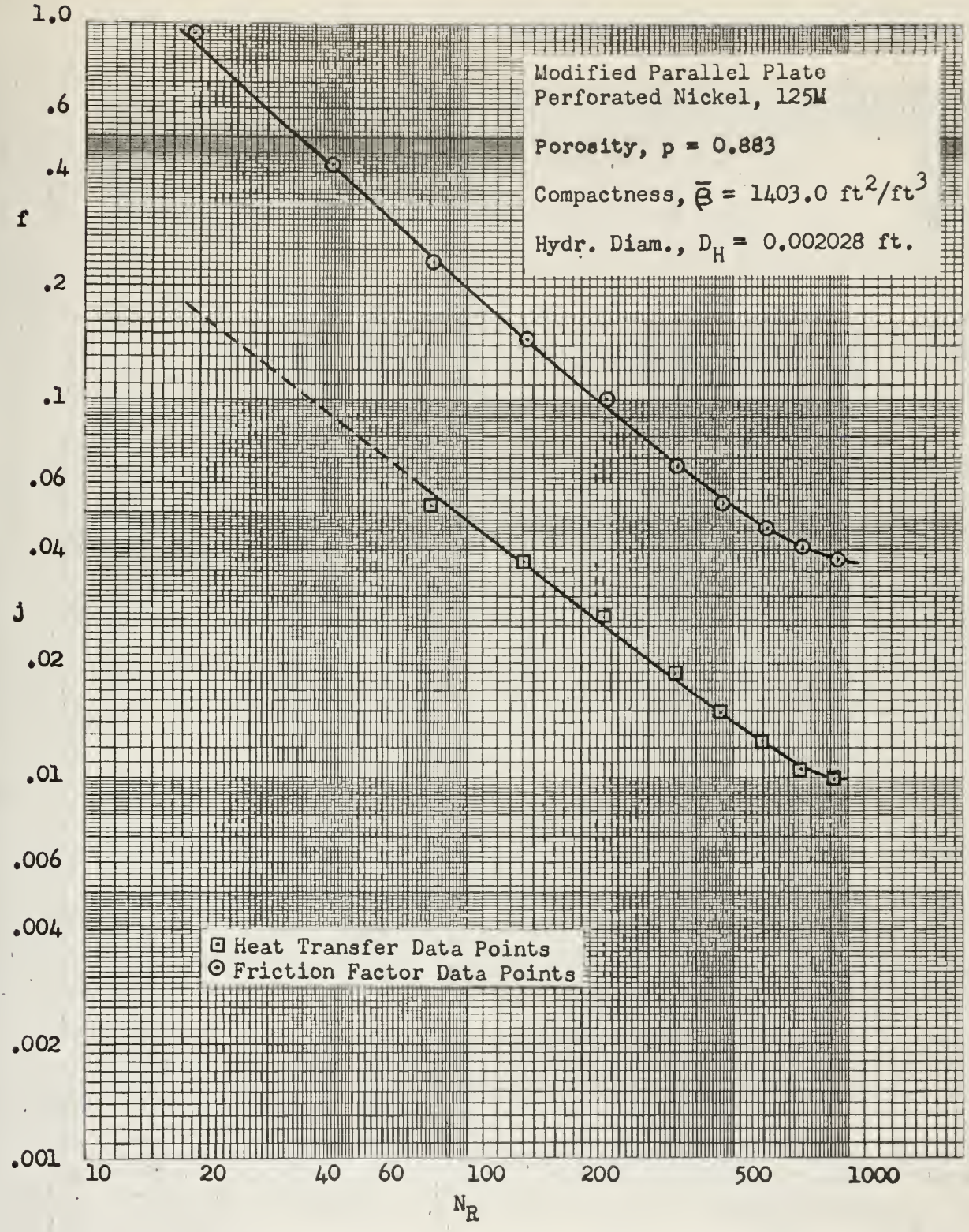

Figure 11. Surface Heat Transfer and Friction Data "Parallel Plate", 125 M Perforated Nickel

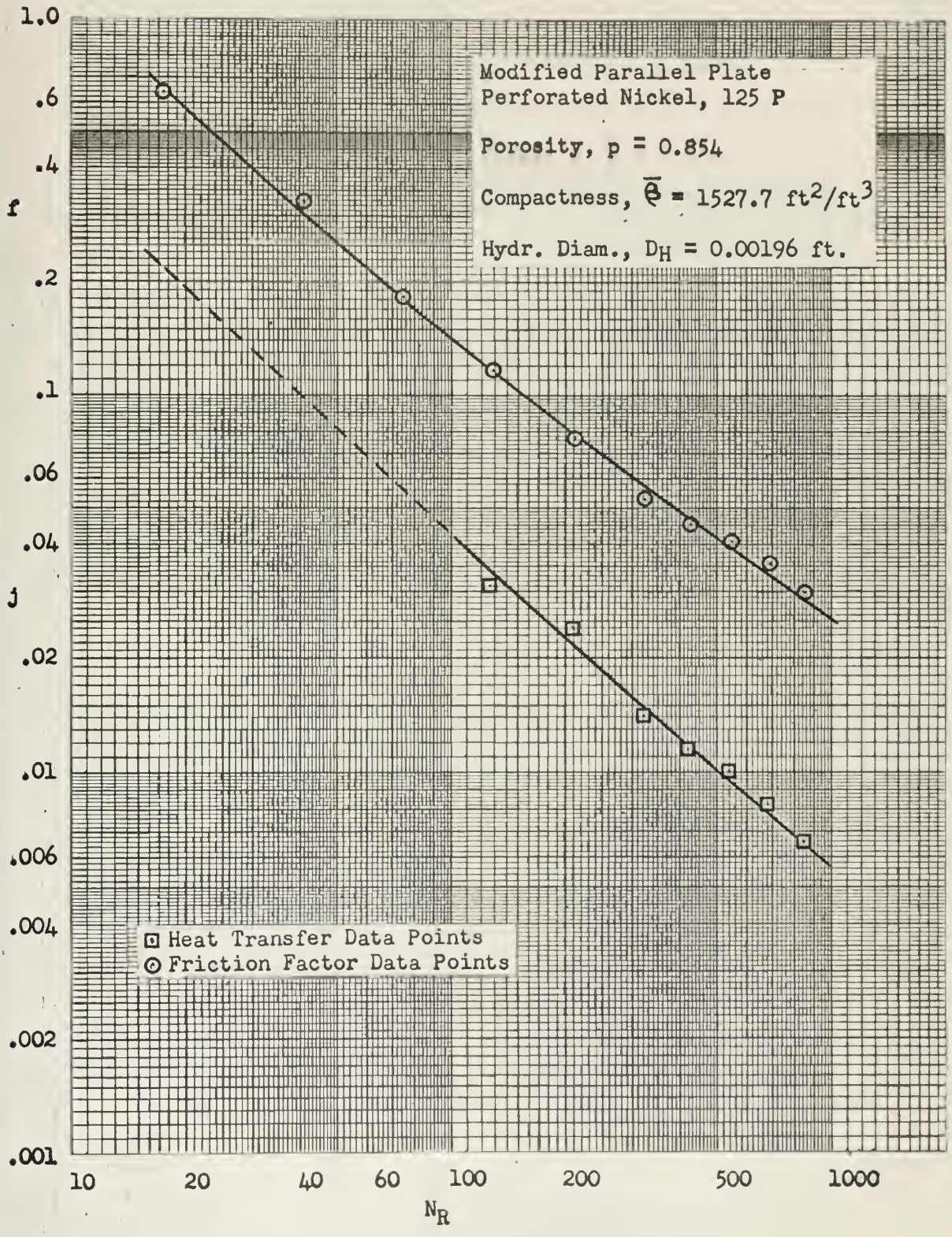

Figure 12. Surface Heat Transfer and Friction Data "Parallel Plate", 125 P Perforated Nickel

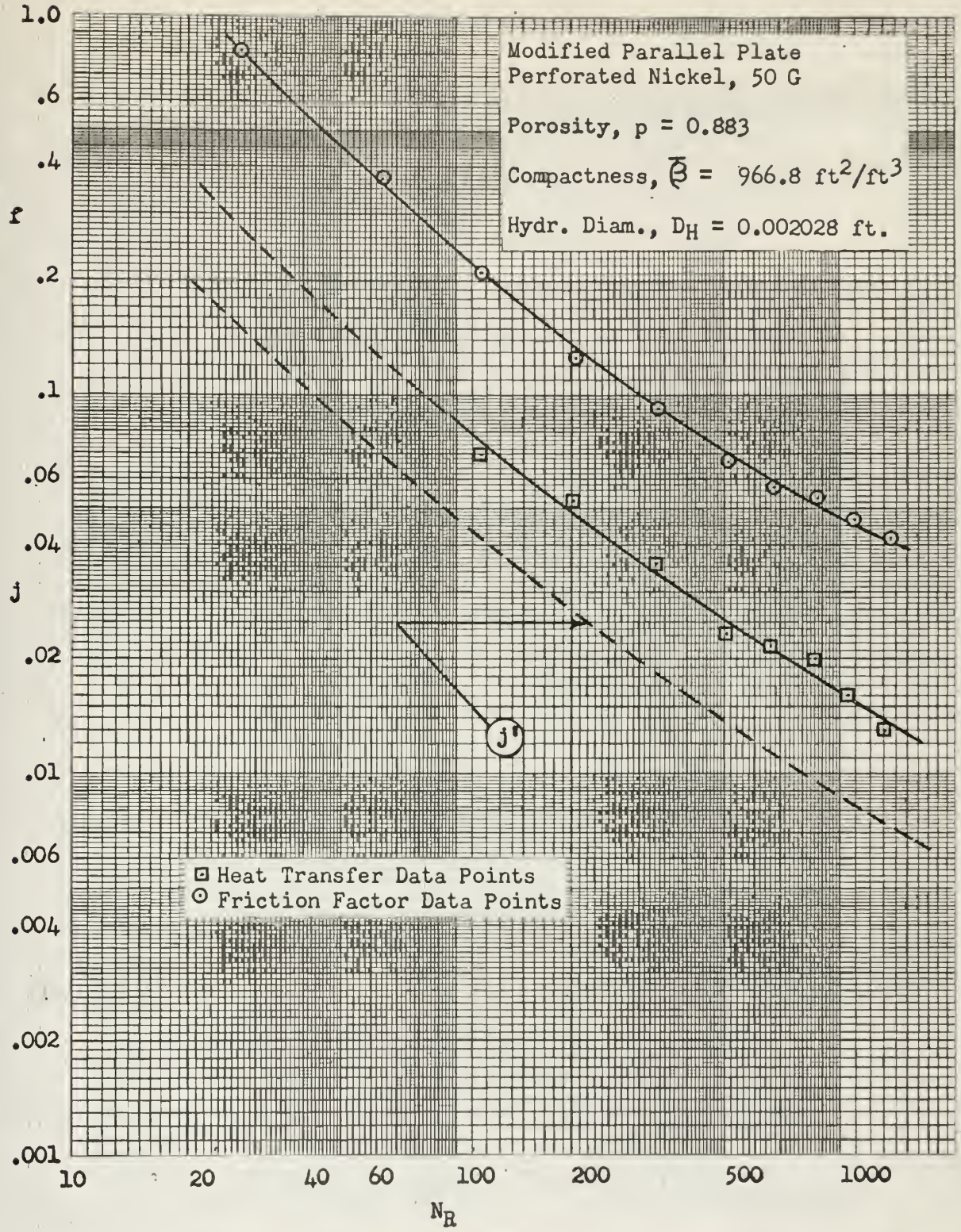

Figure 13. Surface Heat Transfer and Friction Data "Parallel Plate", 50 G Perforated Nickel

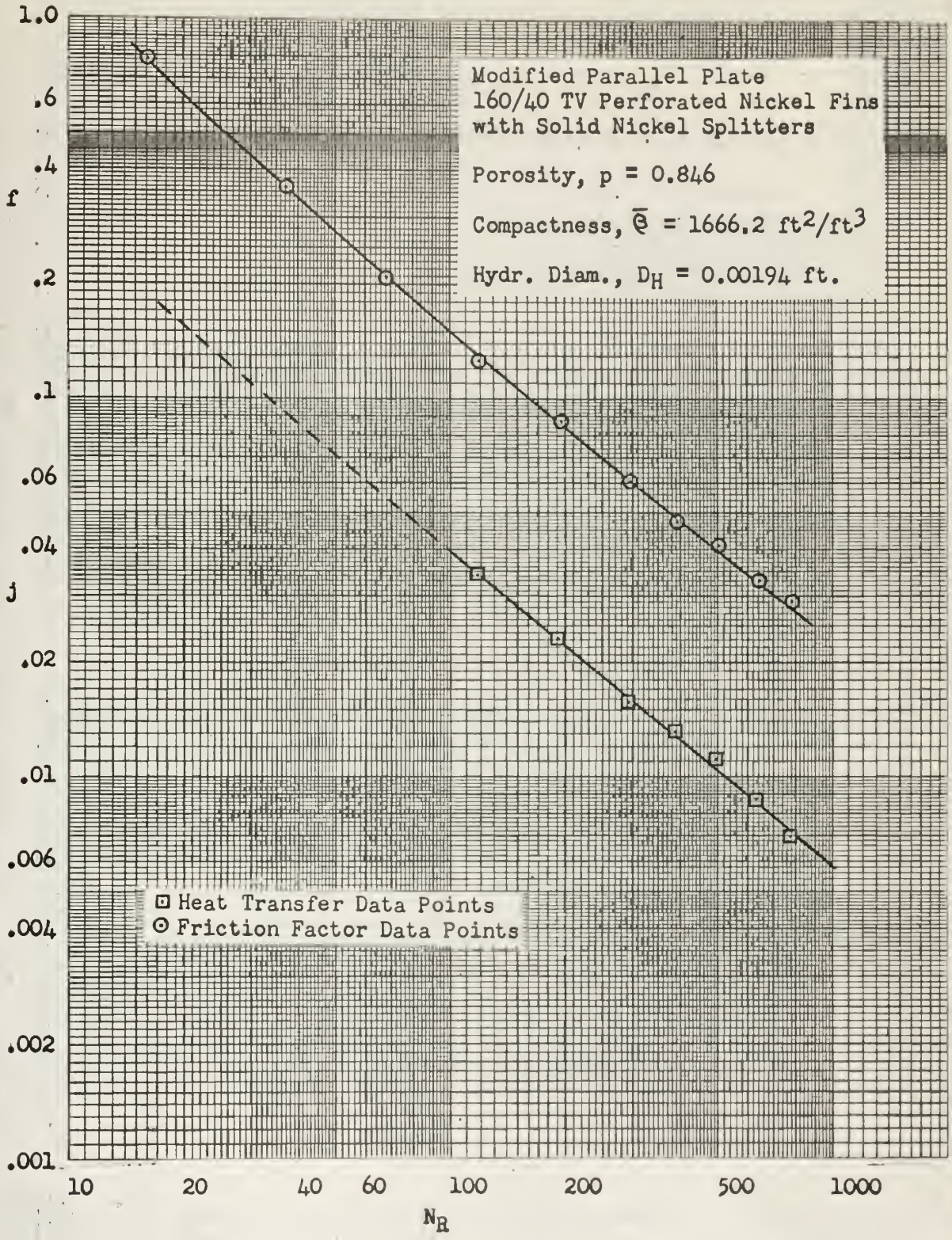

Figure 14. Surface Heat Transfer and Friction Data "Parallel Plate", 160/40 TV Fins with Solid Nickel Splitter Plates

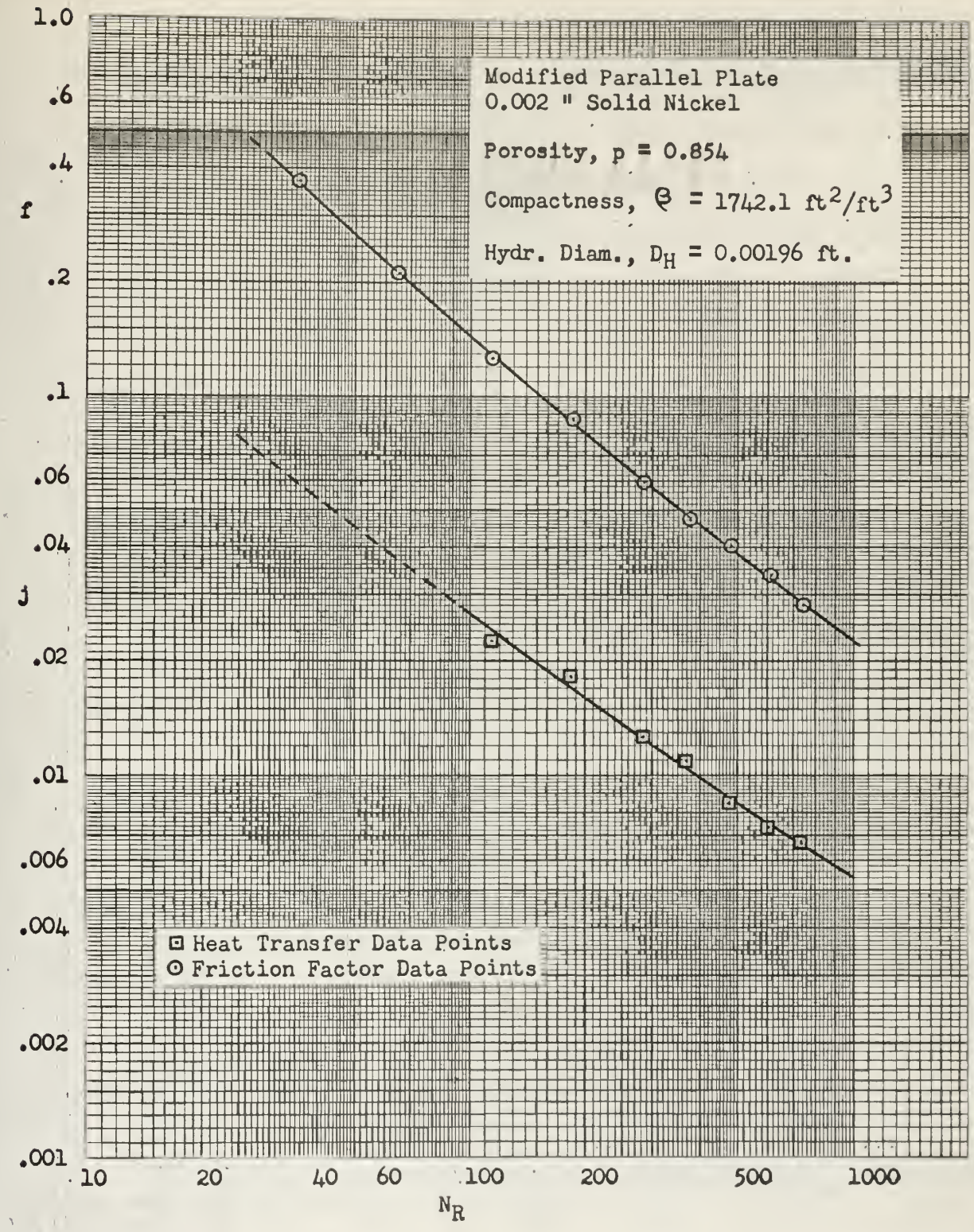

Figure 15. Surface Heat Transfer and Friction Data "Parallel Plate", 0.002" Solid Nickel

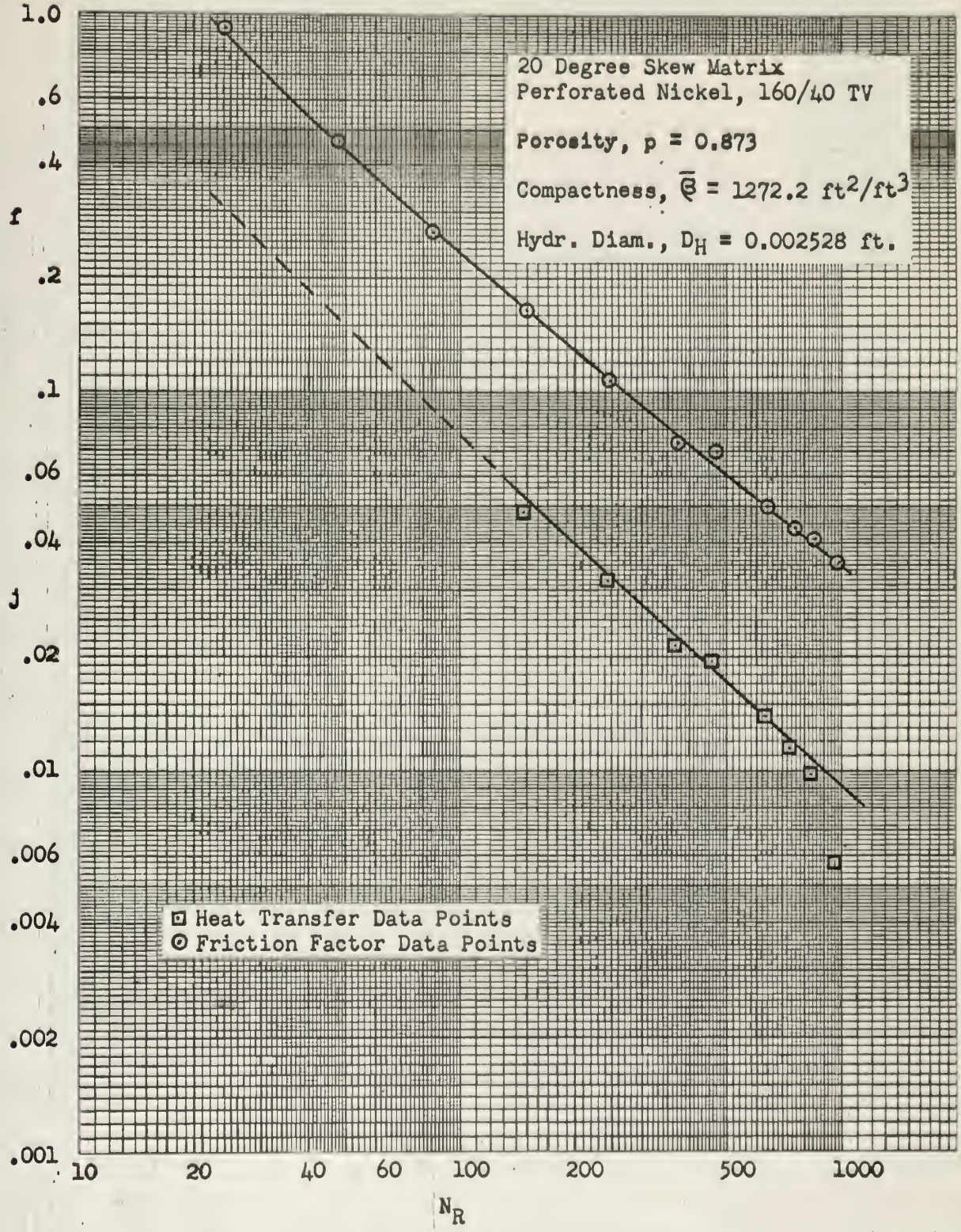

Figure 16. Surface Heat Transfer and Friction Data
20° Skew, 160/40 TV Perforated Nickel

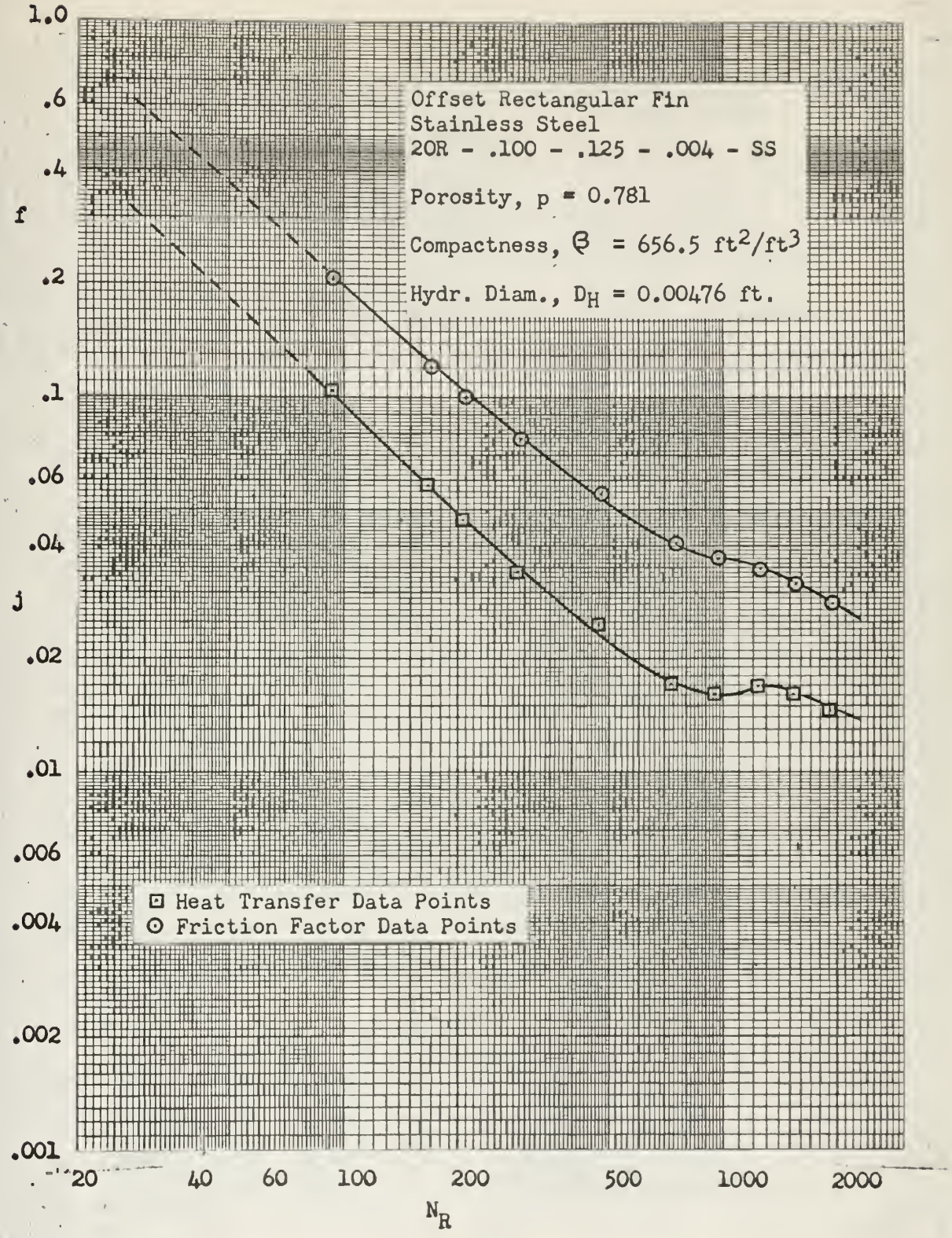

Figure 17. Surface Heat Transfer and Friction Data
Offset Rectangular Fin, 20R -.100 -.125 -.004 - SS

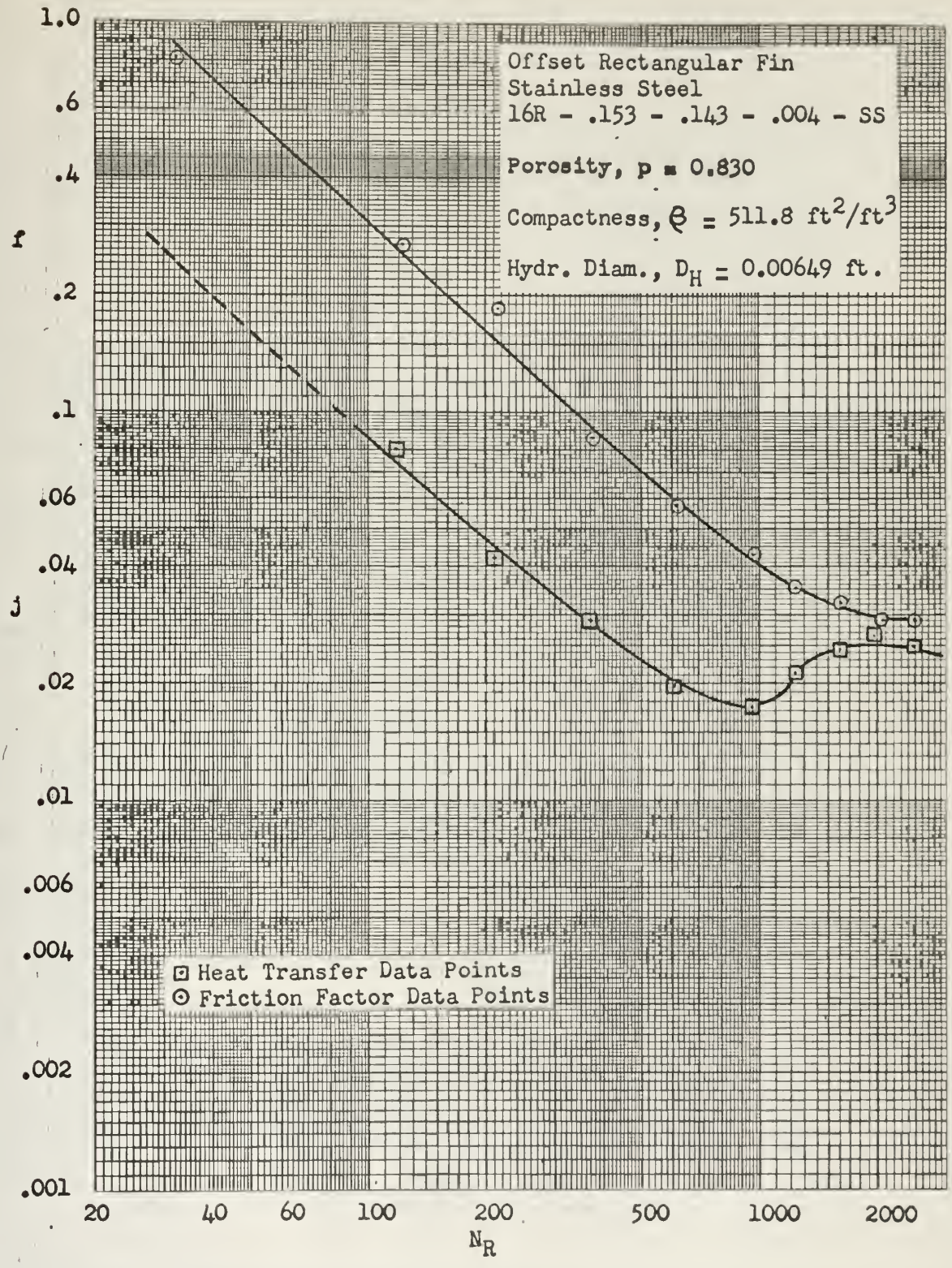

Figure 18. Surface Heat Transfer and Friction Data
Offset Rectangular Fin, 16R -.153 -.143 -.004 - SS

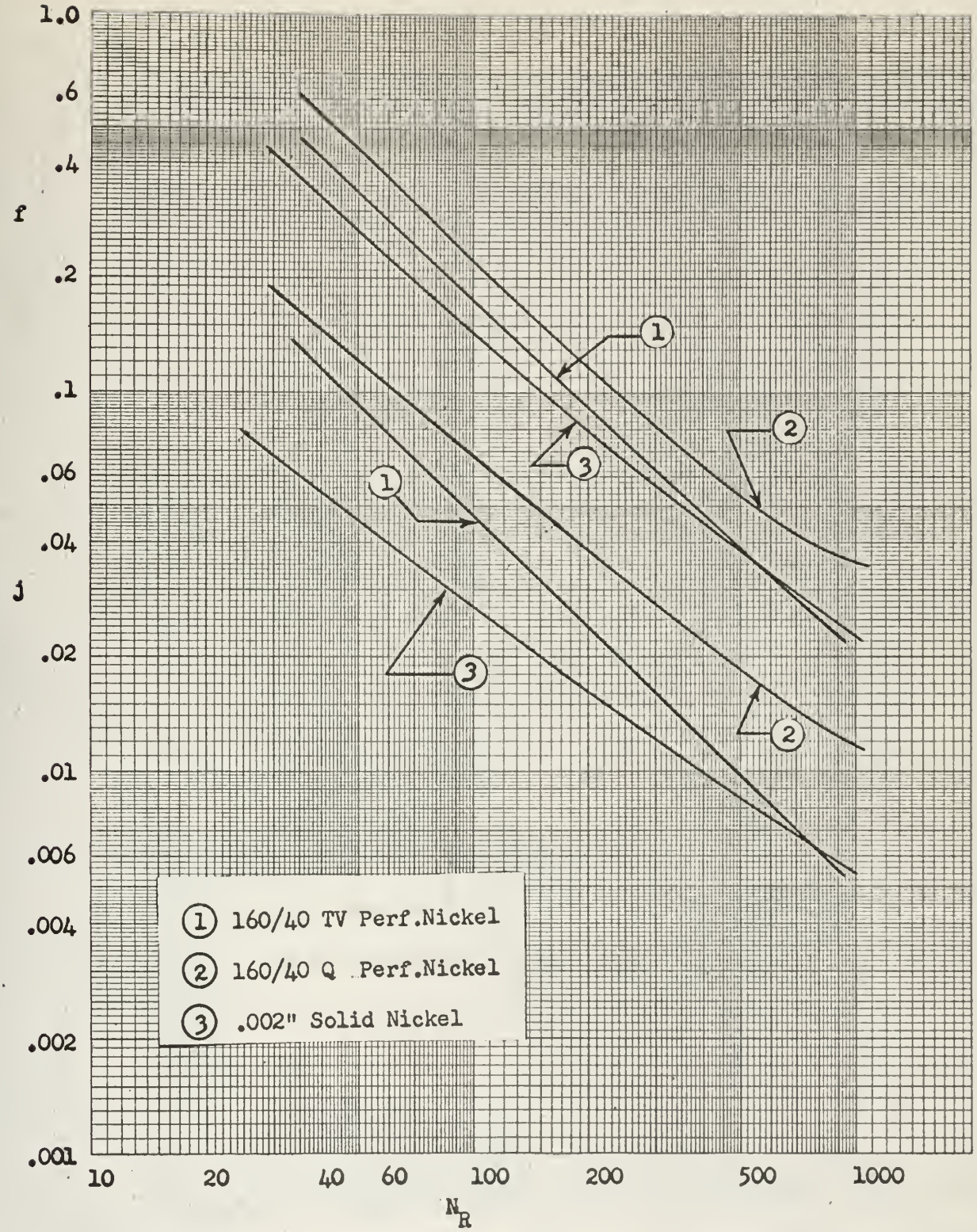

Figure 19. Comparison of Slotted Perforated vs. Solid Nickel "Parallel Plate" Matrices

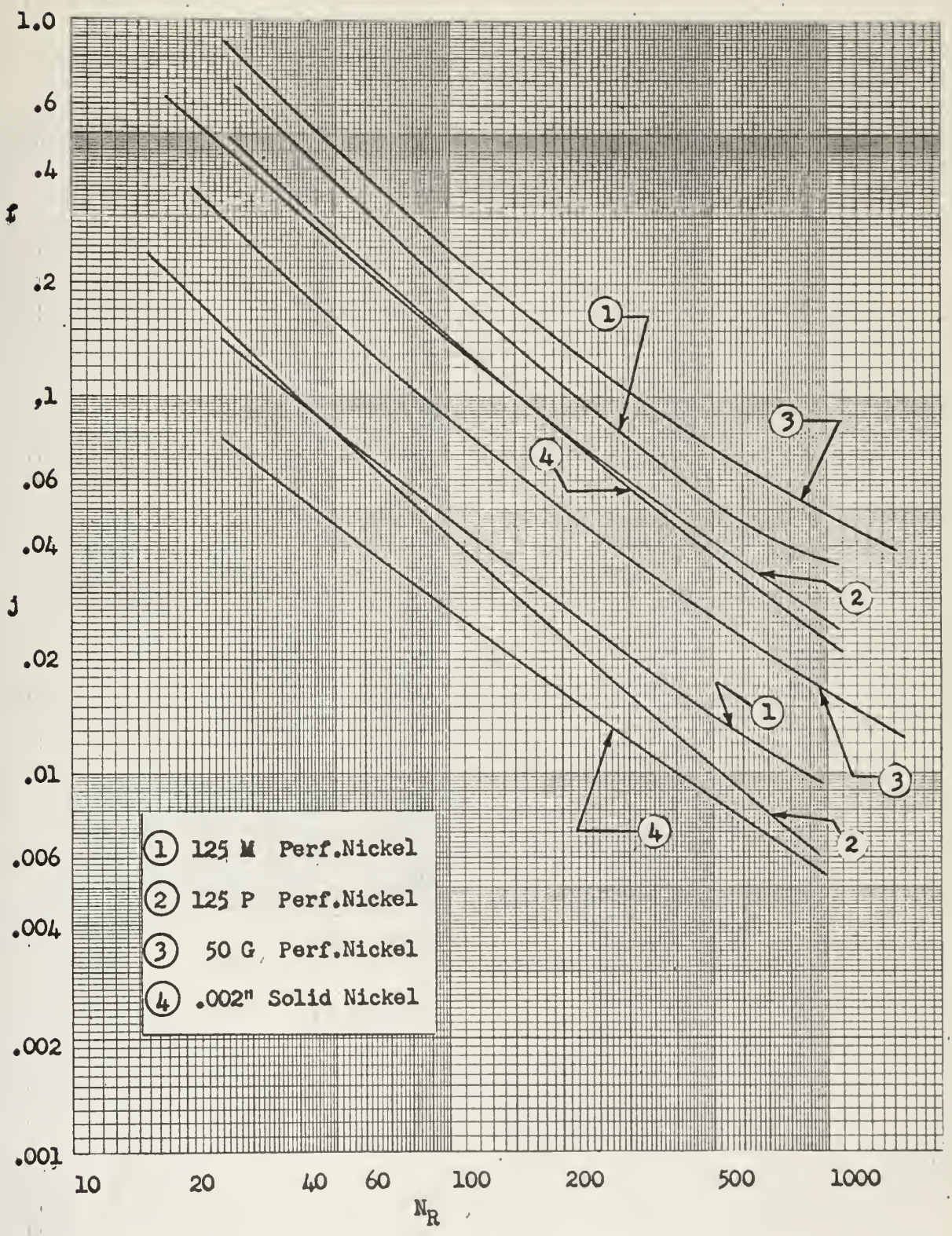

Figure 20. Comparison of Round Perforated vs. Solid Nickel "Parallel Plate" Matrices

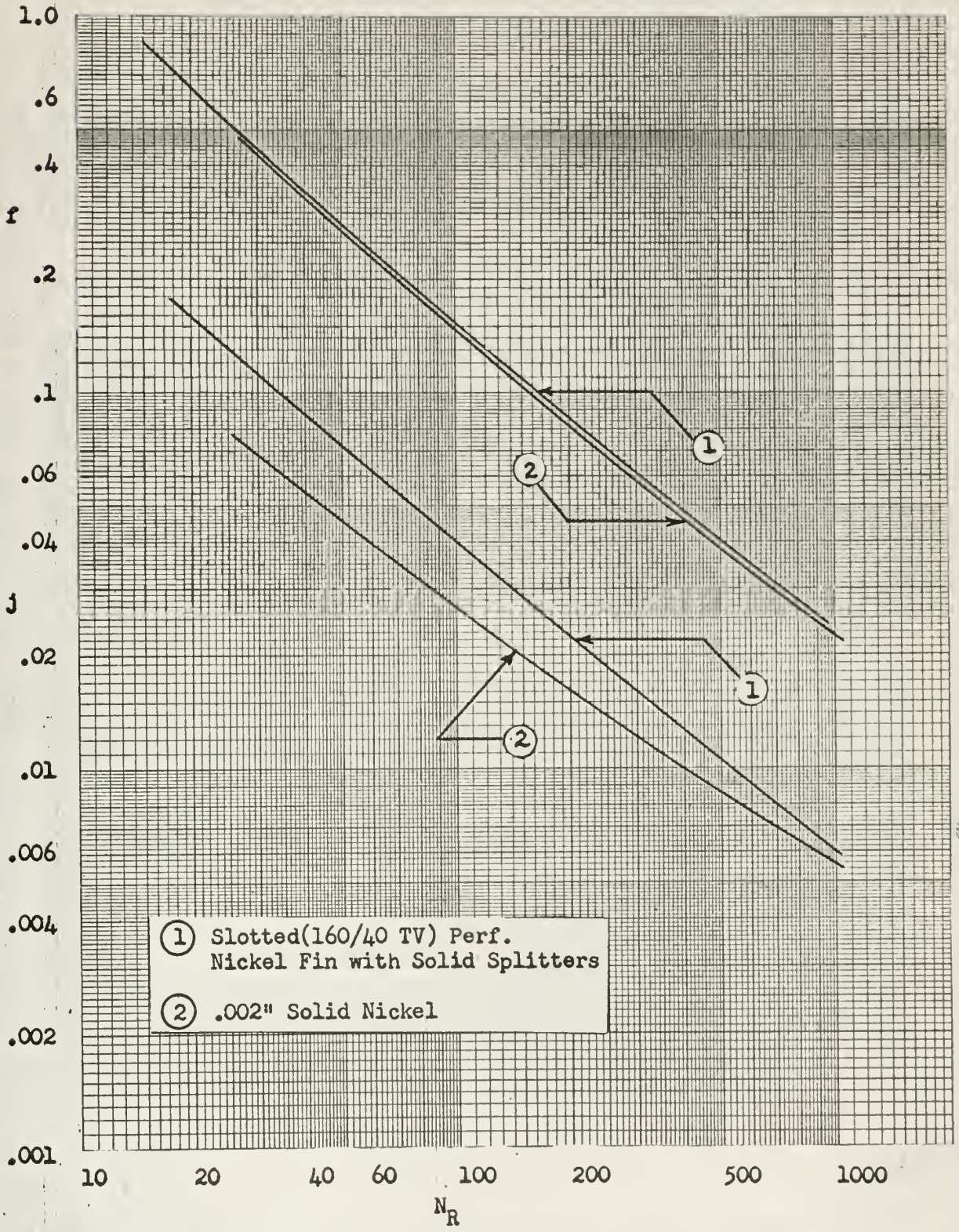

Figure 21. Comparison of Slotted Perforated Fin with Solid Nickel Splitters vs. Solid Nickel "Parallel Plate" Matrices

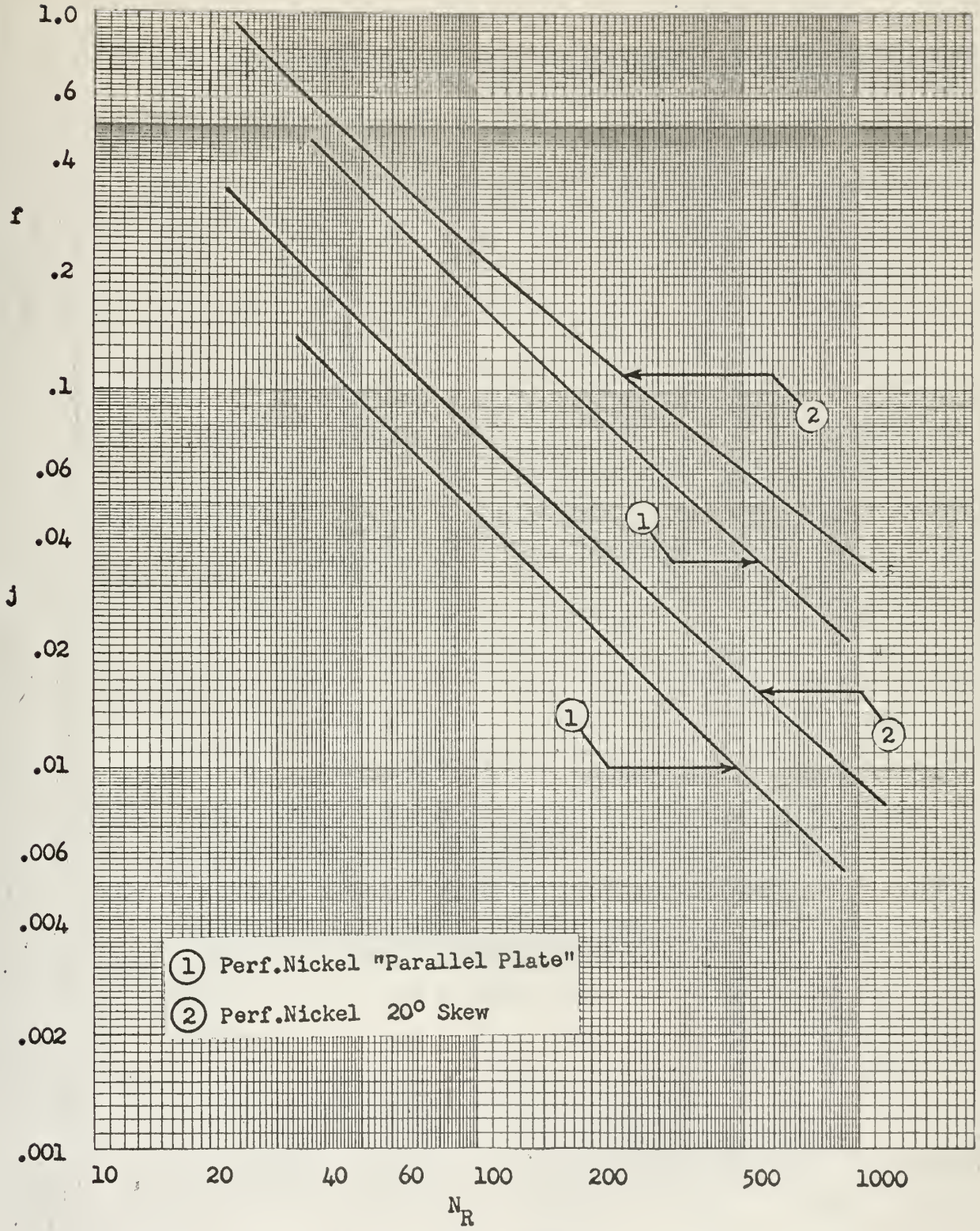

Figure 22. Comparison of Slotted Perforated Nickel "Parallel Plate" vs. Slotted Perforated Nickel 20° Skew Matrix

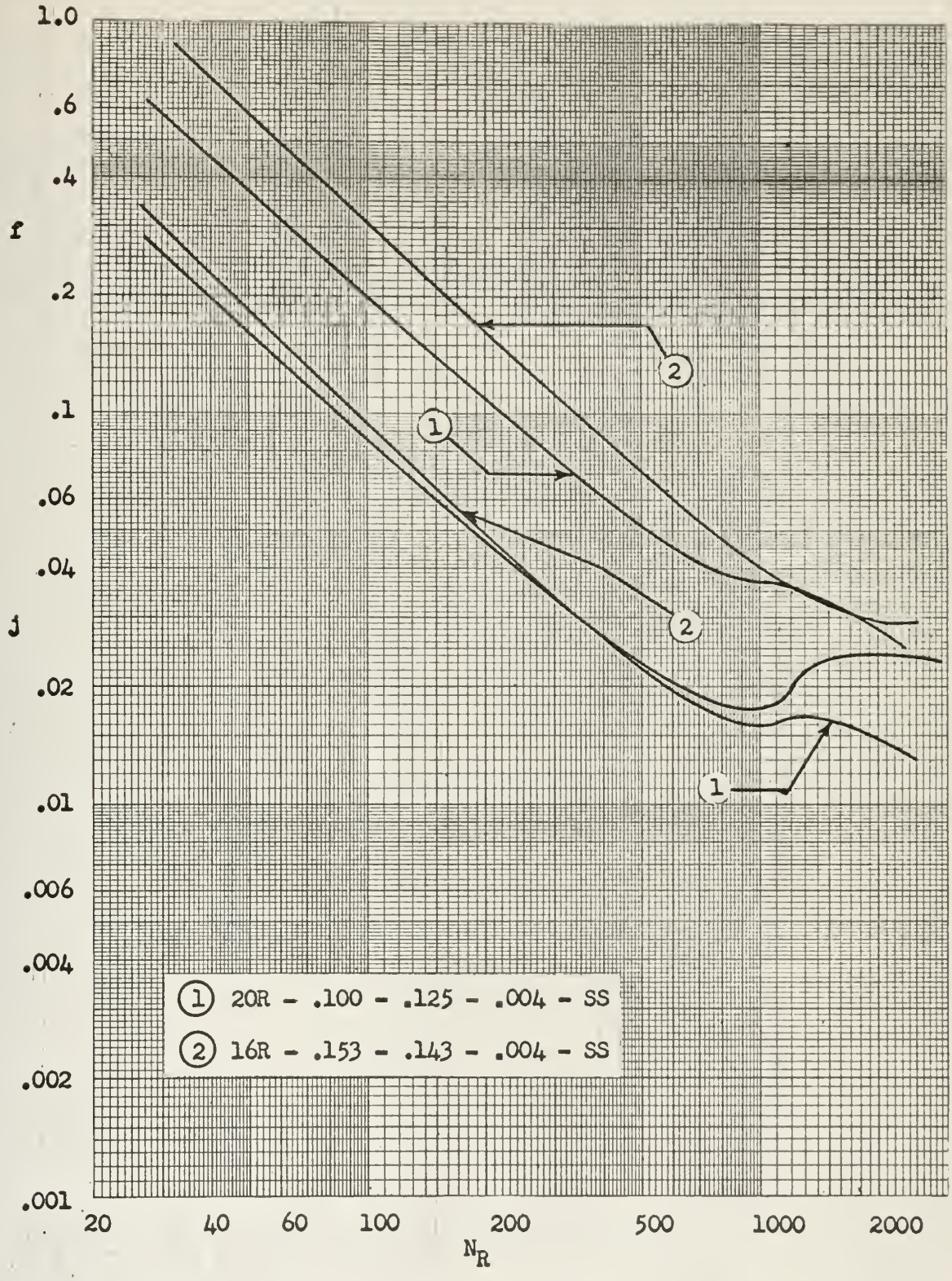

Figure 23. Comparison of Offset Rectangular Fin Matrices

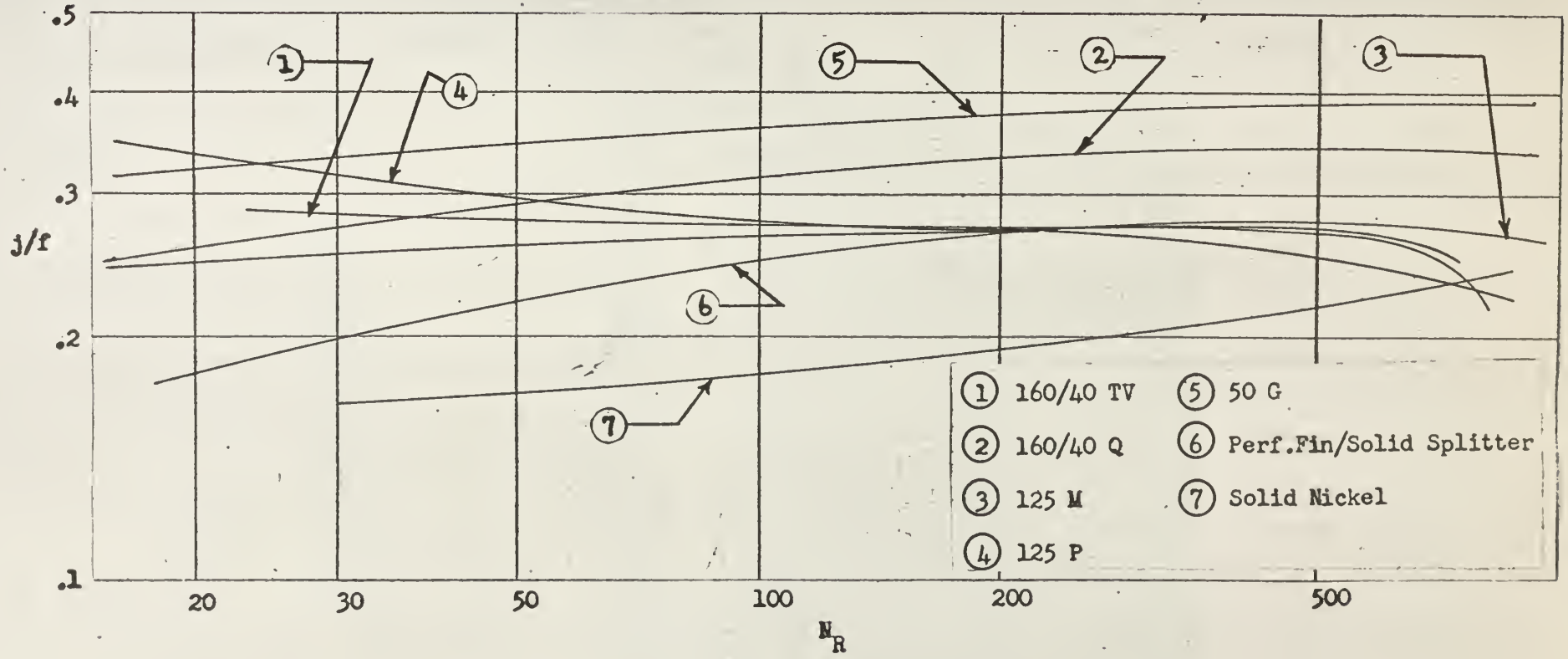

Figure 24. Flow Area Goodness Factors for the Nickel Surfaces

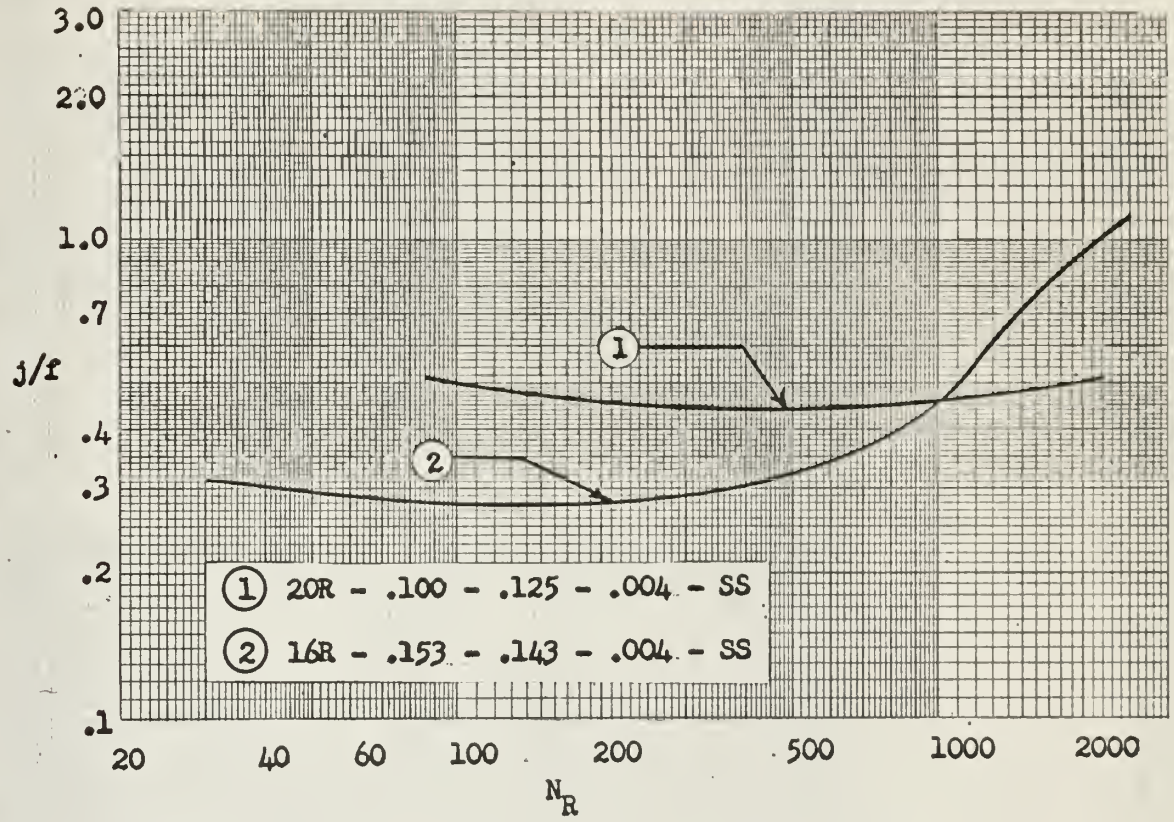

Figure 25. Flow Area Goodness Factors for the Offset Rectangular Fin Surfaces

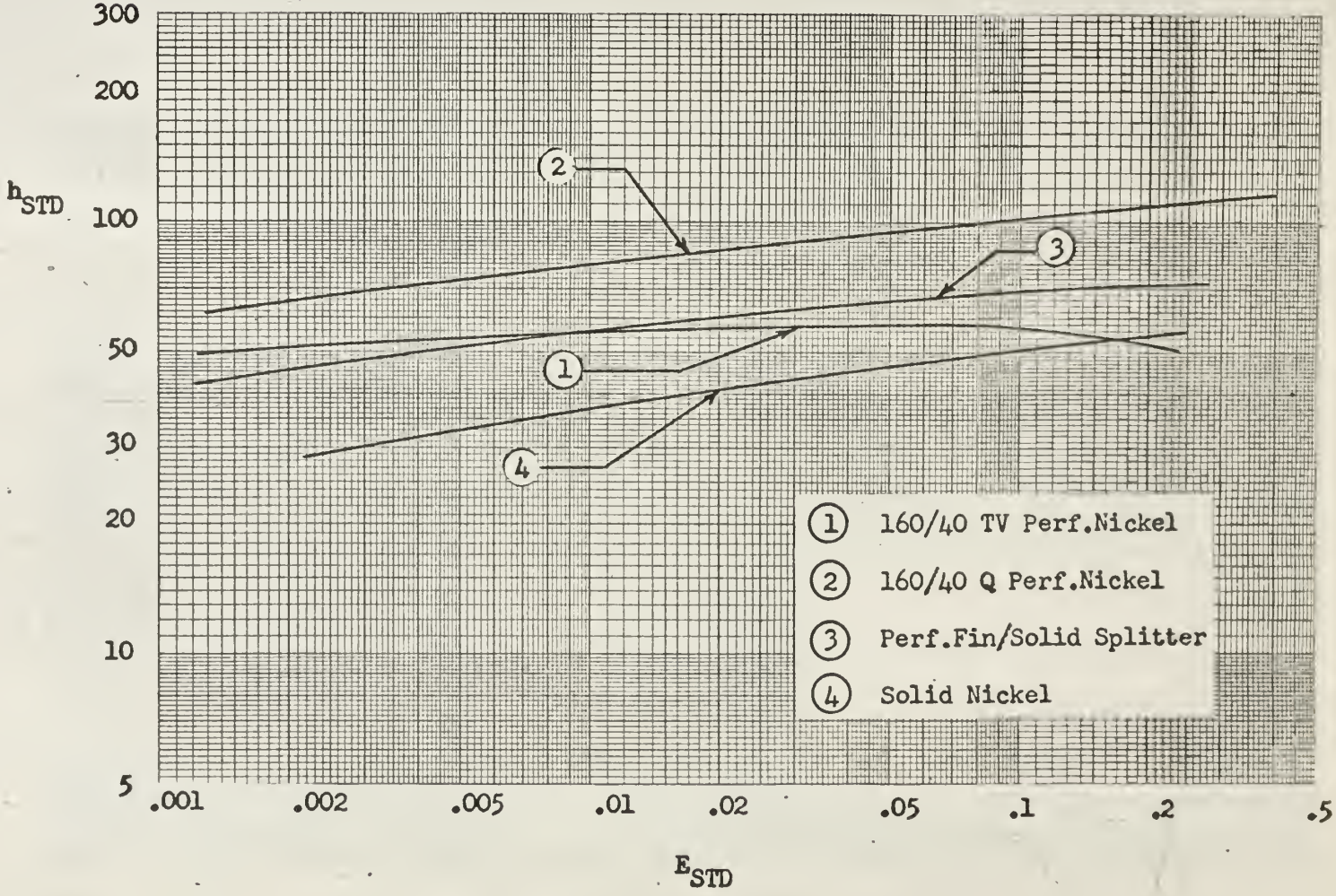

Figure 26. Heat Transfer Power vs. Flow Friction Power per Unit Area for the Slotted Perforated Nickel and Solid Nickel "Parallel Plate" Matrices

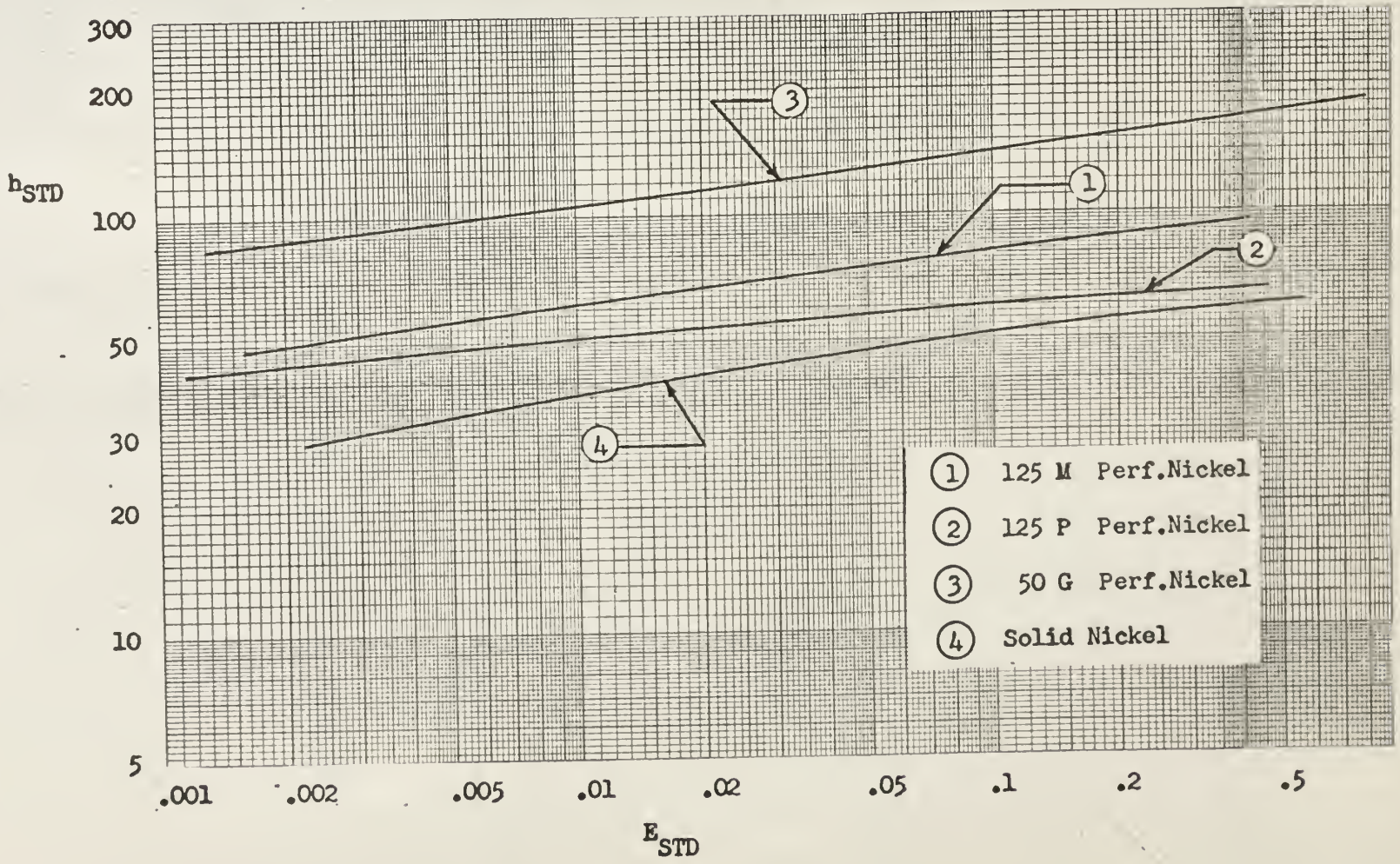

Figure 27. Heat Transfer Power vs. Flow Friction Power per Unit Area for the Round Perforated Nickel and Solid Nickel "Parallel Plate" Matrices

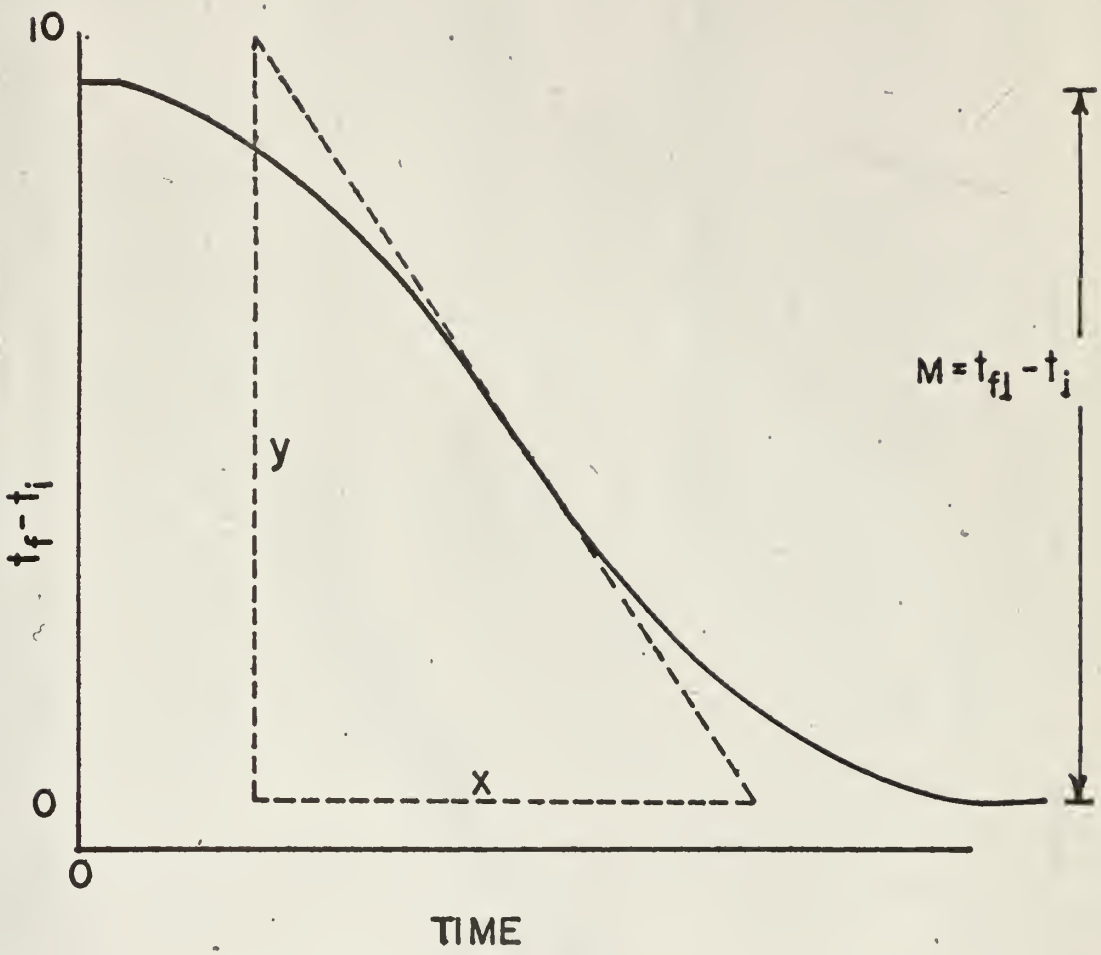

FIGURE 28. GENERALIZED COOLING CURVE

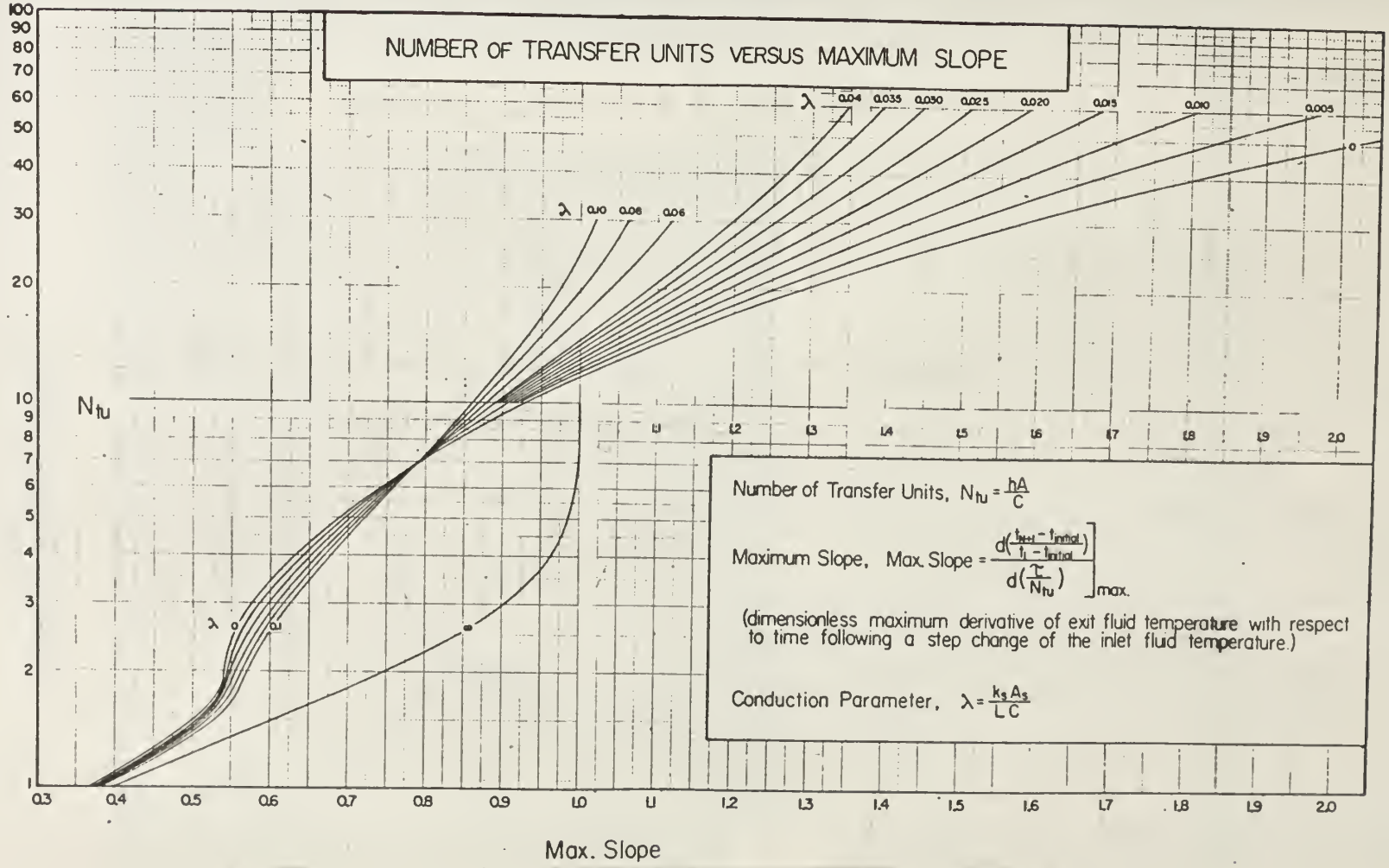

Figure 29. Number of Transfer Units vs. Maximum Slope

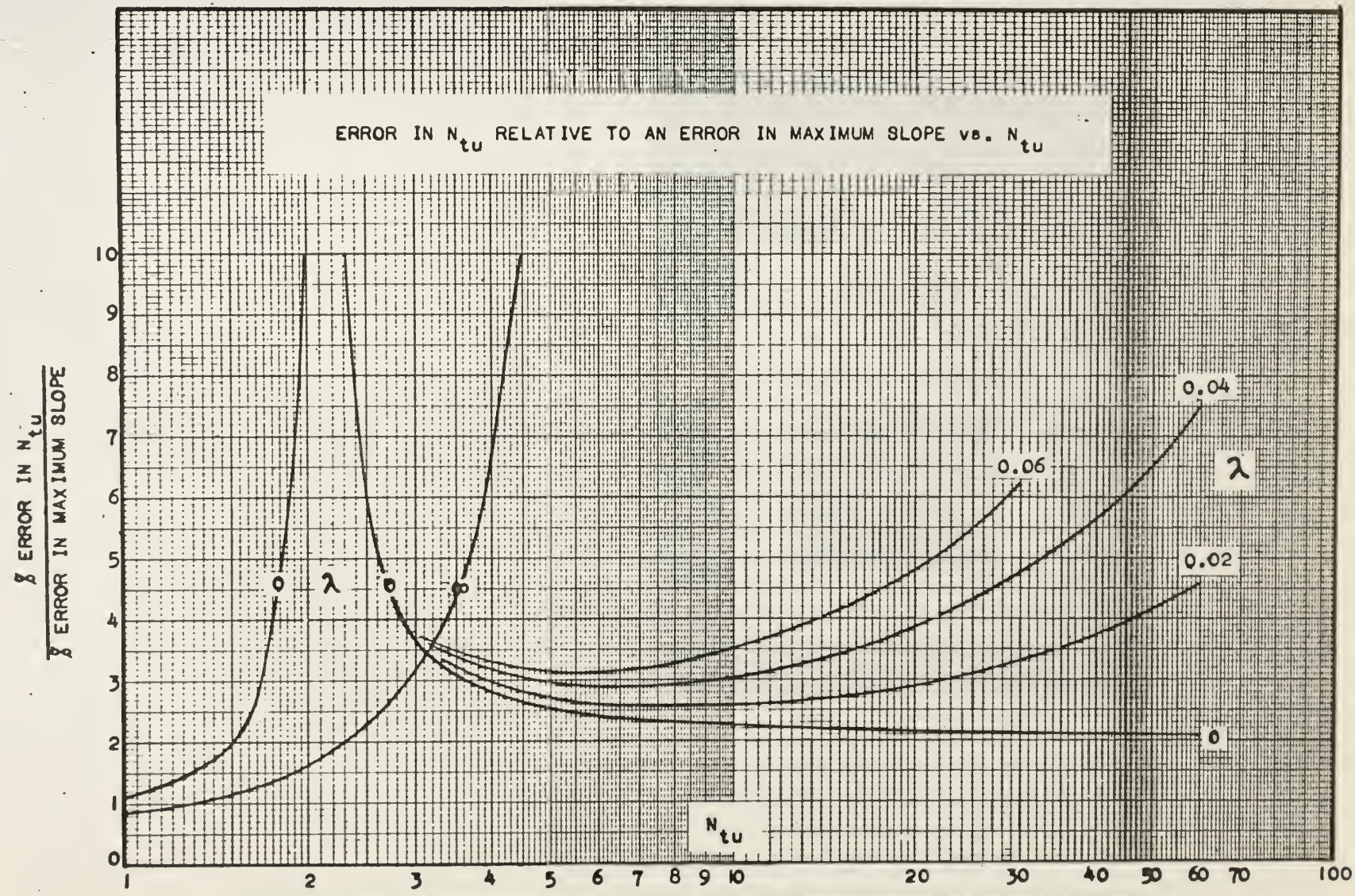

Figure 30. Error in N_{Tu} Relative to an Error in Maximum Slope vs. N_{Tu}

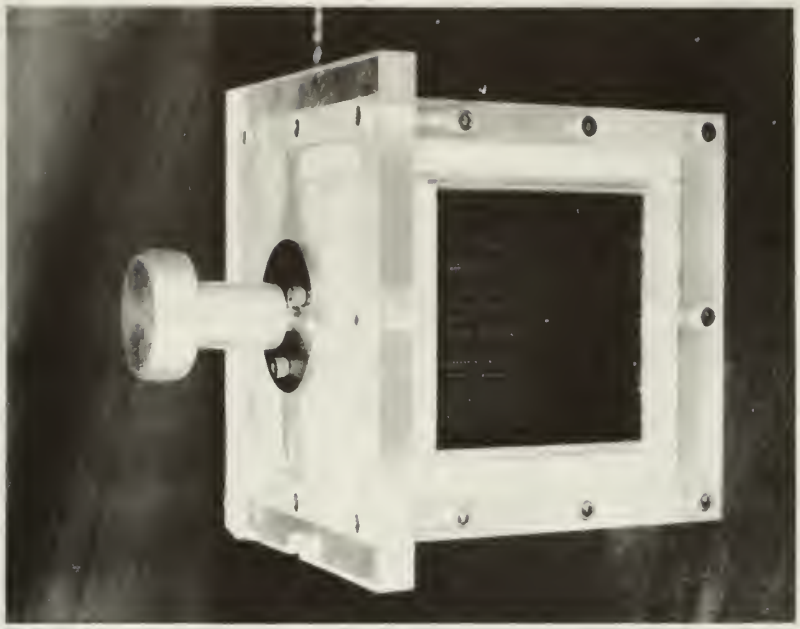

Figure 31. Matrix Holder
(Upstream View)

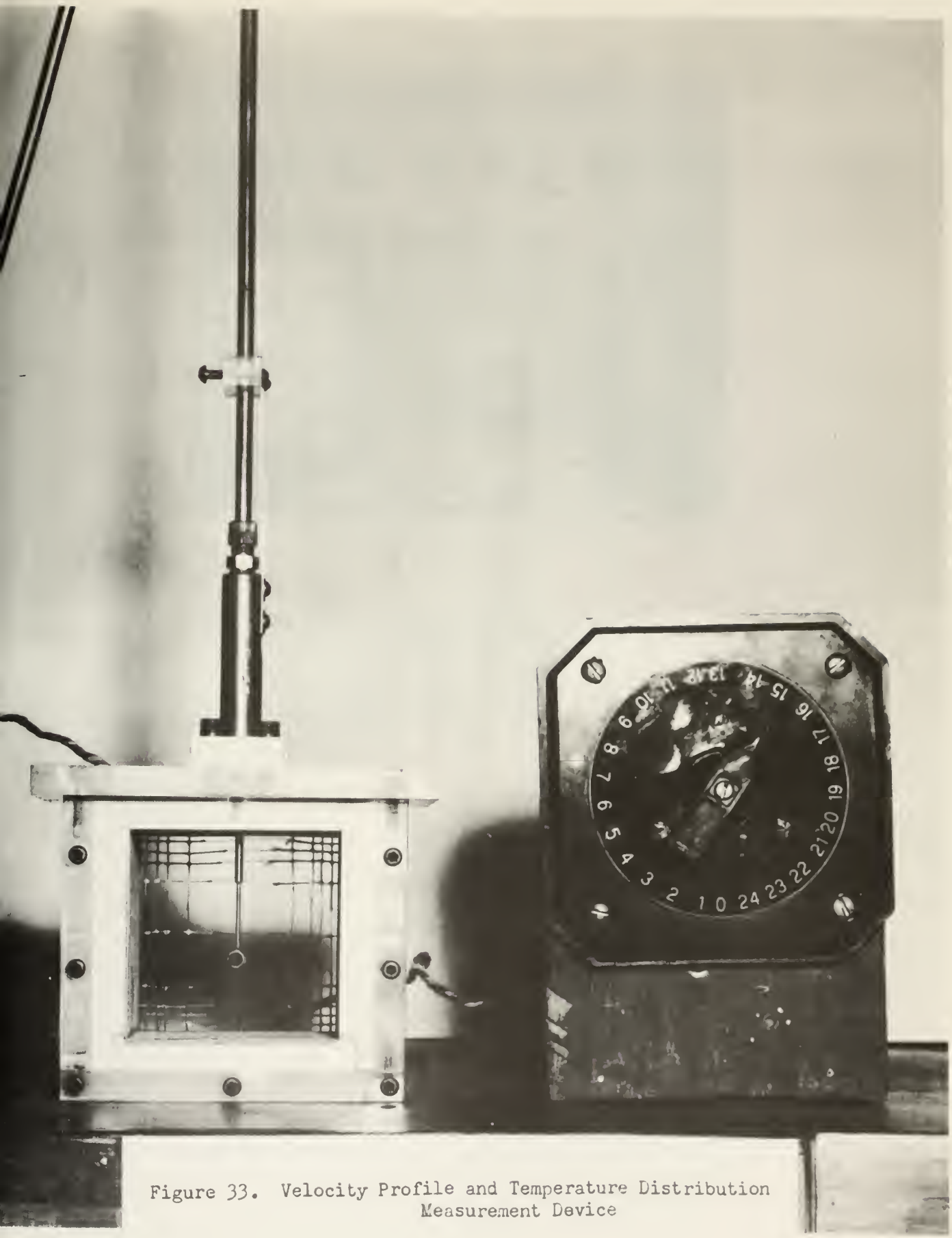

Figure 33. Velocity Profile and Temperature Distribution Measurement Device

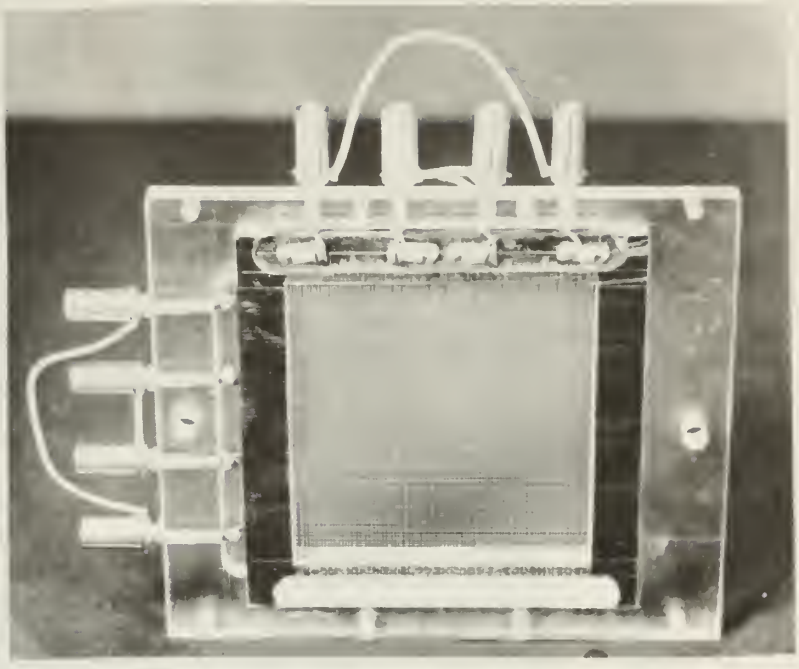

Figure 34. Nichrome Wire Heater
(Upstream View)

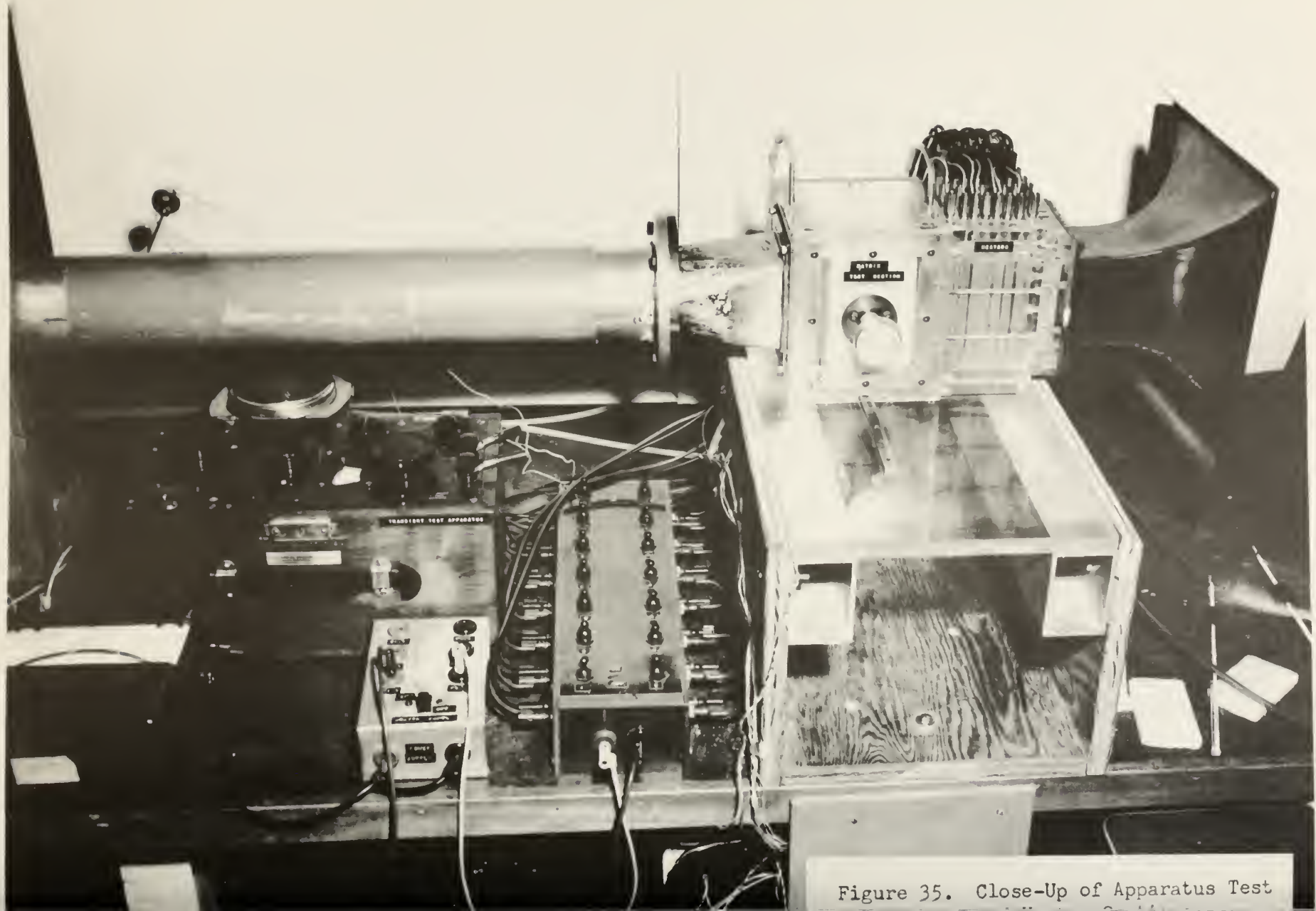

Figure 35. Close-Up of Apparatus Test

Figure 36. Recorder Trace of Actual Cooling Curve for the 160/40 Q Perforated Nickel, "Parallel Plate" Matrix

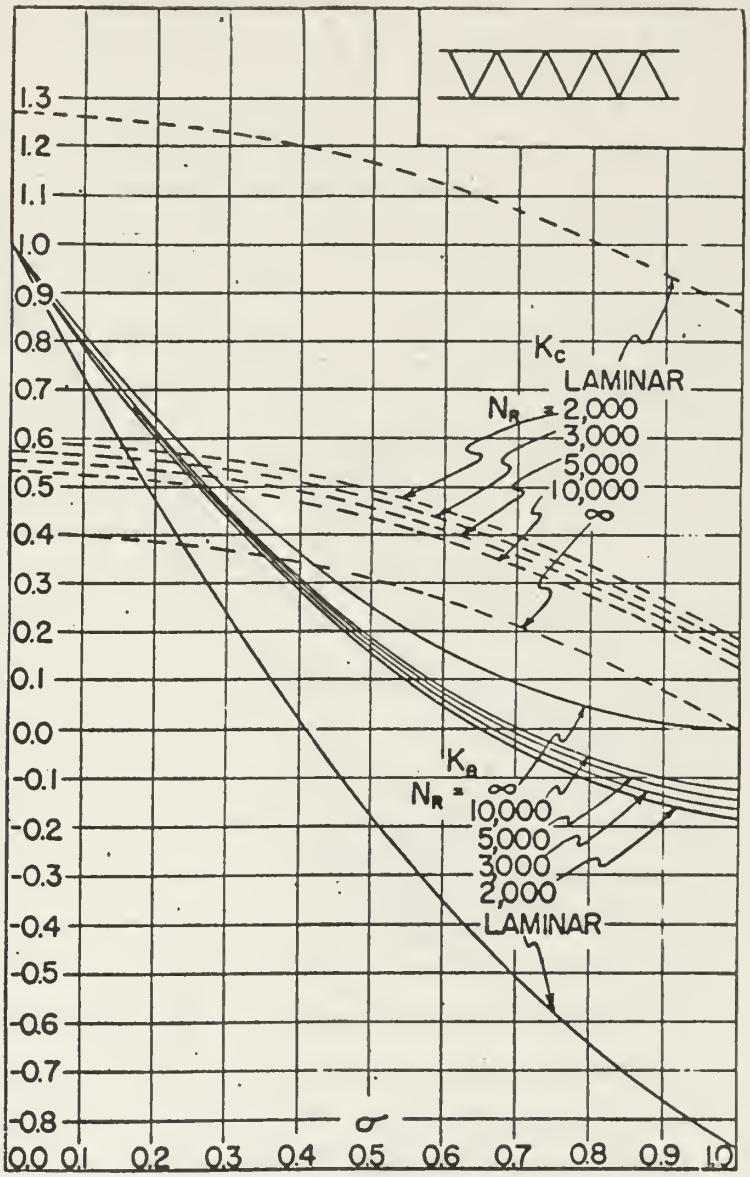

Figure 37. Entrance and Exit Pressure Loss Coefficients for Triangular Cross Section Matrix with Abrupt-Contraction Entrance and Abrupt-Expansion Exit

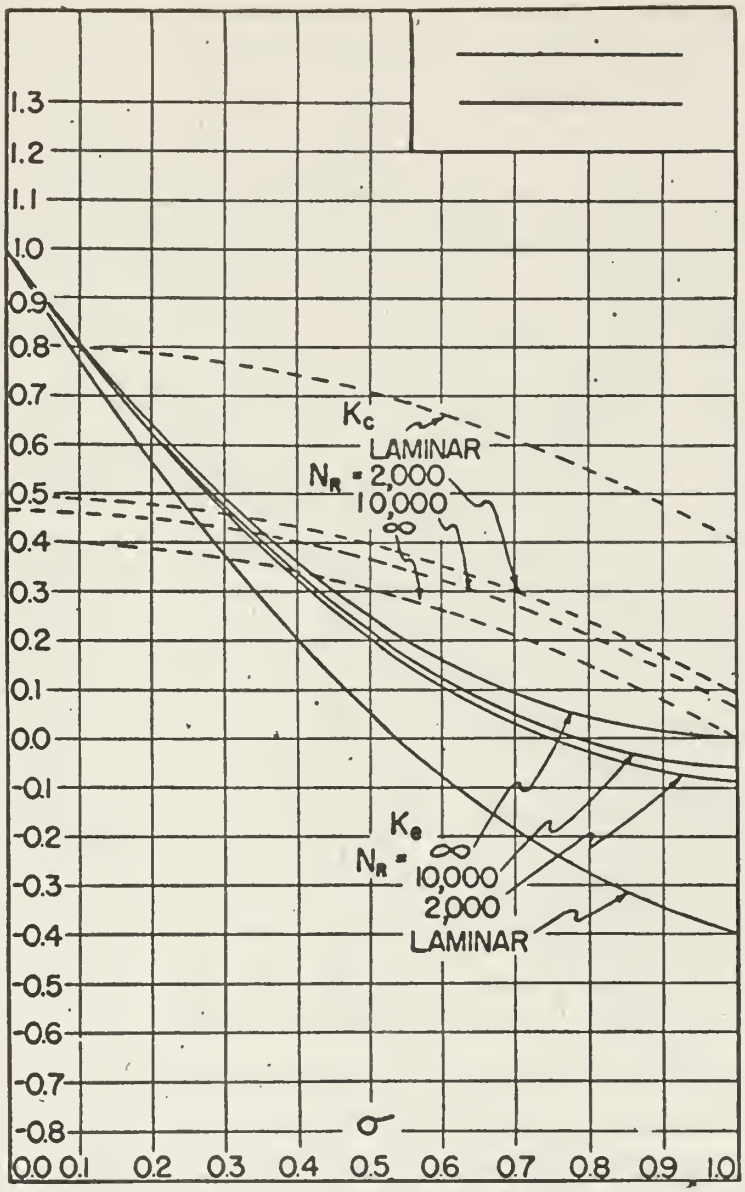

Figure 38. Entrance and Exit Pressure Loss Coefficients for Parallel Plate Cross Section Matrix with Abrupt-Contraction Entrance and Abrupt-Expansion Exit

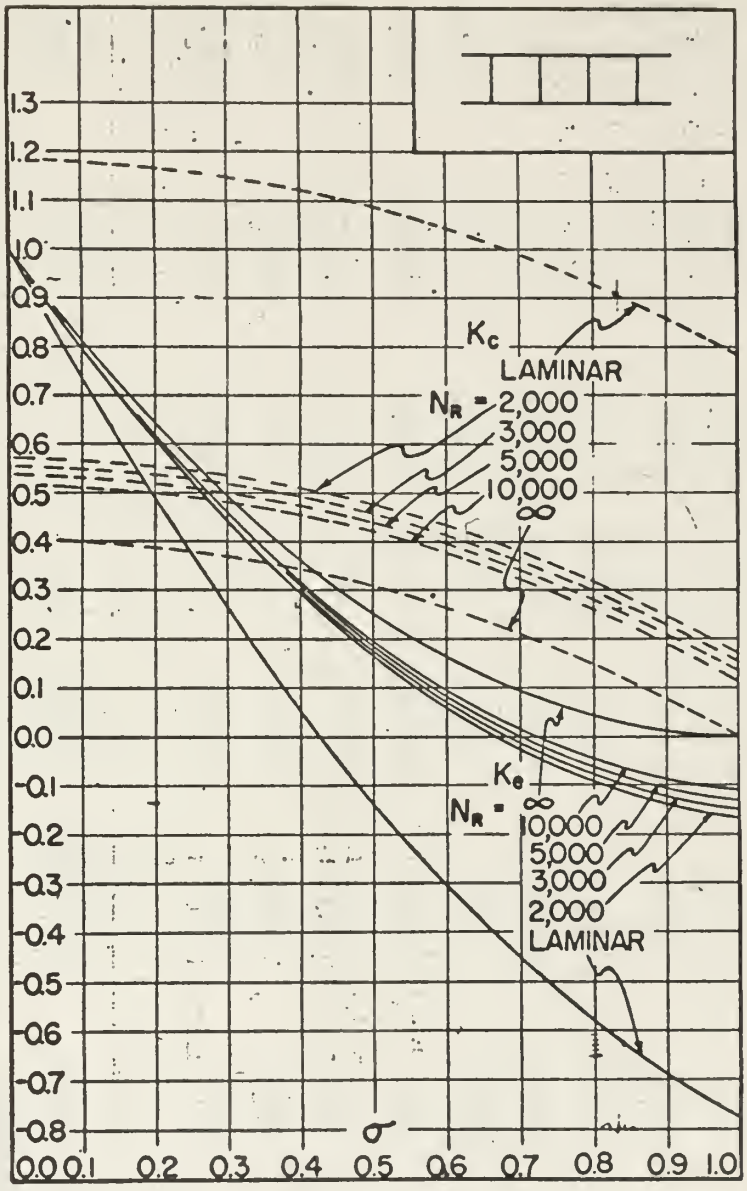

Figure 39. Entrance and Exit Pressure Loss Coefficients for Multiple - Rectangular Cross Section Matrix with Abrupt-Contraction Entrance and Abrupt-Expansion Exit

TABLE I SUMMARY OF HEAT TRANSFER AND FRICTION RESULTS:
160/40 TV PERFORATED NICKEL, MODIFIED PARALLEL PLATE

HEAT TRANSFER RESULTS							ISOTHERMAL FRICTION RESULTS	
RUN NO.	REYNOLD'S NUMBER N_R	$N_{St}N_{Pr}^{2/3}$ j	CONDUCTION PARAMETER λ_K	MAXIMUM SLOPE	N_{Tu}	$j' = j \times s$	REYNOLD'S NUMBER N_R	FRICTION FACTOR f
1	825.76	.00510	.00134	.54186	2.04	.00470	837.82	.02381
2	655.96	.00788	.00169	.58496	3.15	.00726	665.67	.02971
3	526.80	.01075	.00210	.64907	4.30	.00991	534.61	.03631
4	404.33	.01260	.00273	.69503	5.04	.01161	410.22	.04337
5	308.17	.01633	.00359	.77129	6.53	.01505	312.66	.05900
6	204.31	.02375	.00543	.89956	9.50	.02189	207.29	.08664
7	122.62	.03625	.00902	1.07060	14.50	.03341	124.41	.13255
8	68.98	.0675*	.01604	1.1833	27.0*	.06218*	69.99	.23685
9	38.79	.120*	.02851	1.1712	48.0*	.1105*	39.35	.42260

* From Extrapolated Values of j versus N_R Curve

TABLE II SUMMARY OF HEAT TRANSFER AND FRICTION RESULTS:
160/40 Q PERFORATED NICKEL, MODIFIED PARALLEL PLATE

HEAT TRANSFER RESULTS							ISOTHERMAL FRICTION RESULTS	
RUN NO.	REYNOLD'S NUMBER N_R	$N_{St}N_{Pr}^{2/3}$ j	CONDUCTION PARAMETER λ_K	MAXIMUM SLOPE	N_{Tu}	$j' = j \times s$	REYNOLD'S NUMBER N_R	FRICTION FACTOR f
1	911.23	.01217	.00094	.63507	4.05	.00980	924.54	.03686
2	744.10	.01427	.00116	.67558	4.75	.01150	754.96	.04080
3	597.40	.01478	.00144	.68555	4.92	.01191	606.12	.04931
4	458.68	.01953	.00188	.76765	6.50	.01574	465.38	.05785
5	351.29	.02389	.00245	.83415	7.95	.01925	356.42	.06954
6	230.65	.03531	.00373	.99130	11.75	.02845	234.01	.10424
7	138.84	.05077	.00618	1.15746	16.90	.04091	140.86	.15614
8	79.37	.07513	.01084	1.32066	25.00	.06054	80.53	.27078
9	43.37	.1370*	.01981	1.27471	45.6*	.1104*	44.01	.49671
10	18.41	.275*	.04667	1.05193	91.51*	.2216*	18.67	1.07260

* From Extrapolated Values of j versus N_R Curve

TABLE III SUMMARY OF HEAT TRANSFER AND FRICTION RESULTS:
125 M PERFORATED NICKEL, MODIFIED PARALLEL PLATE

HEAT TRANSFER RESULTS							ISOTHERMAL FRICTION RESULTS	
RUN NO.	REYNOLD'S NUMBER N_R	$N_{St}N_{Pr}^{2/3}$ j	CONDUCTION PARAMETER λ_K	MAXIMUM SLOPE	N_{Tu}	$j' = j \times s$	REYNOLD'S NUMBER N_R	FRICTION FACTOR f
1	914.40	.00987	.00351	.59243	3.28	.00795	927.78	.03720
2	747.25	.01044	.00429	.60382	3.47	.00841	758.19	.04033
3	595.23	.01264	.00539	.64508	4.20	.01018	603.95	.04549
4	460.47	.01496	.00697	.68852	4.97	.01205	467.21	.05310
5	352.70	.01878	.00910	.75470	6.24	.01512	357.87	.06680
6	229.81	.02661	.01395	.87198	8.84	.02143	233.17	.10051
7	140.94	.03732	.02279	.97943	12.40	.03006	143.00	.14527
8	80.37	.05222	.03996	1.04961	17.35	.04205	81.55	.23256
9	43.68	.091*	.07341	1.01867	30.23*	.0733*	44.32	.41901
10	18.87	.175*	.17002	.87812	58.14*	.1409*	19.15	.94158

* From Extrapolated Values of j versus N_R Curve

TABLE IV SUMMARY OF HEAT TRANSFER AND FRICTION RESULTS:
125 P PERFORATED NICKEL, MODIFIED PARALLEL PLATE

HEAT TRANSFER RESULTS							ISOTHERMAL FRICTION RESULTS	
RUN NO.	REYNOLD'S NUMBER N_R	$N_{St}N_{Pr}^{2/3}$ j	CONDUCTION PARAMETER λ_K	MAXIMUM SLOPE	N_{Tu}	$j' = j \times s$	REYNOLD'S NUMBER N_R	FRICTION FACTOR f
1	842.66	.00660	.00514	.55199	2.47	.00579	854.98	.02993
2	681.03	.00833	.00634	.58445	3.12	.00730	690.95	.03538
3	539.11	.01009	.00798	.62151	3.78	.00885	546.94	.04075
4	419.77	.01135	.01026	.65278	4.25	.00995	425.88	.04503
5	320.14	.01399	.01345	.70628	5.24	.01227	324.79	.05326
6	209.10	.02419	.02059	.87353	9.06	.02121	212.14	.07662
7	127.02	.03124	.03390	.94586	11.70	.02739	128.87	.11763
8	73.68	.0500*	.05873	.90270	18.73*	.04385*	74.76	.18271
9	40.24	.0990*	.10737	.83740	37.08*	.08681*	40.83	.32765
10	17.33	.2200*	.24936	.70783	82.40*	.19292*	17.58	.64335

* From Extrapolated Values of j versus N_R Curve

TABLE V SUMMARY OF HEAT TRANSFER AND FRICTION RESULTS:
50 G PERFORATED NICKEL, MODIFIED PARALLEL PLATE

HEAT TRANSFER RESULTS							ISOTHERMAL FRICTION RESULTS	
RUN NO.	REYNOLD'S NUMBER N_R	$N_{St}N_{Pr}^{2/3}$ j	CONDUCTION PARAMETER λ_K	MAXIMUM SLOPE	N_{Tu}	$j' = j \times s$	REYNOLD'S NUMBER N_R	FRICTION FACTOR f
1	1327.11	.01286	.00196	.57371	2.95	.00714	1346.50	.04157
2	1077.78	.01613	.00241	.61596	3.70	.00895	1093.53	.04656
3	860.44	.02049	.00302	.67415	4.70	.01137	873.01	.05366
4	660.25	.02167	.00393	.68872	4.97	.01203	669.90	.05654
5	505.10	.02315	.00511	.70620	5.31	.01285	512.43	.06639
6	332.27	.03575	.00777	.84294	8.20	.01984	337.09	.09211
7	202.59	.05275	.01274	.98835	12.10	.02927	205.54	.12593
8	116.91	.06932	.02207	1.06986	15.9	.03847	118.61	.21087
9	63.60	.1250*	.04050	1.04240	28.7*	.0694*	64.52	.37091
10	27.24	.2740*	.09455	.90406	62.8*	.1521*	27.63	.80961

* From Extrapolated Values of j versus N_R Curve

TABLE VI SUMMARY OF HEAT TRANSFER AND FRICTION RESULTS:
160/40TV PERFORATED NICKEL FIN, SOLID SPLITTERS "PARALLEL PLATE"

HEAT TRANSFER RESULTS:						ISOTHERMAL FRICTION RESULTS:	
RUN NO.	REYNOLD'S NUMBER N_R	$N_{St}N_{Pr}^{2/3}$ j	CONDUCTION PARAMETER λ_K	MAXIMUM SLOPE	N_{Tu}	REYNOLD'S NUMBER N_R	FRICTION FACTOR f
1	765.94	.00695	.00451	.56963	2.87	777.13	.02908
2	629.02	.00874	.00549	.61108	3.61	638.20	.03313
3	495.98	.01125	.00696	.67109	4.65	503.22	.04111
4	385.97	.01307	.00895	.71202	5.40	391.60	.04730
5	291.98	.01561	.01179	.76775	6.45	296.23	.06052
6	192.67	.02311	.01787	.88931	9.55	195.47	.08737
7	118.00	.03412	.02920	1.00846	14.1	119.47	.12713
8	67.44	.055*	.05110	.93807	22.6*	68.42	.20821
9	36.73	.0923*	.09375	.85417	37.98*	37.26	.35804
10	15.91	.190*	.21648	.76567	78.2*	16.14	.78018

* From Extrapolated Values of j versus N_R Curve

TABLE VII SUMMARY OF HEAT TRANSFER AND FRICTION RESULTS:
SOLID NICKEL, "PARALLEL PLATE"

HEAT TRANSFER RESULTS:						ISOTHERMAL FRICTION RESULTS:	
RUN NO.	REYNOLD'S NUMBER N_R	$N_{St}N_{Pr}^{2/3}$ j	CONDUCTION PARAMETER λ	MAXIMUM SLOPE	N_{Tu}	REYNOLD'S NUMBER N_R	FRICTION FACTOR f
1	729.78	.00667	.00995	.57372	2.85	740.42	.02836
2	600.20	.00737	.01209	.58983	3.15	608.95	.03389
3	474.84	.00842	.01527	.61607	3.60	481.75	.04027
4	368.55	.01093	.01969	.67998	4.67	373.92	.04731
5	282.69	.01278	.02567	.72287	5.46	286.81	.05896
6	184.45	.01825	.03934	.82225	7.80	187.14	.08669
7	113.77	.02258	.06376	.86518	9.65	115.43	.12779
8	64.14	.0375*	.11308	.81509	16.02*	65.08	.21281
9	35.21	.059*	.20603	.77453	25.2*	35.72	.37241

* From Extrapolated Values of j versus N_R Curve

TABLE VIII SUMMARY OF HEAT TRANSFER AND FRICTION RESULTS:
160/40TV PERFORATED NICKEL, 20° SKEW

HEAT TRANSFER RESULTS:							ISOTHERMAL FRICTION RESULTS:	
RUN NO.	REYNOLD'S NUMBER N_R	$N_{St}N_{Pr}^{2/3}$ j	CONDUCTION PARAMETER λ_K	MAXIMUM SLOPE	N_{Tu}	$j' = j \times s$	REYNOLD'S NUMBER N_R	FRICTION FACTOR f
1	961.20	.00563	.00114	.53466	1.70	.00189	975.26	.03544
2	830.66	.00976	.00132	.57513	2.95	.00327	842.79	.04105
3	735.32	.01165	.00149	.60684	3.52	.00390	746.00	.04399
4	625.93	.01400	.00176	.64507	4.23	.00469	635.11	.05018
5	456.99	.01953	.00241	.73691	5.90	.00654	463.70	.07026
6	365.31	.02105	.00300	.76108	6.36	.00705	370.64	.07379
7	241.54	.03178	.00453	.90357	9.60	.01065	245.05	.10837
8	146.02	.04800	.00750	1.07054	14.5	.01608	148.15	.16407
9	83.40	.09100*	.01313	1.22320	27.5*	.03049*	84.61	.26504
10	47.02	.1570*	.02328	1.28233	47.4*	.05261*	47.70	.46809
11	23.80	.3100*	.04599	1.12518	93.6*	.1039*	24.15	.92250

* From Extrapolated Values of j versus N_R Curve

TABLE IX SUMMARY OF HEAT TRANSFER AND FRICTION RESULTS:
20R - .100 - .125 - .004 - SS, OFFSET RECTANGULAR FIN

HEAT TRANSFER RESULTS:						ISOTHERMAL FRICTION RESULTS:	
RUN NO.	REYNOLD'S NUMBER N_R	$N_{St}N_{Pr}^{2/3}$ j	CONDUCTION PARAMETER λ	MAXIMUM SLOPE	N_{Tu}	REYNOLD'S NUMBER N_R	FRICTION FACTOR f
1	1916.90	.01459	.00242	.62369	3.85	1944.92	.02883
2	1535.99	.01626	.00302	.64867	4.29	1558.44	.03247
3	1236.67	.01687	.00375	.65807	4.45	1254.76	.03573
4	955.33	.01611	.00486	.64354	4.25	969.31	.03777
5	733.27	.01724	.00632	.66540	4.55	743.99	.04121
6	469.32	.02471	.00988	.77128	6.52	476.18	.05636
7	287.45	.03411	.01612	.87728	9.00	291.64	.07842
8	206.93	.04700	.02239	.97627	12.4	209.95	.10055
9	167.11	.05837	.02777	1.03970	15.4	169.55	.12085
10	92.55	.10498	.05011	1.19481	27.7	93.90	.20767

TABLE X SUMMARY OF HEAT TRANSFER AND FRICTION RESULTS:
16R - .153 - .143 - .004 - SS, OFFSET RECTANGULAR FIN

HEAT TRANSFER RESULTS:

ISOTHERMAL FRICTION RESULTS:

RUN NO.	REYNOLD'S NUMBER N_R	$N_{St}N_{Pr}^{2/3}$ j	CONDUCTION PARAMETER λ	MAXIMUM SLOPE	N_{Tu}	REYNOLD'S NUMBER N_R	FRICTION FACTOR f
1	2475.35	0.03040	.00186	.73734	5.88	2511.50	.03010
2	1977.09	0.02678	.00233	.69851	5.18	2005.96	.02993
3	1591.25	0.02451	.00290	.67458	4.74	1614.49	.03309
4	1221.76	0.02146	.00377	.63837	4.15	1239.60	.03596
5	946.83	0.01737	.00486	.59726	3.36	960.65	.04378
6	600.94	0.01970	.00766	.62614	3.81	609.71	.05875
7	371.53	0.02895	.01238	.72367	5.60	376.95	.08702
8	212.24	0.04384	.02171	.85327	8.48	215.34	.18758
9	118.61	0.08065	.03883	1.01893	15.60	120.34	.27030
10	51.12	0.157*	.09037	1.21707	30.37*	51.87	.41484
11	31.66	0.250*	.14580	1.4404	48.36*	32.12	.80995

* From Extrapolated Values of j versus N_R Curve

	Maximum Slope															
N_{Tu} \ λ	0	.005	.010	.015	.020	.025	.030	.035	.040	.060	.080	.100	.500	1.0	10	∞
1.0	.368	-	-	-	.374	-	-	-	.377	.380	.382	.384	-	-	-	.400
1.1	.403	-	-	-	.408	-	-	-	.413	.417	.420	.425	-	-	-	.445
1.2	.434	-	-	-	.440	-	-	-	.445	.447	.452	.459	-	-	-	.488
1.3	.461	-	-	-	.467	-	-	-	.472	.475	.480	.487	.497	-	-	.529
1.4	.483	-	-	-	.489	-	-	-	.494	.498	.503	.511	.522	-	-	.568
1.5	.502	-	-	-	.507	-	-	-	.512	.517	.521	.530	.542	-	-	.603
1.6	.517	-	-	-	.522	-	-	-	.527	.530	.536	.544	.560	-	-	.637
1.8	.536	-	-	-	.539	-	-	-	.542	.547	.553	.561	.589	-	-	.697
2.0	.541	-	-	-	.545	-	-	-	.548	.556	.563	.571	.615	.646	.723	.748
2.2	.544	-	-	-	.549	-	-	-	.557	.566	.574	.582	.640	.677	.764	.791
2.4	.549	-	-	-	.557	-	-	-	.567	.577	.585	.592	.662	.703	.798	.827
2.6	.557	-	-	-	.566	-	-	-	.577	.587	.595	.603	.682	.726	.826	.857
2.8	.567	-	-	-	.577	-	-	-	.587	.598	.606	.615	.699	.745	.850	.882
3.0	.577	-	-	-	.587	-	-	-	.598	.608	.617	.626	.714	.761	.869	.903
3.2	.587	-	-	-	.598	-	-	-	.609	.619	.628	.637	.727	.775	.885	.920
3.4	.598	-	-	-	.610	-	-	-	.620	.630	.640	.647	.738	.787	.899	.934
3.6	.609	-	-	-	.621	-	-	-	.631	.641	.650	.658	.749	.798	.911	.946
3.8	.621	-	-	-	.632	-	-	-	.642	.652	.660	.668	.758	.807	.920	.956
4.0	.632	-	-	-	.643	-	-	-	.653	.662	.670	.678	.767	.815	.928	.964
4.5	.660	-	-	-	.670	-	-	-	.678	.687	.694	.701	.784	.831	.941	.978
5.0	.688	-	-	-	.697	-	-	-	.704	.711	.717	.722	.800	.843	.951	.987
5.5	.715	-	-	-	.722	-	-	-	.727	.733	.737	.742	.812	.852	.956	.992
6.0	.741	-	-	-	.746	-	-	-	.750	.753	.757	.760	.822	.859	.960	.995
6.5	.767	-	-	-	.769	-	-	-	.771	.773	.774	.776	.830	.865	.962	-
7.0	.792	-	-	-	.792	-	-	-	.791	.791	.791	.792	.837	.870	.964	1.000
7.5	.816	-	-	-	.812	-	-	-	.810	.808	.806	.805	.844	.874	.965	-
8.0	.840	-	-	-	.832	-	-	-	.827	.824	.821	.817	.849	.877	.966	-
9.0	.885	-	-	-	.872	-	-	-	.861	.853	.847	.840	.858	.882	.967	-
10.0	.929	.922	.916	.911	.906	.901	.897	.893	.890	.880	.869	.860	.864	.886	.968	1.000
11.0	.970	.959	.953	.946	.939	.933	.927	.921	.917	.901	.888	.878	.870	.889	.968	-
12.0	1.010	.998	.988	.979	.970	.962	.955	.948	.942	.922	.906	.893	.873	-	-	-
13.0	1.049	1.034	1.022	1.009	.999	.990	.980	.973	.965	.941	.922	.907	.875	-	-	-
14.0	1.085	1.068	1.053	1.039	1.027	1.016	1.005	.996	.987	.958	.937	.921	.877	-	-	-
15.0	1.121	1.102	1.085	1.068	1.053	1.040	1.028	1.017	1.007	.975	.950	.932	.879	.893	-	-
16.0	1.156	1.133	1.112	1.094	1.077	1.063	1.049	1.037	1.026	.990	.963	.942	.881	-	-	-
18.0	1.223	1.193	1.167	1.144	1.123	1.105	1.088	1.073	1.060	1.016	.984	.960	.885	-	-	-
20.0	1.286	1.249	1.217	1.189	1.164	1.143	1.123	1.105	1.089	1.039	1.003	.975	.887	.894	-	1.000
22.0	1.347	1.302	1.264	1.231	1.202	1.177	1.154	1.134	1.116	1.059	1.018	.987	.889	-	-	-
24.0	1.404	1.352	1.308	1.269	1.237	1.208	1.182	1.160	1.140	1.077	1.032	.997	.891	-	-	-
26.0	1.460	1.399	1.348	1.305	1.268	1.236	1.208	1.183	1.161	1.092	1.043	1.005	.893	-	-	-
28.0	1.515	1.444	1.387	1.339	1.298	1.262	1.231	1.204	1.180	1.106	1.053	1.013	.894	-	-	-
30.0	1.565	1.487	1.423	1.370	1.325	1.286	1.253	1.224	1.198	1.118	1.061	1.019	.895	.895	-	1.000
32.0	1.617	1.528	1.458	1.399	1.351	1.309	1.273	1.241	1.214	-	-	-	-	-	-	-
34.0	1.665	1.568	1.490	1.427	1.374	1.330	1.291	1.258	1.228	-	-	-	-	-	-	-
36.0	1.712	1.605	1.521	1.453	1.397	1.349	1.308	1.273	1.242	-	-	-	-	-	-	-
38.0	1.757	1.641	1.551	1.478	1.418	1.367	1.324	1.287	1.254	-	-	-	-	-	-	-
40.0	1.801	1.676	1.579	1.501	1.437	1.384	1.339	1.300	1.266	-	-	-	-	-	-	1.000
45.0	1.908	1.757	1.643	1.554	1.481	1.422	1.372	1.328	1.292	-	-	-	-	-	-	-
50.0	2.010	1.833	1.702	1.601	1.520	1.455	1.400	1.353	1.313	-	-	-	-	-	-	1.000
55.0	2.107	1.902	1.756	1.644	1.555	1.483	1.425	1.375	1.332	-	-	-	-	-	-	-
60.0	2.199	1.967	1.803	1.680	1.585	1.508	1.445	1.392	1.347	-	-	-	-	-	-	1.000

TABLE XI Tabulation of N_{Tu} as a Function of the Maximum Slope of the Generalized Cooling Curve at Various Levels of the Material Heat Conduction Parameter (λ) Parallel to the Flow Direction

APPENDIX A

DATA REDUCTION RELATIONSHIPS

Summarized herein are those data reduction relationships which are of prime importance in obtaining the heat transfer and flow friction characteristics as presented from the raw data taken. Before the data on the matrices tested can be reduced, or a comparison of the different matrices can be made, it is essential to obtain accurate geometrical dimensions. The geometrical factors of interest are the porosity, p, the hydraulic diameter, D_H, and the area compactness, β . Determination of any of these fixes the third since it may be shown that

$$\beta = \frac{4p}{D_H} \qquad [14] \qquad \text{(A-1)}$$

The definitions of these terms are:

(1) $$p = \frac{\text{Free Flow Area}}{\text{Frontal Area}} = \frac{A_c}{A_{fr}} \qquad \text{(A-2)}$$

(2) $$D_H = \frac{4 \times \text{Free Flow Area}}{\text{Heat Transfer Surface Area}} = 4\frac{A_c}{A}L \qquad \text{(A-3)}$$

(3) $$\beta = \frac{\text{Heat Transfer Surface Area}}{\text{Frontal Area x Flow Length}} = \frac{A}{A_{fr}L} \qquad \text{(A-4)}$$

MAXIMUM SLOPE

As presented earlier, the maximum slope of the generalized cooling curve is a unique function of N_{Tu} and λ .

$$\left[\frac{d\left[\frac{t_{f2}-t_i}{t_{f1}-t_i}\right]}{d\left[\tau/N_{Tu}\right]}\right]_{max} = \varphi\left(N_{Tu}, \lambda\right) \qquad \text{(A-5)}$$

τ and N_{Tu} have both been previously defined, but for convenience the relationships are restated:

$$\tau \approx \frac{hA}{W_s c_s}\,\theta \qquad \text{and} \qquad N_{Tu} = \frac{hA}{\dot{m} c_p}$$

Therefore:

$$\tau / N_{Tu} = \left(\dot{m} c_p / W_s c_s\right)\theta$$

and

$$d\left(\tau / N_{Tu}\right) = \dot{m} c_p / W_s c_s)\, d\theta = \left(C/\bar{C}_s\right) d\theta \qquad \text{(A-6)}$$

Furthermore:

$$\frac{t_{f2}-t_i}{t_{f1}-t_i} = \frac{t_{f2}-t_{f1}}{t_{f1}-t_i} + 1 \qquad [7]$$

and

$$d\left[\frac{t_{f2}-t_i}{t_{f1}-t_i}\right] = \frac{1}{t_{f1}-t_i}\; d\left[t_{f2}-t_{f1}\right] \qquad \text{(A-7)}$$

Combining (A-6) and (A-7)

$$\left[\frac{d\left[\frac{t_{f2}-t_i}{t_{f1}-t_i}\right]}{d\left[\tau/N_{Tu}\right]}\right]_{max} = \left[\frac{\bar{C}_s}{C}\right]\frac{1}{t_{f1}-t_i}\,\frac{d\left[t_{f2}-t_{f1}\right]}{d\theta} \qquad \text{(A-8)}$$

From Figure 28:

(1) $$\left[\frac{d\left[t_{f2}-t_{f1}\right]}{d\theta}\right]_{max} = \frac{y}{x}$$

(2) $$\frac{x}{\text{Chart speed}} = d\theta \text{ , sec}$$

(3) $y = d(t_{f2} - t_{f1})$, inches

(4) $M = (t_{f1} - t_i)$, inches

Combining these determined values into (A-8) yields:

$$\left[\frac{d\left[\frac{t_{f2}-t_i}{t_{f1}-t_i}\right]}{d\left[\tau/N_{Tu}\right]}\right]_{max} = \frac{\bar{C}_s}{C} \cdot \frac{1}{M} \cdot \frac{y}{x} \cdot \text{Chart speed} \quad \text{(A-9)}$$

With this value of maximum slope and $\lambda = \frac{k_s A_s}{\dot{m} c_p L}$, enter TABLE XI or Figure 29 to obtain a corresponding N_{Tu} value.

MASS RATE OF FLOW:

The mass rate of flow is calculated from the method given in reference [16] with necessary rearrangements in order to reduce unnecessary hand calculations and to gain the full benefits of Murdock [15]:

$$\dot{m} = 359 K d_o^{\,2} F_a Y \sqrt{\Delta P_o \gamma} \quad \text{(A-10)}$$

where: K = flow coefficient, including velocity of approach = $\frac{C}{\sqrt{1-\beta^4}}$ with C = orifice coefficient of discharge (obtained from [15]) and β = ratio of orifice diameter to internal pipe diameter, d_o/d

d_o = orifice diameter, inches

F_a = thermal expansion factor

Y = expansion factor

γ = specific weight of fluid flowing = $\frac{P}{RT}$

with P in #/ft^2

R = 53.35 ft - #/lb °R for air

T = t(°F) + 459.7 = degrees Rankine (°R)

ΔP_o = Pressure drop across the orifice, inches H_2O

substituting $\frac{P}{R\,T}$ for γ, since the magnitude of the local acceleration of gravity, g, is taken as being equal to the magnitude of standard acceleration of gravity, g_c; and $\frac{C}{\sqrt{1-\beta^4}}$ for K.

gives:

$$\dot{m} = \frac{359\,C}{\sqrt{1-\beta^4}}\, d_o^2\, F_a\, Y \sqrt{\Delta P_o \cdot \frac{P}{RT}} \qquad \text{(A-11)}$$

Inserting the numerical value for R and converting P to units of $\#/in^2$ yields:

$$\dot{m} = \frac{589.81\,C\,d_o^2\,F_a\,Y}{\sqrt{1-\beta^4}} \sqrt{\Delta P_o \cdot \frac{P(psia)}{T}} \qquad \text{(A-12)}$$

From Figure 38, reference [16] : $F_a \approx 1.00$

From Figure 40b, reference [16] : $Y = 0.9985 \approx 1.0$

The pressure, P, in (A-12), is hereafter referred to as P_3 and is determined by the following relationship:

$$P_3 = (P_{atm} - P_o / 13.6)\ 0.4912,\ \#/in^2 \qquad \text{(A-13)}$$

Where P_{atm} is the atmospheric pressure in inches of mercury,

P_o is the static pressure upstream of the orifice in inches of H_2O

13.6 inches of H_2O/ inches of mercury

0.4912 $\#/in^2$/ inches of mercury

The temperature, T, in (A-12) is the air temperature at the orifice in degrees Rankine (T_o):

$$T_o = t_o + 459.7 \qquad \text{(A-14)}$$

Replacing F_a and Y in (A-12) with their numerical values, the equation reduces to the working form:

$$\dot{m} = \frac{589.81\, C\, d_o^2}{\sqrt{1-\beta^4}} \sqrt{\Delta P_o \cdot \frac{P_3}{T_o}} \qquad \text{(A-15)}$$

REYNOLDS NUMBER

Reynolds number is defined as:

$$N_R = \frac{D_H\, G}{\mu} \qquad \text{(A-16)}$$

where G is the mass flow velocity based on the free flow area, A_c.

$$G = \frac{\dot{m}}{A_c} = \frac{\dot{m}}{p\, A_{fr}} \qquad \text{(A-17)}$$

Substituting (A-17) into (A-16):

$$N_R = \frac{\dot{m}}{\mu\, A_{fr}} \frac{D_H}{p} \qquad \text{(A-18)}$$

But from (A-1) $D_H/p = \frac{4}{\beta}$, therefore: $N_R = \frac{4\dot{m}}{\mu A_{fr}}\left(\frac{1}{\beta}\right)$ (A-19)

Equation (A-19) shows that for a given matrix and mass flow rate the Reynolds number is inversely proportional to the compactness. Substituting (A-4) into (A-19) yields the working equation:

$$N_R = \frac{4\, L\, \dot{m}}{\mu\, A} \qquad \text{(A-20)}$$

FANNING FRICTION FACTOR:

The following sketch together with equation (A-21) describes the flow system under consideration: [11]

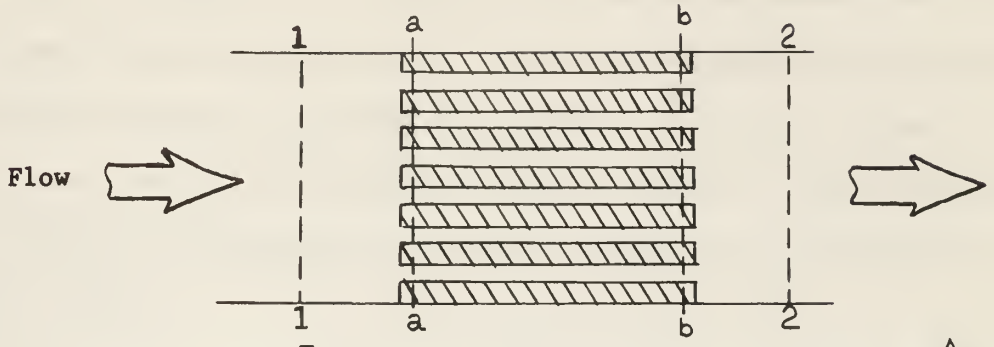

$$\frac{\Delta P}{P_1} = \frac{G^2}{2g_c}\ \frac{v_1}{P_1}\left[(K_c - 1 - \rho^2) - 2\left(\frac{v_2}{v_1} - 1\right) + f\ \frac{A}{A_c}\ \frac{v_m}{v_1}\right.$$

entrance effect; flow acceleration; core friction

$$\left. - (1 - \rho^2 - K_e)\ \frac{v_2}{v_1}\right] \qquad \text{(A-21)}$$

exit effect

It is important to note that $v_a \approx v_1$ and $v_b \approx v_2$ in the above sketch as the pressure changes (for gas flow heat exchanger application) from section 1 to a and b to 2, respectively, are very small relative to the total pressure. Inasmuch as the testing is performed with air at moderate temperatures and pressures, the perfect gas law is applicable ($P = \rho RT$).

Substituting $v = \frac{1}{\rho}$ and recalling that $\frac{D_H}{4L} = \frac{A_c}{A}$ or $\frac{r_H}{L} = \frac{A_c}{A}$ from equation (A-3), equation (A-21) solved for f for the isothermal case becomes:

$$f = \left[2g_c \rho_m \left(\frac{\Delta P}{G^2}\right) - \frac{P_1 + P_2}{2}\left(\frac{K_c}{P_1} + \frac{K_e}{P_2}\right) -\right.$$

con't on next page

(con't.)

$$\left(\frac{P_1 + P_2}{2}\right)\left(\frac{1}{P_2} - \frac{1}{P_1}\right)\left(1 + p^2\right)\Bigg]\frac{r_H}{L} \qquad \text{(A-22)}$$

where $\rho_m = \frac{\rho_1 + \rho_2}{2}$ with the upstream values subscripted by 1 and the downstream subscripted by 2. K_c is the entrance coefficient and K_e the exit coefficient, and both are dependent on porosity, shape of the flow cross section and the matrix Reynolds number. Values of K_c and K_e are obtained from Figures 37, 38, or 39, which were reprinted from reference [11].

If we consider an order of magnitude approximation, the first term in (A-22) is by far the greatest contributor to friction factor for small pressure differentials.

The approximation, therefore, that $\frac{P_1+P_2}{2} = P_m \approx P_1 \approx P_2$

reduces (A-22) to the following

$$f = \left[2g_c \rho_m\left(\frac{\Delta P}{G^2}\right) - (K_c + K_e) + \frac{\Delta P}{P_m}\left(1 + p^2\right)\right]\frac{r_H}{L} \qquad \text{(A-23)}$$

Reference [14] points out that the relationships given here can be recombined in such a manner so as to show that f is proportional to the porosity cubed and inversely proportional to the compactness ($f \propto p^3/\beta$).

COLBURN J FACTOR:

Colburn j factor is defined as:

$$j = N_{St} N_{Pr}^{2/3} = \frac{h}{Gc_p} N_{Pr}^{2/3} \qquad \text{(A-24)}$$

Substituting (A-17) for G and multiplying by A/A yields

$$j = \frac{h A}{\dot{m} c_p} \frac{A_c}{A} N_{Pr}^{2/3} \qquad \text{(A-25)}$$

but $$\frac{h A}{\dot{m} c_p} = N_{Tu}$$

therefore:

$$j = N_{Tu} \frac{A_c}{A} N_{Pr}^{2/3} \qquad \text{(A-26)}$$

Combining equations (A-1) and (A-3):

$$\frac{A_c}{A} = \frac{P}{\beta L}$$

thus:

$$j = N_{Tu} N_{Pr}^{2/3} \frac{1}{L} \frac{P}{\beta} \qquad \text{(A-27)}$$

It is apparent from equation (A-27) that the Colburn j factor is directly proportional to porosity and inversely proportional to compactness ($j \propto P/\beta$).

HEAT TRANSFER POWER AND FLOW FRICTION POWER:

An evaluation of the heat transfer power versus flow friction power is of interest in that it is a measure of relative performance.

The heat transfer power per unit area per degree temperature difference is [11]:

$$h = \frac{c_p \mu}{N_{Pr}^{2/3}} \frac{1}{D_H} j N_R \qquad \text{(A-28)}$$

Equation (A-28) with the properties evaluated at standard conditions of dry air at 500 F and one atmosphere becomes:

$$h_{STD} = 0.02195 \left(\frac{1}{D_H}\right)\left(N_R\, j\right) \quad \text{Btu/hr ft}^2\ ^\circ\text{F} \qquad \text{(A-29)}$$

where $c_p = 0.2477$ Btu/lb °F

$\mu = 0.0678$ lb/hr ft

$\rho = 0.0413$ lb/ft^3

$N_{Pr} = 0.671$

The flow friction power per unit area is [11] :

$$E = \frac{1}{2g_c}\,\frac{\mu^3}{\rho^2}\left(\frac{1}{D_H}\right)^3 f\, N_R^{\,3} \qquad \text{(A-30)}$$

When equation (A-30) is evaluated at standard conditions (μ and ρ values given above), the flow friction power per unit area at standard conditions is:

$$E_{STD} = 1.11 \times 10^{-7} \left(\frac{1}{D_H}\right)^3 f \left(\frac{N_R}{1000}\right)^3 \quad \text{HP/ft}^2$$

For comparison purposes the surface geometries were reduced to a common hydraulic diameter of $D_H = 2 \times 10^{-3}$ ft. Figures 26 and 27 show such comparisons for the nickel surfaces.

APPENDIX B

DESCRIPTION OF EQUIPMENT

Heat transfer data was obtained utilizing the "single blow" technique which consists briefly of monitoring the fluid temperature response at the test matrix exit while subjecting the inlet to the test matrix to a step change in fluid temperature.

Friction factor was determined from pressure drop data obtained from static pressure taps located in the test section - one at inlet, the other at the exit.

Necessary equipment to perform such an experiment falls into one of the following categories:

(1) Fluid source

(2) Flow metering system

(3) Temperature measuring system

(4) Pressure measuring system

(5) Fluid heater system

(6) Matrix holder and test section casing

FLUID SOURCE:

Air, the working fluid, was provided to the test apparatus by connecting the rig to the inlet of a 30HP, multistage, Spencer Turbo-Compressor rated for 550cfm operating on a 220 volt a.c. power supply.

FLOW METERING SYSTEM: (See Figure 1)

The flow metering system consisted of an ASME standard orifice section constructed for d and d/2 pressure taps in a 3.08" inside diameter metal tube. [16]. A wide flow range was obtained by utilizing thin plate concentric

orifices of throat diameter 2.310, 1.971, 1.232, 1.540, 0.462, and 0.308 inches respectively.

Control of the pressure drop across the orifice was maintained by a gate valve downstream of the apparatus, ahead of the compressor inlet and another gate valve on the compressor inlet. The blast gate on the compressor discharge was pre-set so that the unit could not be operated beyond the full load rating of the turbo.

This turbo-compressor had many distinct advantages over the one used in reference [1] : some of the more pertinent being (1) a 550 cfm capacity; (2) essentially constant pressure throughout the range of the machine; (3) the load decreases as less air is used so that the problem of stalling at low flow rates is non-existent.

TEMPERATURE MEASURING SYSTEM: (See Figure 1)

The majority of the temperatures were measured with iron-constantan thermocouples. These thermocouples use iron for the positive conductor and constantan for the negative conductor. Measuring T_1 is a group of five thermocouples in series, bound together and insulated from each other by teflon tape and inserted in a 1/8" diameter aluminum tube to serve as a radiation shield. A small aperature was cut in the inserted tube facing upstream. T_2 and T_4 are five wire thermocouple grids, connected in series, mounted permanently in the test section casing. T_3 is a movable five wire series connected thermocouple grid located in the matrix holder so that it is adjacent to the downstream side of the matrix. The purpose of connecting the thermocouples in series was to magnify the emf output so that the instrument sensitivity to small temperature changes would be enhanced. With T_2 bucked against T_4, it is possible to determine the temperature uniformity

across the matrix. T_1 versus T_3 indicates the difference between upstream and downstream temperatures; thus, it is this combination which is used to record the rate of change of upstream and downstream temperatures with time, resulting from the step change in fluid temperature upstream. This differential is recorded on a Minneapolis-Honeywell "Brown" Recorder and serves as the primary data for heat transfer evaluation of the matrix. The recorder has variable chart speeds so that acceptable cooling curves for maximum slope determination can be generated. This instrument has a span adjustment which permits the span to be varied continuosuly from the narrowest to the widest span desired from 0 to 55 millivolts. For the work performed herein, the recorder was precalibrated for a 0 - 3 millivolt scale. This unit also has adjustable supression and damping adjustment features. The damping adjustment provides a filter network for removing a.c. strays, and provides correct damping so that neither undershoot nor overshoot in the response curves is experienced.

A copper constantan thermocouple was inserted into the duct just ahead of the orifice to measure T_o, orifice temperature. This temperature was read in millivolts on a Rubicon Company Portable Precision Potentiometer, converted to degrees Fahrenheit and recorded for each run.

A copper constantan thermocouple grid was inserted in place of T_3 to determine the temperature distribution across the cross section during initial check out of the apparatus. This thermocouple arrangement was part of a special holder lined with balsa wood to provide a smooth, continuous flow passage, which also contained an impact tube used for checking the velocity profiles (See Figure 33).

PRESSURE MEASURING SYSTEM: (See Figure 1)

Pressure taps are located upstream and downstream of the matrix and on

either side of the orifice. Each tap is connected to an appropriate manometer or draft gage via Imperial Company "poly-flo" tubing. Quick closing valves were installed at various positions in the line to permit isolation of sections and as a safety feature.

The following instruments were utilized:

(1) Meriam Instrument Company, 0 - 50" manometer

(2) Meriam Instrument Company, -8" to +8" manometer

(3) Ellison Differential Direct Draft Gages, 0 - 6", 0 - 8".

(4) Ellison Inclined Draft Gages, 0 - 0.5", 0 - 6".

(5) E. Vernon Hill and Company Type "C" Micromanometer, 0 - 1.25".

Any one of these instruments or a combination can be used to measure the differential pressures of the orifice or matrix or the required static pressures - upstream of matrix and upstream of the orifice. Cross checking of the various instruments assured reliable operation.

FLUID HEATER SYSTEM: (See Figure 1)

The heater section is comprised of 28 nichrome wire heaters of 0.0031" diameter. The heater system was designed to elevate the air temperature 20 $^{\circ}$F above ambient for a mass rate of flow of 1000 lb/hour. The nichrome material was selected because it has high resistivity, low thermal conductivity and specific heat, and has a very small time constant so that it permits one to approach the idealized step function. [1]

The wire heaters are wound two to a bakelite frame, 1/32" between each wire, with 50 and 52 wires respectively to each heater on a frame. These heaters are connected in parallel, then via a switch to a variable voltage bus. The heater frame and its electrical connections are apparent in

Figures 34 and 35.

A schematic wiring diagram for one of the two heater complexes is shown below [1] . A total of 14 frames are wired in this fashion, thereby putting all 28 heaters in parallel, permitting two to be switched on or off at a time.

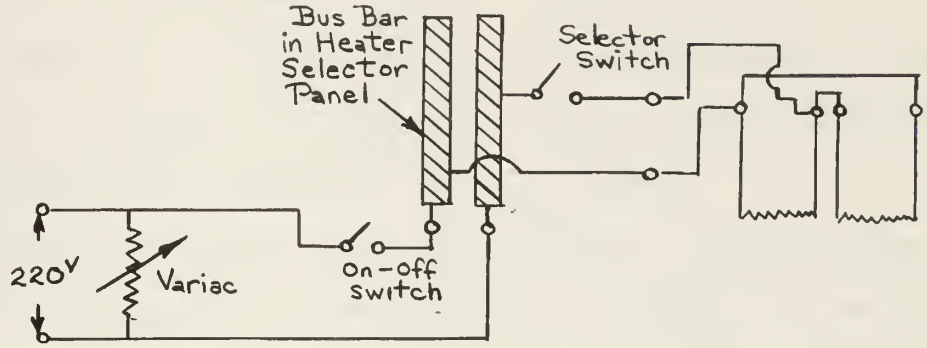

The number of heaters in use decreases as flow rate decreases. The necessary voltage variations are obtainable by a General Radio Company Type W20HM "Variac" Autotransformer, 0 - 280 volt, 8 amp load from a 240 volt 50 - 60 cycle line.

The recommended procedure is to decrease the number of heaters insofar as practical while maintaining a high voltage. When there are only four heaters in use, voltage reduction becomes necessary to obtain the required 20° temperature rise, keeping the number of heaters constant. Meeting the current requirement is the dictating factor. It is noteworthy that the heaters should never be energized unless sufficient air is flowing, otherwise the wires will sag and short circuiting will result.

MATRIX HOLDER AND TEST SECTION: (See Figures 31, 32, and 35)

The matrix holder and test section are made of polyethylene plastic. The test section casing holds the T_2 and T_4 thermocouple grids permanently mounted, as well as the upstream and downstream static pressure taps required for determining friction factor. All parts were machined to close tolerance to assure a snug fit for the matrix holder and to guarantee good alignment of the flow channel through the heater and test sections. The flow channel is 3 - 3/16" x 3 - 3/16" and matrices of flow lengths up to 3" may be tested. As mentioned previously under Temperature Measuring System, the T_3 thermocouple grid is located in the matrix holder.

Correct positioning of the test matrices in the flow channel is ensured by using styrofoam plastic inserts. In addition to the aforementioned systems, one item remains to be considered - the Inlet Cone and Screen Straightener Section. The inlet cone was designed using Smith and Wang [18] as a guide. Although this reference pertained to contracting cones for circular duct, the resultant inlet cone for this rig proved very satisfactory. To assist in guaranteeing a uniform velocity at the throat, a stainless steel 60 mesh screen was installed (See Figure 1). Space is available in the screen straightening section to add additional screens if they should be required for flow rates beyond the range of this investigation.

APPENDIX C

PERFORATED NICKEL GEOMETRIC PROPERTIES

The material used in the perforated plate matrices was pure nickel, electro-deposited sheet of integral structure manufactured by Perforated Products, Incorporated. Types 160/40TV, 160/40Q, 50G, 125M and 125P were utilized in the matrices - the first two of these having slotted openings and the remaining three having round openings. A brief description of each of the aforementioned types as specified by the manufacturer is set forth in Table C-1.

Inasmuch as the perforations in all cases were conical, the use of the average slot length or average hole diameter was considered à propos. Close examination of each of the different types revealed that this average value was somewhat less than the dimensions specified by the manufacturer in each case. In addition to the requirements for determining porosity of the plate, a correction for the increased longitudinal conduction length due to the perforations as well as a correction to the solid conduction cross-sectional area was performed. The following idealized patterns for each type used, best illustrate these corrections.

160/40TV

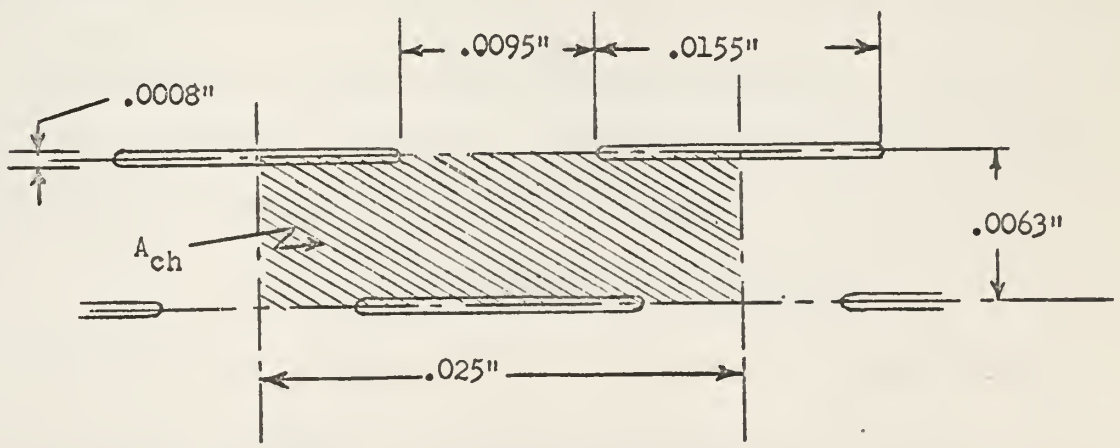

Cross Hatched Area, A_{ch} = (.0063) (.025) = .0001575 in.^{2}

Slotted Area, A_{sl}, in A_{ch} = (.0008) (.0155) = .0000124 in.^{2}

Plate Porosity, the fraction of open or slotted area,

$$\nu = \frac{A_{sl}}{A_{ch}}$$

Solidity, s, is $1 - \nu = 1 - \frac{A_{sl}}{A_{ch}}$

$$s = 1 - \frac{.0000124}{.0001575} = 0.9212$$

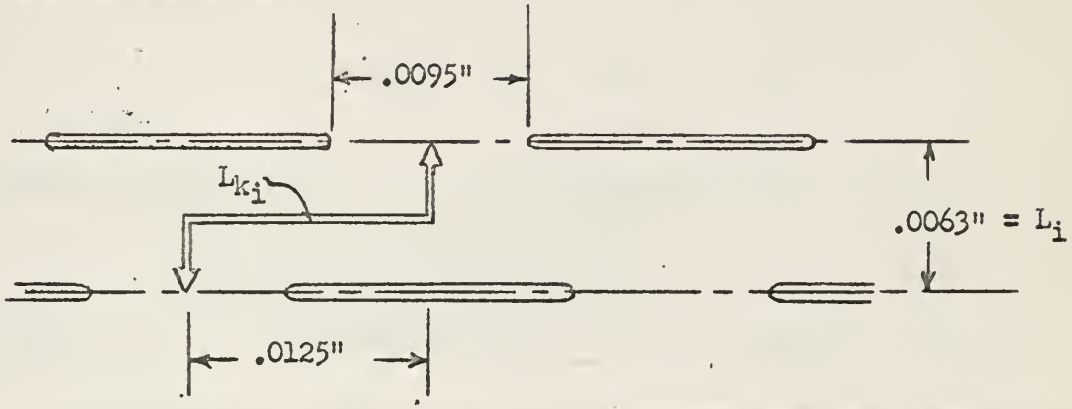

L_{k_i}, conduction path length, = 0.0125 + 0.0063 = 0.0188"

$$\frac{L_i}{L_{k_i}} = \frac{.0063}{.0188} = 0.3351$$

The solid cross sectional area for heat conduction, A_{k_i} varies along the path length. The area, A_{k_i}, selected was the cross sectional area between the slots normal to the flow direction, i.e.,

$$A_{k_i} = (0.0095)(0.0022) = 0.0000209 \text{ in.}^2$$

Just as $L = \sum L_i$ where L is the total matrix flow length and L_i is the flow length between two successive perforations; so does $L_k = \sum L_{k_i}$

and $A_k = \sum A_{k_i}$. In evaluating A_k, a conduction area reduction ratio is employed and is defined as $\xi = \frac{\text{cross sectional area of perforations}}{\text{cross sectional area}}$;

therefore, A_k, is the solid cross sectional area multiplied by $1 - \xi$

i.e.,

$$A_k = A_s (1 - \xi)$$
$$= 1.6058 \left\{ 1 - \frac{(.0155)(.0022)}{(.025)(.0022)} \right\} = 0.6102 \text{ in}^2$$
$$= 0.00424 \text{ ft.}^2$$

160/40Q

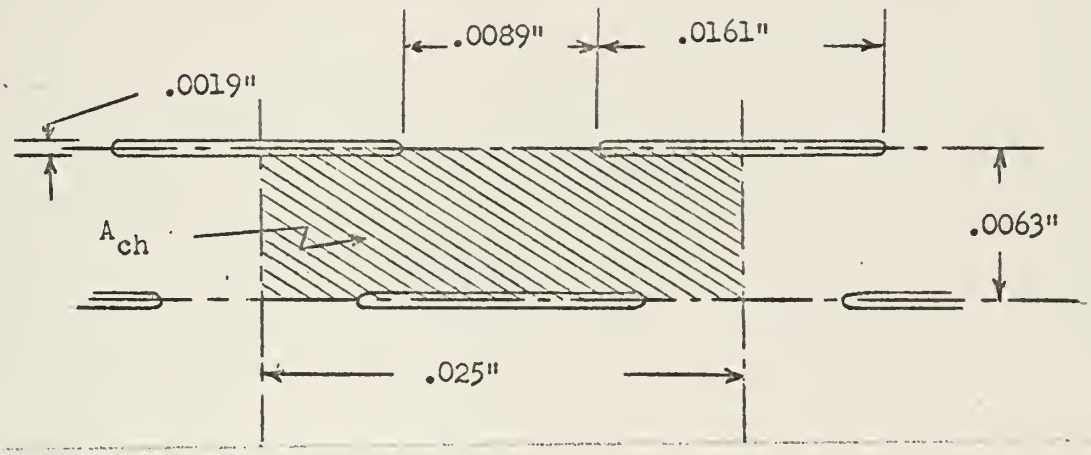

$A_{ch} = (.0063)(.025) = .0001575 \text{ in.}^2$

$A_{sl} = (.0019)(.0161) = .00003059 \text{ in.}^2$

$\nu = .1942$

$s = .8058$

$\frac{L}{L_k} = 0.3351$, same as 160/40TV

$\xi = .644$

$A_k = A_s (1 - \xi) = .002887 \text{ ft.}^2$

125M

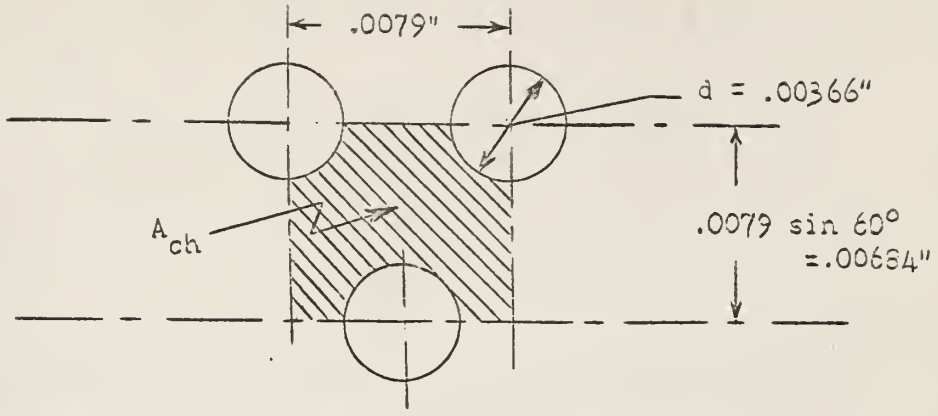

$$A_{ch} = (.00684)(.0079) = .00005404 \text{ in.}^2$$

$$A_{hole} = \frac{\pi}{4} (.00366)^2 = .00001052 \text{ in.}^2$$

$$\nu = \frac{A_{hole}}{A_{ch}} = \frac{.00001052}{.00005404} = 0.19466$$

$$s = .8053$$

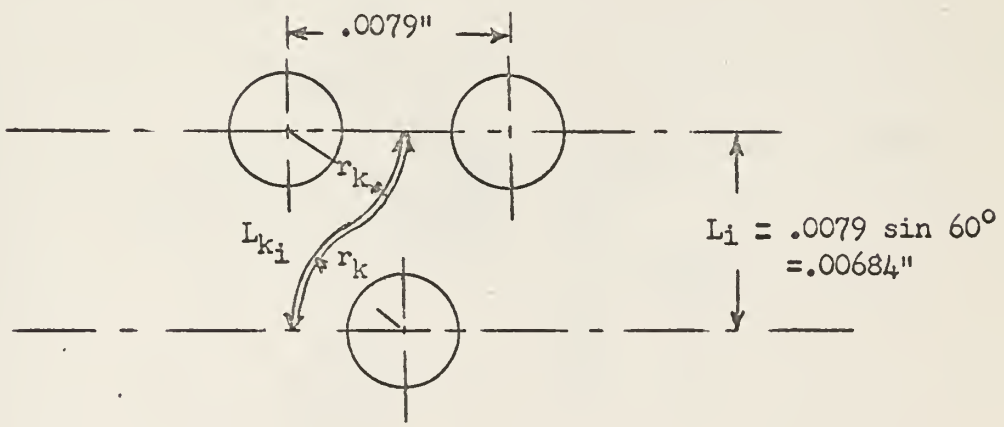

The equivalent conduction length, L_{k_i}, is computed in the case of round perforations assuming the path to be as shown above, i.e., $\frac{2\pi r_k}{3}$ where r_k is the radial distance equal to one-half the center to center distance. Thus

$$L_{k_i} = \frac{2\pi}{3} \frac{(.0079)}{2} = .00827"$$

and

$$\frac{L_i}{L_{k_i}} = \frac{.00684}{.00827} = .82709$$

A_k is determined as in the case of the slotted perforations.

$$\phi = \frac{\text{diam. of hole x plate thickness}}{\text{center to center distance x plate thickness}}$$

$$= \frac{(.00366)(.0016)}{(.0079)(.0016)} = .4633$$

Therefore, $A_k = A_s (1 - \phi) = 1.1679 \text{in.}^2 (1 - .4633)$

$= .6268 \text{ in.}^2 = .00435 \text{ ft.}^2$

125P

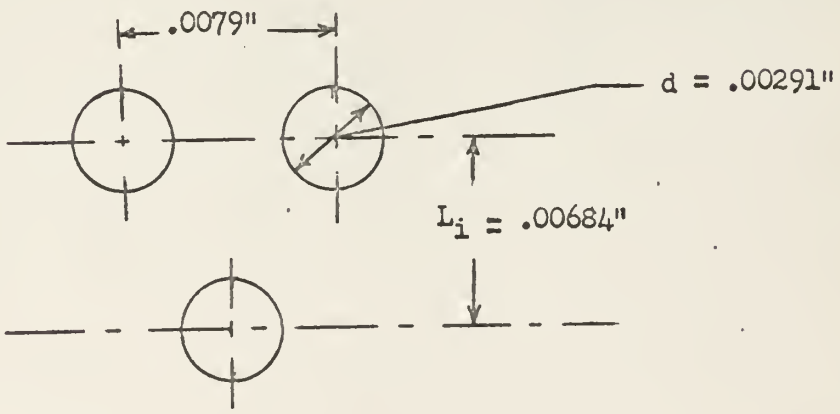

$A_{ch} = (.00684)(.0079) = .00005404 \text{ in}^2$

$A_{hole} = \frac{\pi}{4} (.00291)^2 = .00000665$

$\nu = 0.12307$

$s = 0.8769$

$L_{ki} = .00827"$

$\frac{L_i}{L_{ki}} = .82709$

$\xi = 0.3684$

$A_k = A_s(1 - \xi) = .00640 \text{ ft}^2$

50G

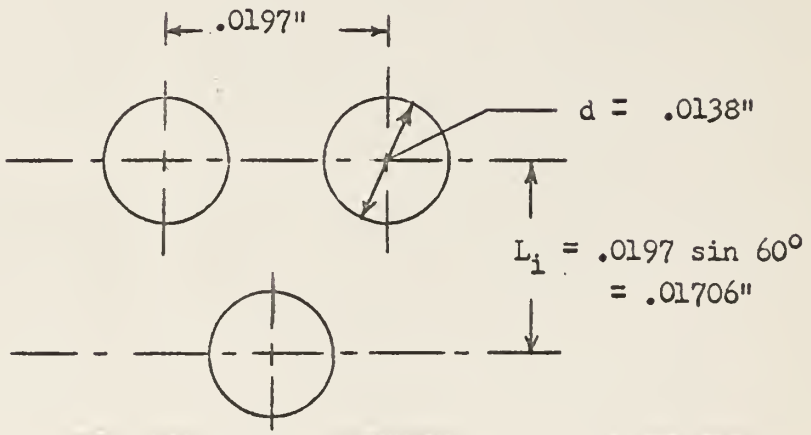

$$A_{ch} = (.01706)(.0197) = .00033608 \text{ in.}^2$$

$$A_{hole} = \frac{\pi}{4} (.0138)^2 = .00014957 \text{ in.}^2$$

$$\mathcal{V} = .44504$$

$$s = .55496$$

$$L_{k_i} = .02063"$$

$$\frac{L_i}{L_{k_i}} = .82697$$

$$\mathcal{F} = .7005$$

$$A_k = A_s (1 - \mathcal{F}) = .00243 \text{ ft.}^2$$

Type	Opening	Hole Diameter (inches)	Plate Thickness (inches)	Center to Center Distance, (inches)	% Open Area
160/40TV	slotted	0.0008x0.017	0.0022	0.0063x0.025	12.0
160/40Q	slotted	0.0019x0.018	0.0016	0.0063x0.025	24.5
50G	round	0.0145	0.0016	0.020	50.0
125M	round	0.0039	0.0016	0.0079	22.5
125P	round	0.003	0.002	0.0079	14.5

TABLE C-1 Geometric Properties of Perforated Nickel

APPENDIX D

SAMPLE CALCULATIONS

The following sample calculations are based on data obtained from Run #1 for the modified parallel plate matrix constructed from the 160/40Q perforated nickel material. The basic geometric parameters are illustrated in Appendix A.

Prior to the reduction of data, several fixed parameters must be evaluated.

DIMENSIONS OF FINNED SHEETS: 3.9375" x 2.00" x .0016"
(BEFORE FORMING)

DIMENSIONS OF SPLITTER PLATES: 3.1875" x 2.00" x 0016"

NUMBER OF FINNED SHEETS: 102

NUMBER OF SPLITTER PLATES: 103

WEIGHT OF MATRIX: 311.0979gms/453.6gm/lb = 0.68584 lb.

MATERIAL CONSTANTS:

k_s = 38.7 Btu/hr - F - ft

c_s = 0.1065 Btu/lb - F

ϱ_s = 0.321 lb/in^3 = 554.7 lb/ft^3

PLANE SURFACE AREA, A*, $= \frac{(102)(2)(2)(3.9375 + 3.1875)}{144} =$

20.1875 ft^2

HEAT TRANSFER AREA, A, = PLANE SURFACE AREA x SOLIDITY

$A = A^*s$

$= (20.1875)(.8058)$

$\boxed{A = 16.2667 \text{ ft}^2}$

FRONTAL AREA, A_{fr}, = 3.141" x 3.1875" = 10.012 in^2

$\boxed{A_{fr} = 0.06953 \text{ ft}^2}$

It has been shown in Appendix A; however, that this can be alternately expressed as:

$$D_H = 4 \frac{p}{\beta}$$

Inasmuch as the perforations have no effect on the hydraulic diameter the value of β rather than $\overline{\beta}$ is used.

$$D_H = \frac{(4)\quad(0.8834)}{(1742.1)} = \boxed{0.002028 \text{ ft}}$$

Now, we are in a position to reduce the data. The following presentation outlines the steps required; however, as far as practicable the actual evaluation is performed by the digital computer program set forth in Appendix E.

RECORDED DATA:

$d_o = 2.310"$

$\Delta P_o = 6.69$ in H_2O

$\Delta P_m = 10.15$ in H_2O

$P_s = 10.65$ in H_2O

$P_o = 20.80$ in H_2O

$T_o = 69.0\ ^\circ F$

$P_{atm} = 30.140$ in Hg.

Chart Speed = 4 in/sec.

$\beta = d_o/d = \frac{2.310}{3.08} = 0.75$

DETERMINATION OF MASS RATE OF FLOW: (See Appendix A)

$$\dot{m} = \frac{589.81\ Fa\ Y\ d_o^2\ C}{\sqrt{1-\beta^4}} \sqrt{\Delta P_o \times \frac{P_3}{T_o}}$$

where: $C = C_o + \Delta C \left[\frac{10^4}{N_{R(d_o)}} \right]$ from reference [15]

$P_3 = (P_{atm} - P_o/13.6)\ 0.4912$; $T_o = t_o\ (^\circ F) + 459.7$

$Y \cong 1.0$ Fig. 40b of Reference [16]

$F_a \cong 1.0$ Fig. 30 of Reference [16]

For $\mathcal{B}$ = 0.75 and d = 3.08", C_o = 0.60691 and ΔC = 0.03839, respectively

$$P_3 = \left[30.140 - \frac{20.80}{13.6}\right] \times 0.4912 = 14.0537 \text{ psi}$$

SOLID MATRIX CROSS SECTIONAL AREA, A_s,

A_s = 102 x 3.9375" x .0016" + 103 x 3.1875" x .0016"

= 1.1679 in^2

$$\boxed{A_s = 0.00811 \text{ ft}^2}$$

FREE FLOW AREA, A_c, = FRONTAL AREA - SOLID CROSS SECTIONAL AREA

$A_c = A_{fr} - A_s$

$$\boxed{A_c = 0.06142 \text{ ft}^2}$$

CONDUCTION AREA CORRECTED FOR EFFECTS OF PERFORATIONS, A_k,

$A_k = A_s (1 - \mathcal{S})$ where $\mathcal{S}$ is the conduction area reduction ratio (See Appendix C).

= 0.00811 (1-0.644)

$$\boxed{A_k = 0.00288 \text{ ft}^2}$$

POROSITY, p, = $\frac{\text{MATRIX FLOW VOID VOLUME}}{\text{MATRIX VOLUME}} = \frac{Vm - Vs}{Vm} = 1 - \frac{Vs}{Vm}$

$$p = 1 - \frac{0.00135}{0.01159} = \boxed{0.8834}$$

COMPACTNESS, $\bar{\mathcal{B}}$ = $\frac{\text{TOTAL HEAT TRANSFER AREA}}{\text{MATRIX VOLUME}}$

$$= \frac{A}{Vm} - \frac{16.2667}{0.01159} = \boxed{1403.75 \text{ ft}^2/\text{ft}^3}$$

Note that $\bar{\mathcal{B}}$ includes the effect of area reduction due to perforations.

$\mathcal{B}$ for an unperforated surface would therefore simply be the plane surface area divided by the matrix volume.

$$\beta = \frac{A^*}{Vm} = \frac{20.1875}{0.01159} = 1742.1 \text{ ft}^2/\text{ft}^3$$

THE HYDRAULIC DIAMETER, D_H, $= 4r_h =$

$$4 \frac{\text{FLOW CROSS SECTIONAL AREA}}{\text{WETTED PERIMETER}}$$

$T_o = 69.0 + 459.7 = 528.7 \ ^\circ R$

$$\dot{m} = \frac{(589.81\ (2.310)^2}{\sqrt{1 - (0.75)^4}} \quad C \quad \sqrt{6.69 \times \frac{14.0537}{528.7}}$$

$$\dot{m} = 1605.242\ C$$

assume $C = 0.6000$

then $\dot{m} = 963.145$ lb/hr

$$C = C_o + \Delta C \left[\frac{10^4}{N_{R(d_o)}} \right] \qquad \text{where} \quad N_{R(d_o)} = \frac{(4)\ (12)\ \dot{m}}{(3.1416)(3.08)\mu}$$

$$= 4.961 \frac{\dot{m}}{\mu}$$

μ is evaluated at temperature t_o by means of the linear approximation

$$\mu = 0.0395 + 0.64167 \times 10^{-4}\ t_o = 0.0395 + 0.64167 \times 10^{-4}\ (69.0)$$

$$= 0.04392 \text{ lb/ft - hr}$$

therefore,

$$C = 0.60691 + 0.03839 \left[\frac{(10^4)(0.04392)}{(4.961)(963.145)} \right]$$

$$C = 0.6104$$

This value of C is compared with the assumed value of C and successive iterations are performed until the two values are equal. The iterative process shows that a value of C = 0.6172 satisfies this requirement and thus

$$\boxed{\dot{m} = 990.756 \text{ lb/hr}}$$

MATRIX REYNOLDS NUMBERS:

Two values for Reynolds number are required, one for the isothermal flow friction factor evaluation and second for the heat transfer evaluation. The two values differ only in so far as the difference in the absolute viscosities. μ_f is evaluated at orifice temperature (t_o) whereas μ_H (heat transfer) is evaluated at average bulk fluid temperature which is assumed to be at t_o + 10 °F.

$$N_{Rf} = \frac{4L\dot{m}}{A\mu_f} = \frac{(4)\ \frac{2}{12}\ (990.756)}{(16.2667)(.04392)} = \boxed{924.54}$$

$$N_{RH} = \frac{4L\dot{m}}{A\mu_H} = N_{Rf}\frac{\mu_f}{\mu_H} = 924.54\ \frac{(.04392)}{(.04456)} = \boxed{911.23}$$

CONDUCTION PARAMETER:

$$\lambda = \frac{k_s A_k}{L \dot{m} c_p} = \frac{(38.7)(0.00288)}{(2/12)(990.756)(.24)} = 0.00282$$

$$\lambda_k = \lambda \frac{L}{L_k} \quad ; \quad \frac{L}{L_k} = 0.3351 \text{ from Appendix C.}$$

therefore $\lambda_k = (.00282)(.3351) = \boxed{0.000944}$

MAXIMUM SLOPE:

The slope of the cooling curve was determined by the method prescribed in Appendix A from Figure 36. Slopes were determined for each of the curves and the average value was used.

$$\text{MAXIMUM SLOPE} = \frac{\bar{C}_s}{C}\left[\frac{dT}{d\Theta}\right]_{max} = \frac{\bar{C}_s}{C} \times \text{SLOPE} \times \text{CHART SPEED}$$

$$\bar{C}_s = W_s c_s = (0.68584\ \text{lb})(0.1065\ \text{Btu/lb °F}) = 0.07304$$

$$C = \dot{m} c_p = (990.756\ \text{lb/hr})(0.24\ \text{Btu/lb °F})\ \frac{1}{3600}\ \frac{\text{hr}}{\text{sec}} = 0.06605$$

SLOPE = 0.14357 (See Figure 36)

whence,

$$\text{MAXIMUM SLOPE} = \frac{(.07304)}{(.06605)} \quad (0.14357)\ (4) = \boxed{0.63507}$$

COLBURN j FACTOR:

Enter Table XI with the values of λ_k and MAXIMUM SLOPE to determine $N_{Tu} = 4.05$. Linear interpolation from this table is sufficient.

$$j = N_{Tu} \frac{A_c}{A} N_{PR}^{2/3} \quad \text{from Appendix A,}$$

$N_{PR}^{2/3} = 0.8017 - 0.82353 \times 10^{-4}\ t_o$ using a linear approximation; therefore

$$j = (4.05)\frac{(0.06142)}{(16.2667)}\ (.7960) = \boxed{0.01217}$$

FANNING FRICTION FACTOR:

From Appendix A, the friction factor is:

$$f = \left[2 g_c \rho_m \left(\frac{\Delta P}{G^2}\right) - (K_c - K_e) - \frac{\Delta P_m}{P_{mean}}(1+\rho^2)\right]\frac{r_H}{L}$$

$$P_{atm} = 30.140 \text{ in Hg} \times 0.4912 \frac{\text{psi}}{\text{in Hg}} = 14.8048 \text{ psi}$$

$$P_s = 10.65 \text{ in } H_2O \times 5.204 \frac{\text{psf}}{\text{in } H_2O} = 55.42 \text{ psf} = 0.3849 \text{ psi}$$

$$P_m = 10.15 \text{ in } H_2O \times 5.204 \frac{\text{psf}}{\text{in } H_2O} = 52.82 \text{ psf} = 0.3668 \text{ psi}$$

$$P_1 = P_{atm} - P_s = 14.8048 - 0.3849 = 14.4199 \text{ psi}$$

$$P_2 = P_1 - \Delta P_m = 14.4199 - 0.3668 = 14.0531 \text{ psi}$$

$$P_{mean} = \frac{P_1 + P_2}{2} = 14.2365 \text{ psi}$$

$$\rho_{mean} = \frac{(P_{mean})\ (144)}{R(t_o + 459.7)} = \frac{(14.2365)(144)}{(53.35)(528.7)} = 0.07268 \text{ lb/ft}^3$$

$$G = \frac{\dot{m}}{A_c} = \frac{990.756}{0.06142} = 16130.84 \text{ lb/hr - ft}^2 = 4.481 \text{ lb/sec - ft}^2$$

$$\frac{r_H}{L} = \frac{0.000507}{2/12} = 0.00304$$

$K_c = 0.48$ and $K_e = -0.33$ from Figure 38.

$$(1 + p^2) = 1 + (0.8834)^2 = 1.7804$$

$$f = \left[\frac{(2)(32.2)(0.07268)(52.82)}{(4.481)^2} - (0.48 - 0.33) - \frac{.3668}{14.2365} (1.7804) \right] (0.00304)$$

$$= (12.3126 - 0.150 - 0.04587)(0.00304)$$

$$\boxed{f = 0.03686}$$

The thermal properties, μ and $N_{PR}^{2/3}$, were obtained by linear interpolation of data from reference [6]. The values of k_s and c_s were obtained directly from references [5] and [4] for nickel and stainless steel respectively.

APPENDIX E

FORTRAN 60 DATA REDUCTION COMPUTER PROGRAM FOR A CDC 1604 DIGITAL COMPUTER

A computer program was formulated in order that as much data reduction as practicable would be performed by the digital computer. (See Table E-1).

It was hoped that this program together with a subroutine would produce Colburn j factor directly. An unsuccessful attempt was made to fill out table values of N_{Tu} (TABLE XI) by curve fitting using Aitken's iterative method for fitting an nth degree Lagrange polynomial to the n + 1 given points - allowing for unequal spacing. As a result of reference [8], this approach was abandoned; however, the computer program presented is still helpful in that values of conduction parameter and maximum slope are end results.

Entering TABLE XI with these parameters yields a value of N_{Tu}, which when multiplied by C1 ($C1 = N_{Pr}^{2/3} * A_c/A$) produces the Colburn j factor. A linear approximation for values of viscosity and $N_{Pr}^{2/3}$ as functions of temperature is included. An added convenience in the computer program is the evaluation of the orifice constant, K. Using [15], an assumed value for C (a slowly varying function) was made. The correct value for C was then evaluated by an iterative process by the computer. With the value of C determined, K (a rapidly varying function) was found from the following simple relationship:

$$K = \frac{C}{\sqrt{1 - \beta^4}}$$

where β is the ratio of the orifice diameter to the inside pipe diameter.

With the computer program presented, an unlimited number of matrices can be reduced by simply changing the first card of the program. (L = number of matrices for which data is to be reduced).

The following is a list of the input data for the FORTRAN 60 program:

(See sample input data in TABLE E - 2)

CARD NO.		
30	XML	Matrix length, ft
	AS	Solid conduction area, ft^2
	RH	Hydraulic radius, ft
	POR	Porosity
	AFL	Free flow area, ft^2
	AHT	Matrix heat transfer area, ft^2
	WM	Matrix weight, lbs.
40	EK	Exit flow coefficient
	CK	Entrance flow coefficient
	SK	Solid thermal conductivity, Btu/hr ft °F
	CM	Matrix material specific heat, Btu/lb °F
	XLR	Ratio of L/L_K (Flow length/Equivalent conduction length)
	N	Number of runs
10	DO	Diameter of orifice plate opening, inches
	DELPO	Pressure drop across orifice, inches H_2O
	PO	Static pressure upstream of orifice, inches H_2O
	ATMP	Atmospheric pressure, inches Hg
	BETA	Ratio of orifice diameter to inside pipe diameter
10 + 2	CS	Chart speed, sec/inch
	DELH	Pressure drop across matrix, inches H_2O
	HS	Static pressure at matrix inlet, inches H_2O
	SLO	Slope of generalized cooling curve, $(inches)^{-1}$
	TEMPO	Fluid temperature at orifice (t_o), °F

The output from the program is as follows:

EMDOT	Mass rate of flow ($\dot{m}$), lb/hr
RNUMP	Reynolds number for the pipe
RNUMH	Reynolds number for heat transfer
CAPFL	Thermal capacitance of the fluid (C), Btu/sec °F
CAPS	Thermal capacitance of the solid ($\bar{C}_s$), Btu/ °F
CONDPAR	Conduction parameter (λ)
SLOMAX	Maximum slope of generalized cooling curve
CONPARE	Equivalent conduction parameter (λ_K)
G	Mass flow velocity ($\dot{m}/A_c$), lb/sec - ft^2
RNUMFR	Reynolds number for friction
FFR	Fanning friction factor
ORIFICE K	Orifice constant, K
PRANDTL NO. 2/3	(Prandtl number)$^{2/3}$, $N_{Pr}^{2/3}$
C1	Parameter = $N_{Pr}^{2/3} \times A_c/A$
UFR	Fluid viscosity, μ , lb/hr-ft (evaluated at fluid temperature at orifice)
ESTD	Flow friction power per unit area (E_{STD}), HP/ft^2
STDH	Parameter for evaluating heat transfer power per unit area (h_{STD}), Btu/hr ft^2 °F. (STDH x N_{Tu} = h_{STD})

```
      PROGRAM SINGBLO
      L=1
      K=1
   30 READ 300,XML,AS,RH,POR,AFL,AHT,WM
  300 FORMAT(7F10.5)
   40 READ 400,EK,CK,SK,CM,XLR,N
  400 FORMAT(5F10.5,I2)
      M=1
   10 READ 100,DO,DELPO,PO,ATMP,BETA
  100 FORMAT(5F10.5)
      READ 101,CS,DELH ,HS,SLO,TEMPO
  101 FORMAT(5F10.5)
      P3=(ATMP-(PO/13.6))*.4912
      TO=TEMPO+459.7
      UFR=0.0395+0.64167E-4*TEMPO
      TB=TEMPO+10.0
      UH=0.0395+0.64167E-4*TB
      WRITE OUTPUT TAPE 4,9
    9 FORMAT(1H1)
      WRITE OUTPUT TAPE 4,4,M
    4 FORMAT(9H RUN NO. I2///)
   11 IF(ABSF(BETA-.75)-.000001)27,27,12
   12 IF(ABSF(BETA-.64)-.000001)26,26,13
   13 IF(ABSF(BETA-.50)-.000001)25,25,14
   14 IF(ABSF(BETA-.40)-.000001)24,24,15
   15 IF(ABSF(BETA-.25)-.000001)23,23,16
   16 IF(ABSF(BETA-.15)-.000001)22,22,17
   17 GO TO 80
   21 X2=0.59225
      DELX=0.01916
      ASSUM=0.6000
      GO TO 28
   22 X2=0.59171
      DELX=0.01691
      ASSUM=0.6000
      GO TO 28
   23 X2=0.59184
      DELX=0.01622
      ASSUM=0.6000
      GO TO 28
   24 X2=0.59448
      DELX=0.01867
      ASSUM=0.6000
      GO TO 28
```

TABLE E-1

```
25 X2=0.59850
   DELX=0.02125
   ASSUM=0.6000
   GO TO 28
26 X2=0.60575
   DELX=0.02595
   ASSUM=0.6000
   GO TO 28
27 X2=0.60691
   DELX=0.03839
   ASSUM=0.6000
28 COR=ASSUM
   NC=0
   B1=1./SQRTF(1.-BETA**4)
31 NC=NC+1
   IF(NC-4)29,29,60
29 EMDOT=589.81*DO*DO*SQRTF(DELPO*P3/T0)*COR*B1
   RNUMO=(4.961*EMDOT/UFR)/BETA
   CORA=X2+DELX*SQRTF(10000./RNUMO)
   WRITE OUTPUT TAPE 4,8,CORA
 8 FORMAT(6H CORA=F10.5//)
32 COR=CORA
   GO TO 31
60 PR=0.8017-.82353E-4*TEMPO
   C1=PR*AFL/AHT
   CP=0.24
   RNUMP=5.09*EMDOT/UFR
   RNUMH=(4.0*XML*EMDOT)/(AHT*UH)
   RNUMFR=RNUMH*UH/UFR
   CAPFL=EMDOT*CP/3600.0
   CAPS=WM*CM
   SLOMAX=(CAPS*SLO)/(CAPFL*CS)
   CONDPAR=(SK*AS)/(XML*EMDOT*CP)
   CONPARE=CONDPAR*XLR
   B=CK+EK
   C=1.0+POR**2
   G=EMDOT/(AFL*3600.0)
   DELP=DELH*.03613
   PS=HS*.03613
   PA=ATMP*.4912
   P1=PA-PS
   P2=P1-DELP
   PM=(P1+P2)/2.
   RHOM=(PM*144.0)/(53.3*(TEMPO+460.0))
```

TABLE E-1

```
      FF1=((64.4*RHOM*DELP*144.0)/(G*G))
      FF2=C*DELP/PV
      FF3=FF1-FF2-B
      FFR=FF3*RH/XML
      CONST=COR*B1
      STDH=(0.02195*RNUMH*C1)/(4.*RH)
      ESTD=1.11E-7*(1.0/(4.*RH))**3*FFR*(RNUMFR/1000.)**3
      WRITE OUTPUT TAPE 4,7,STDH,ESTD
    7 FORMAT(19H CONSTANT FOR HSTD=F10.5,3X,6H ESTD=F10.5///)
      WRITE OUTPUT TAPE 4,1,EMDOT,RNUMP,RNUMH,CAPFL,CAPS
    1 FORMAT(7H EMDOT=F10.5,3X,7H RNUMP=E20.8,3X,7H RNUMH=F10.5,3X,
     17H CAPFL=F10.5,3X,6H CAPS=F10.5///)
      WRITE OUTPUT TAPE 4,2,CONDPAR,SLOMAX,CONPARE
    2 FORMAT(9H CONDPAR=F10.5,3X,8H SLOMAX=F10.5,3X,9H CONPARE=F10.5///)
      WRITE OUTPUT TAPE 4,3,G,RNUMFR,FFR,CONST
   30 FORMAT(3H G=F10.5,3X,8H RNUMFR=F10.5,3X,5H FFR=F10.5,3X,11H ORIFIC
     1E K=F10.5///)
      WRITE OUTPUT TAPE 4,5,PR,C1,UFR
    5 FORMAT(16H PRANDTL NO.2/3=F10.5,3X,4H C1=F10.5,3X,5H UFR=F10.5///)
      M=M+1
      IF(N-M)50,10,10
   50 K=K+1
      IF(L-K)20,30,30
   80 PRINT 81
   81 FORMAT(30H ORIFICE CONSTANT ERROR EXISTS)
      GO TO 20
   20 STOP
      END
      END
```

TABLE E-1

SAMPLE INPUT DATA FOR PROGRAM SINGBLO

```
0.1667    .00640    .00049     .8542     .05939    17.70242   .4844
-.32      .51       38.7       .1065     .82709    11
2.310     6.78      21.5      30.140     .75
.25       9.30      12.2       .17768   68.5
2.310     4.40      15.45     30.120     .75
.25       7.15       8.30      .15259   71.0
2.310     2.74      10.95     30.120     .75
.25       5.15       5.80      .12882   73.0
1.971     3.82       7.10     30.120     .64
.50       3.40       3.50      .21040   72.0
1.540     6.89       4.50     30.120     .50
.50       2.33       2.06      .17379   72.7
1.540     2.91       2.60     30.110     .50
.50       1.42       0.95      .14039   72.7
1.232     2.75       1.40     30.110     .40
.50       0.80       0.43      .09232   72.5
0.775     6.00       0.68     30.110     .25
1.00      0.41       0.18      .10170   69.0
0.775     5.98       0.67     30.110     .25
1.00      0.40       0.178     .10316   69.0
0.775     1.78       0.35     30.110     .25
2.00      0.22       0.075     .10321   70.0
0.462     2.60       0.15     30.110     .15
4.00      0.080      0.025     .07513   70.0
```

TABLE E - 2